UNIVERSIDAD AUTÓNOMA DE MADRID

School of Medicine

Anatomy, Histology and Neuroscience Department

Basal Forebrain-Cortical circuits in rodents. Implications of anatomical pathways and cell toxicity in Alzheimer´s Disease.

Doctoral Thesis **Irene Chaves-Coira**

2017

UNIVERSIDAD AUTÓNOMA DE MADRID
Facultad de Medicina
Departamento de Anatomía, Histología y Neurociencia

Basal Forebrain-Cortical circuits in rodents.

Implications of anatomical pathways and cell toxicity in Alzheimer´s Disease.

Memory presented by Irene Chaves Coira to qualify for the Doctor's Degree by the Autonomous University of Madrid (UAM) in the Program of Doctorate in Neuroscience, in agreement to the work realized under the direction of the Teachers Margarita Rodrigo Angulo and Ángel Núñez Molina in the Department of Anatomy, Histology and Neuroscience of Medical School of the UAM.

Memoria presentada por Irene Chaves Coira para optar al título de Doctor por la Universidad Autónoma de Madrid (UAM) en el Programa de Doctorado en Neurociencia, de acuerdo al trabajo realizado bajo la dirección de los Profesores Margarita Rodrigo Angulo y Ángel Núñez Molina en el Departamento de Anatomía, Histología y Neurociencia de la Facultad de Medicina de la UAM.

List of contents

LIST OF CONTENTS

A1: primary auditory cortex

ac: anterior comissure

aca: anterior commissure, anterior part

AD: Alzheimer disease

AHP: anterior hypothalamic area, posterior part

Arc: arcuate hypothalamic nucleus

B: nucleus basalis magnocellularis

BF: basal forebrain

BLA: basolateral amygdaloid nucleus,

CA3: field CA3 of the hippocampus

cc: corpus callosus

CeC: central amygdaloid nucleus, capsular part

CeM: central amygdaloid nucleus, medial division

cg: cingulum

Cg1: cingulate cortex

ChAT: choline acetyl transferase

CPu: caudate putamen (striatum)

D3V: dorsal 3rd ventricle

DCl: dorsal part of claustrum

Den: dorsal endopiriform nucleus

EAC: sublenticular extended amygdala, central part

ec: external capsule

EGP: external globus pallidus

f: fornix

FB: Fast Blue fluorochrome

FlGo Fluoro-Gold fluorochrome

HDB: horizontal limb of the diagonal band of Broca

IAD: interanterodorsal thalamic nucleus

ic: internal capsule

Il: infralimbic cortex

Ld: lambdoid septal zone

Lo: lateral olfactory tract

LSD: lateral septal nucleus, dorsal part

LSI: lateral septal nucleus, intermediate part

LSV: lateral septal nucleus, ventral part

LV: lateral ventricle

M1: primary motor cortex

MCPO: magnocellular preoptic nucleus

mfb: medial forebrain bundle

MnPO: medial preoptic nucleus

mPfC: medial prefrontal cortex

MS: medial septal nucleus

mt: mamillothalamic tract

och: optic chiasm

opt: optic tract

PeFLH: perifornical part of lateral hypothalamus

PrL: prelimbic cortex

PT: paratenial thalamic nucleus

PV: paraventricular thalamic nucleus

PVA: paraventricular thalamic nucleus, anterior part

RCh: retrochiasmatic area

RChL: retrochiasmatic area, lateral part

Re: reuniens thalamic nucleus

Rt: reticular thalamic nucleus

S1: primary somatosensory cortex

S1BF: S1 barrel field cortex

S1FL: S1 fore limb cortex

S2: secundary somatosensory cortical area

ScHVM: suprachiasmatic nucleus, ventromedial part

SHi: septohippocampal nucleus

SHy: septohypotalamic nucleus

SI: sustantia innominata

SIB: substantia innominate, basal part

sm: stria medullaris of the thalamus

SNR: sustantia nigra pars reticulata

SO: supraoptic nucleus

sod: supraoptic decussation

st: stria terminalis

StHy: striohypothalamic nucleus

TS: triangular septal nucleis

V1: primary visual cortical area

VA/VL: región where VA and VL overlap

VA: ventral anterios thalamic nucleus

VCl: ventral part of claustrum

VDB: vertical limb of the diagonal band of Broca

VM: ventromedial thalamic nucleus

VP: ventral pallidum

VP: ventral pallidum

ZI: zona incerta

Summary

SUMMARY

The mammalian cerebral cortex receives consistent projections of cholinergic and non-cholinergic neurons from the basal forebrain (BF). Different structures and nuclei have been historically included in the BF by different authors, including the medial septum, the horizontal and vertical limbs of the Broca diagonal band (HDB and VDB, respectively), the substancia innominata and the nucleus Basal magnocellular (B nucleus, Meynert basal magnocellular nucleus in humans). BF structures provide the major source of cholinergic innervation to the sensory, motor and prefrontal cortex (mPfC), and to the hippocampus, which exert extensive modulatory actions on mood and cognition. Specific reciprocal projections between different BF nuclei and their cortical targets are necessary to control the sensory information processed in the different cortices. Cholinergic cortical innervation plays a fundamental role in the processes of attention, learning, memory and in the processing of sensory information. The cholinergic hypothesis of Alzheimer's disease (AD) arose from evidence of loss of cholinergic markers in the cortex. The loss of neuronal cholinergic projections in AD causes severe disorders in learning, memory and sensory processing, which are the main causes of disability in patients, all of them showing extensive neuronal loss. The deregulation of some of the process where TDP-43 is implicated might lead to an abberant aggregation and modification of TDP-43 in the affected cells.

The aim of this Thesis is, firstly, to elucidate if different neuronal populations of BF modulate specific sensitive cortical areas through separate neural networks, and, second, to study the possible involvement of these BF circuits in AD, which may be altered by neuronal loss, or by cellular toxicity hypothesis as the cause of such neuronal death. For these purposes, anatomical techniques of neural tracing were used in rodents by injecting retrograde and anterograde tracers into cortical areas and in different BF nuclei that were combined with sensory and optogenetic stimulation to determine the functionality of the different reciprocal pathways between BF and the cortical areas. Cell culture

methods were also used to study the possible cellular toxicity by studying TDP-43 function. Anatomic and optogenetic results indicate that while VDB/HDB exhibit more specific cortical targets, B nucleus shows wider non-specific targets in the cortex. In addition, the VDB/HDB comprises reciprocal projections to the mPfC and sensory cortices. Although the B nucleus is involved in the projection to sensory pathways, it does not project to mPfC. We also observed a loss of neurons in the HDB in the case of APP/PS1 mice accompanied by increased expression of the IGF1 receptor in their cholinergic neurons. Therefore, we can conclude that the B nucleus does not present specific circuits for the different cortices but presents a non-specific pattern of projections and does not show a B nucleus-mPfC connecting circuit, which could mean that this nucleus does not play a decisive role in sensory input discrimination. Conversely, the cholinergic projection of HDB may be important in AD during the early stages of its development due to the specific neuronal projection circuit patterns present in this nucleus and linked to the greater expression of IGF1 present in its cholinergic neurons, which might be exerting a protective effect on them.

Resumen

RESUMEN

La corteza cerebral de los mamíferos recibe proyecciones consistentes de las neuronas colinérgicas y no-colinérgicas desde el prosencéfalo basal (BF). Diferentes estructuras y núcleos han sido históricamente incluidos en el BF por diferentes autores, entre ellos están el septo medial, los brazos horizontal y vertical de la banda diagonal de Broca (HDB y VDB, respectivamente), la sustancia innominada (SI) y el núcleo basal magnocelular (Núcleo B, núcleo magnocelular basal de Meynert en humanos). Las estructuras del BF proporcionan la mayor fuente de inervación colinérgica a las cortezas sensoriales, motora y prefrontal, y al hipocampo, que ejercen amplias acciones moduladoras sobre el estado de ánimo y la cognición. Proyecciones recíprocas específicas entre diferentes estructuras del BF y sus dianas corticales son necesarias para controlar la información sensorial procesada en las diferentes cortezas. La inervación cortical colinérgica desempeña un papel fundamental en los procesos de atención, aprendizaje, memoria y en el procesamiento de la información sensorial. La hipótesis colinérgica de la Enfermedad de Alzheimer (EA), surgió a partir de evidencias de pérdida de marcadores colinérgicos en la corteza. La pérdida de neuronas y proyecciones colinérgicas en la EA provoca graves trastornos en el aprendizaje, la memoria y el procesamiento sensorial, que son las principales causas de discapacidad en los pacientes. La desregulación de algunos de los procesos en los que está implicado el TDP-43, cuyo papel en relación con EA está siendo estudiado actualmente, podría estar implicada en la agregación y modificación de TDP-43 en las células afectadas.

Los objetivo de esta Tesis son, en primer lugar, elucidar si diferentes poblaciones neuronales del BF modulan áreas corticales sensitivas específicas a través de redes neuronales independientes, y, en segundo lugar, estudiar la posible implicación de estos circuitos en la EA, que se puedan ver alterados por pérdida neuronal, o por toxicidad celular como causa de muerte neuronal. Para estos propósitos se utilizaron técnicas anatómicas de trazado neuronal en roedores por medio de la inyección de trazadores retrógrados y anterógrados en áreas corticales

y en diferentes núcleos del BF que se combinaron con estimulación sensorial y optogenética para determinar la funcionalidad de las diferentes vías recíprocas entre el BF y las áreas corticales. Se emplearon métodos de cultivo celular para estudiar la posible toxicidad celular por pérdida de función del TDP-43. Los resultados anatómicos y optogenéticos indican que mientras, VDB/HDB tienen objetivos corticales más específicos, el núcleo B no presenta dianas específicas a la corteza. El VDB/HDB mantiene proyecciones recíprocas a las cortezas prefrontal medial (mPfC) y somatosensoriales. Aunque el núcleo B está involucrado en la proyección a vías somatosensoriales, no proyecta a mPfC. También se observó una pérdida de neuronas en el HDB en el caso de ratones APP/PS1 acompañado de una mayor expresión del receptor de IGF1 en sus neuronas colinérgicas. Con todos estos datos, podemos concluir que el núcleo B no presenta circuitos específicos para las distintas cortezas, sino que presenta un patrón inespecífico de proyecciones y no muestra un circuito núcleo B-mPfC. Esto podría significar que éste núcleo no desempeña un papel decisivo en la discriminación de la entrada sensorial. En contraposición, la proyección colinérgica de HDB podría ser importante en las primeras etapas de la EA debido a que sus patrones de proyección neuronal específicos podrían estar ejerciendo bajo un efecto protector del IGF1 mediado por su mayor expresión en las neuronas colinérgicas.

Introduction

1. INTRODUCTION

1.1. BASAL FOREBRAIN

The basal forebrain (BF) is a brain region located, as its name indicates, in the basal part of the forebrain. It includes several structures distributed al along the brain from rostral to caudal. A global and detailed Knowledge of the neuronal connectivity, as well as of the central nervous system is crucial for the well understanding of how the brain Works, both in physiological and pathological conditions.The mammalian cerebral cortex receives consistent projections from cholinergic and non-cholinergic neurons in the BF.

Many classic classifications of the BF have been done based on different criteria such as anatomy, citoarchitectonic, biochemical features or electrophysiological properties.

From an anatomical point of view, we have followed the classification that Kristt et al did in 1985, where he divided the BF fibers in 3 pathways:

1) Anterior pathway: In sagittal sections fiber bundles can be traced from the SI / B region to the frontal cortex. After passing through the neoestriatum the fibers cross the outer capsule and curl dorsally to enter the VI layer of the frontal cortex. Another small group of AChE-rich fibers that runs dorso-ventrally anterior to the neo-striatum appear to attach to a major trajectory before entering the cortex. This second path could be originated in the hypothalamus, according to retrograde transport data. The entry point in the cortex of all fascicles is close to the transition zone with the olfactory cortex.

2) Medial pathway: The existence of a medial pathway rich in AChE in rat was histologically described by Shute and Lewis. Emerging from the AChE rich sums in the HDB is a bundle of fibers with a dorso-lateral course and entering layer VI of the anterior medial cortex, area 24. In this sheet the fibers continue dorsally

in a coronal plane Tilted 10-20º rostrally. Additional fibers of a more caudal and / or mid-lateral origin seem to attach to the medial bundle, probably outside of HDB (as for example SI). These fibers of the medial bundle disappear from the coronal plane as it approaches the back of the minor forceps. In sagittal planes, the beam is rotated caudally and continues along the deep margin of the medial cortex above the corpus callosum. In horizontal sections these fibers seem to extend to reach the cingular cortex and also within of the medial parts of the occipital cortex.

3) Lateral pathway: Seems to innervate the frontal-lateral, parieto-temporal and latero-occipital cortex. With B and SI as a concentrator, there are groups of fibers that flow into temporal, parietal and frontal fields in an elaborate three-dimensional variety. Most fibers pass sequentially through the balloon, neoestriatum, and the outer capsule. Commonly, upon entering layer VI of the fronto-parietal cortex, these "striatal radiations" seem to turn abruptly dorsum-medially in the plane of entry. In sagittal sections passing tangentially through layer VI of the fronto-parietal cortex, this pivot point appears as a dense horizontal band from which individual fibers emerge. At levels progressively more caudal or rostral to the fronto-parietal cortex no beams of direct connection with the B / SI nucleus can be traced, not even in immature animals. In contrast, numerous short segments of AChE positive fibers are found between the microstructure (or the outer capsule) and the layer VI of the cortex. This can be interpreted as an indication that at caudal and rostral levels in the lateral cortex the BF afferents enter the cortex at relatively acute angles. Some fibers rich in AChE follow a dorsomedial course from the neoestriado, probably to innervate the cortical regions in the proximity of the cíngulo, where they could partially overlap with the territory of the medial path. The medial occipital cortex is innervated from the anterior SI and the HDB. This can be explained in terms of the spatial distribution of the medial path. Fibers in this path cross these anterior regions of the BF with the cx both cingular and occipital-medial. The other regions in the postero-lateral cortex of the rat that are innervated by caudal regions of the nucleus B surely receive inputs via the lateral pathway.

In three dimensions, the fibers constitute a structure like that of a leaf, connecting the anterior BF with the polar cortex. The fibers of the lateral path radiate multidirectionally. Similarly, lateral fibers enter the cortex and rotate

dorsally within the plane of entry. The anterior fibers that penetrate the cortex rotate 90 ° medially and out of the plane of entry. The anterior fibers that penetrate the cortex rotate 90º medially and out of the plane of entry. The topography of the fibers in each system cannot be duplicated simply by rotating the subcortical portion of the lateral fibers or above, a second rotation is necessary to be topographically congruent. For example, lateral and medial pathways seem to innervate medial regions of the occipital cortex. Medial injections of the tracer to this area are expected to retrograde HDB neurons, whereas more lateral injections may reveal marked neurons in later parts of B nucleus (Kristt, et al 1985).

From a biochemical point of view based on the classification of Mesulam of 1983 we can make a classification of the neurons in 6 groups (Figure 1.1).

There is an organization of ascending cholinergic projections: the BF and the brainstem in the rat, which contain six groups of cholinergic projection neurons, designated Ch1-Ch6 based on cytoarchitectonic criteria and connectivity patterns. Since ChAT is the most specific marker for cholinergic neurons, it can be said that the projections to the neocortex, olfactory bulb, hippocampus and thalamus arise, at least in part, from the cholinergic cell bodies of Ch1-Ch6. Pharmacological experiments showed that most cortical cholinergic innervation was extrinsic and originated in the subcortical cholinergic neurons of BF and reticular formation.

In the rat brain, the Ch1-Ch2 sectors are contained within the medial septum and VDB, respectively. They provide the main cholinergic projection to hippocampus formation. The Ch3 sector is mostly contained within the lateral side of the HDB and provides the main cholinergic projection to the olfactory bulb. The Ch4 sector contains the cholinergic neurons of nucleus B, the SI and probably also neurons located laterally of VDB. One criterion for unification of Ch4 is that its components provide the main cholinergic innervation to neo-cortical targets. Ch4 mainly innervates the amygdala. The Ch5-Ch6 sectors are located in the pontomesencephalic reticular formation and provide the main cholinergic innervation to the thalamus. There is overlap in connectivity whereby individual sectors of Ch also provide a smaller source of cholinergic innervation for areas other than their main targets. The cortical mantle is under a dual cholinergic

influence. On the one hand, there is a monosynaptic corticopetal cholinergic pathway that comes mainly from Ch4. On the other hand, there is also an indirect pathway that has a cholinergic segment from Ch5-Ch6 to the thalamus and a non-cholinergic segment from the thalamus to the cortex.

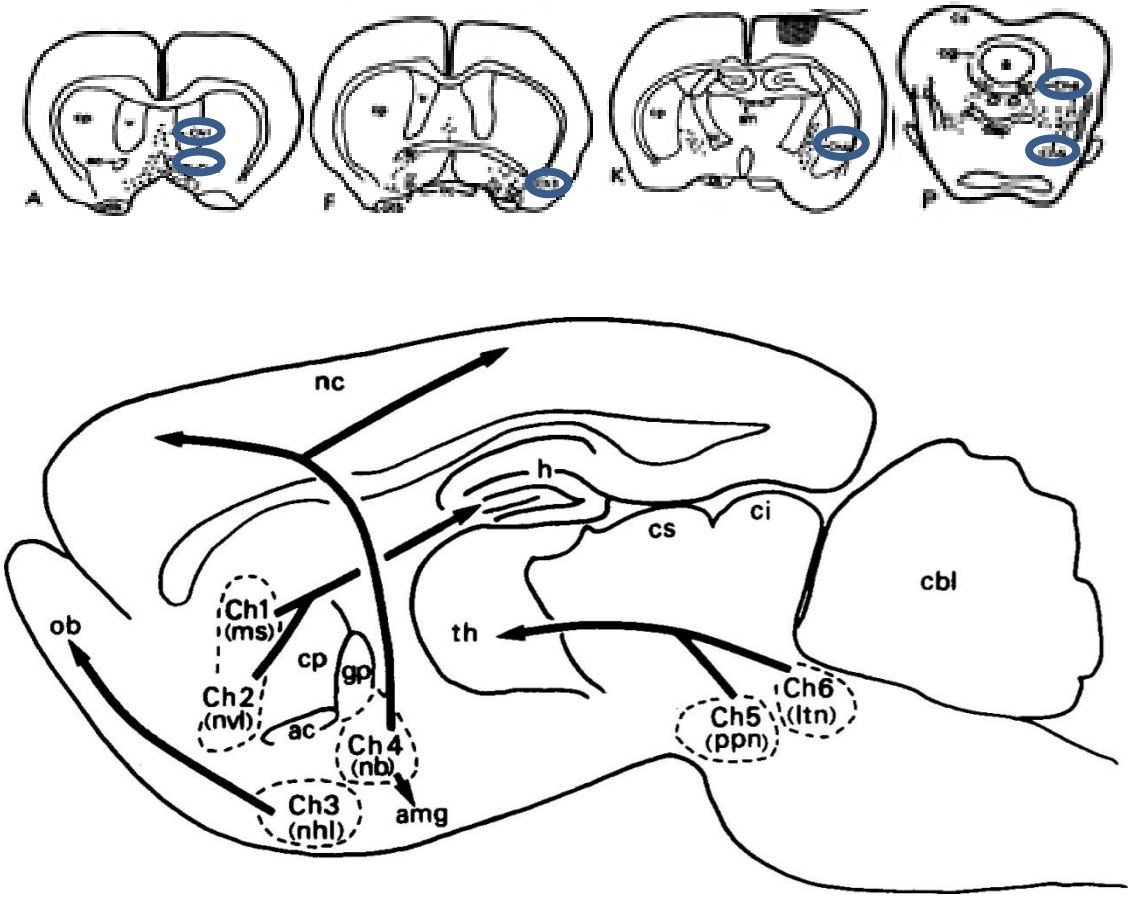

Figure 1.1: Schematic drawing of Mesulam classification (1983) of cholinergic neurons, Ch1-Ch6 groups.

We can also make a classification of BF neurons based on electrophysiological criteria. BF cholinergic neurons can be subdivided into two populations based on their trigger times in response to depolarizing currents. Therefore, we refer to them as early-firing (EF) that constitute 70% of the neuronal population present in the BF, and late-firing (LF) neurons that make up the remaining 30%. EF neurons discharge at higher frequencies in response to intracellular injections of current, but this is accompanied by a prominent ear of adaptive frequency. In many cases, these neurons stop firing after an initial

discharge. On the other hand, LF neurons are less excitable, but are able to maintain a tonic firing pattern in response to longer (10 second) injections of current. This heterogeneity is achieved through an intricate role between different voltage-mediated calcium and K conductance's (Unal et al 2015).

Different authors have included distinct structures and nuclei the BF which are distributed from rostral to caudal all over the brain. It is formed of several heterogeneous structures, which include, depending on the author, the following nuclei: the medial septum, the horizontal and vertical limbs of the diagonal band of Broca (HDB and VDB, respectively), the substantia innominata (SI), the extended amigdala, subpalial regions and the nucleus basalis magnocellularis (B nucleus, or in humans, Maynert basal magnocellular nucleus). These nuclei are conformed of a broad variety of neurons of different biochemical characteristics; they contain gabaergic, cholinergic and glutamatergic projecting neurons, as well as interneurons. These structures provide most of the cholinergic innervation to sensory, motor and prefrontal cortices and the hippocampus (Houser et al., 1985; Semba and Fibiger, 1989; Mesulam et al., 1992; Gritti et al., 1997; Semba, 2000; Bloem et al., 2014; Zaborszky et al., 2015; Kim et al., 2016). There is abundant evidence that the BF cortical projections play an essential role in cognitive functions such as attention states, learning and memory, wakefulness and processing of sensory information (e.g. Manns et al., 2001; Broussard et al., 2009, Sarter et al., 2014; Zant et al., 2016).

Anatomical studies have indicated the existence of a highly structured and topographic organization of BF efferent projections to sensory cortices (Zaborszky, 2002; Zaborszky et al., 2005, 2015). The above-mentioned authors propose that cholinergic and non-cholinergic projections to the neocortex are not diffuse but are instead organized into segregated or overlapped neuronal groups (Zaborszky et al., 2015). Rodent studies of the anatomical pathways linking the BF with primary somatosensory (S1), auditory (A1) and visual (V1) cortical areas studied have shown that separate or partially overlapping groups of BF neurons display specific projection pathways to primary sensory cortices of different modalities (Zaborsky et al., 2015; Chaves-Coira et al., 2016). In the same way, the rostro caudal

distribution of retrogradely-labeled neurons in BF shows that neurons projecting to the medial prefrontal cortex (mPfC) tended to cluster in the rostral portion of the BF region (Chandler et al., 2013). Moreover, cholinergic pathways originated in different BF nuclei have been described following four different routes, depending on their location, to reach different layers of the mPfC (Bloem et al., 2014). The mPfC is a brain region involved in a wide range of diseases. It maintains a large number of connections to other cortical and subcortical regions (Groenewegen et al 1997) and should act as a control station, integrating information it receives from numerous structures and sending this updated or integrated information to target structures (Miller and Cohen, 2001). Consistent with this organization of anatomical pathways, optogenetic activation of cholinergic neurons in BF subnuclei induces modality-selective desynchronization in specific sensory cortices (Kim et al., 2016) and sensory modulation (Chaves-Coira et al., 2016). Moreover, projections from the prefrontal cortex to the BF have been observed (Zaborszky et al., 1997) and posited to contribute to the top-down regulation of this area.

Despite many studies on the relations between the location of different BF nuclei and their projection areas, the question of how specific these projections are and how precisely different regions in the BF map on their cortical targets are still unanswered.

1.2 Acetylcholine

As mentioned above, the BF constitues the main source of ACh to the cortex. Acetylcholine (ACh) is essential to normal central nervous system (CNS) function, modulating the activity of the thalamocortical network in many important brain functions, such as arousal (e.g., (Buzsaki et al., 1988, Détári, 2000, Szymusiak et al., 2000, Lee et al., 2004, Goard and Dan, 2009), attention (Chiba et al., 1999, Sarter et al., 2003), learning (Wilson and Rolls, 1990a, b) and memory ((Pauli and O'Reilly, 2008, Hasselmo and Sarter, 2011, Luchicchi et al., 2014, Sarter et al., 2014). Moreover, ACh enhances synaptic plasticity in the hippocampus (e.g. (Doralp and

Leung, 2008, Fernandez de Sevilla et al., 2008, Navarrete et al., 2012)) and neocortex (e.g. (Metherate and Ashe, 1993, Kuo et al., 2009, Bueno-Junior et al., 2012, Nuñez et al., 2012, Barros-Zulaica et al., 2014).

Ach is a simple molecule synthesized from choline and acetyl-CoA (Figure 1.2) by the action of choline acetyltransferase. The neurons that synthesize and release Ach are called cholinergic neurons.

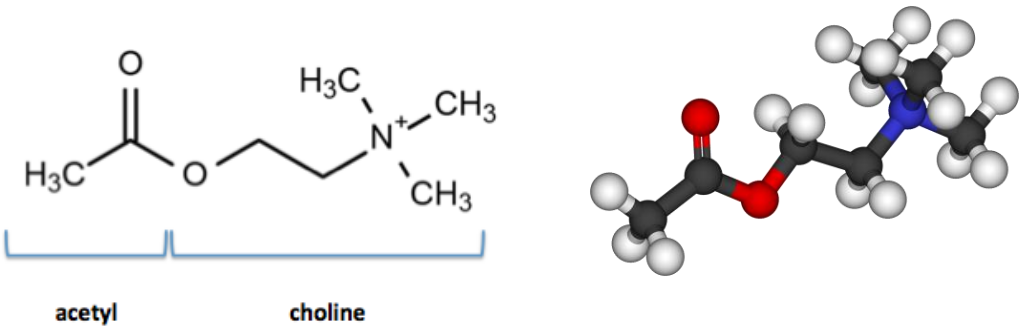

Figure 1.2: Acetylcholine molecule representation

When an action potential reaches the terminal button of a pre-synaptic neuron a calcium channel opens. The entry of calcium ions stimulates the exocytosis of the presynaptic vesicles containing Ach, which is consequently released into the synaptic gap. Once released, the Ach is carried out by the enzyme acetylcholinesterase. Acetylcholinesterase, which is found in the nerve terminals, is anchored to plasma membranes through a glycolipid. Ach receptors are cation channels composed of four disperse polypeptide subunits (alpha2 beta gamma). Two major classes of Ach receptors have been identified: muscarinic receptors and nicotinic receptors. Both kinds of receptors exist with abundance in the human. Nicotinic receptors are eventually divided into receptors found in neuromuscular junctions and those found in neuronal synapses. Activation of Ach receptors by binding to their ligand leads to sodium intake to the cell and K^+ output, resulting in depolarization of the post-synaptic neuron and initiation of a new action potential.

The synthesis of ACh involves the reaction of choline with acetyl co-enzyme A. Much of the choline used in this process is recycled but it can also be synthesized de novo in the neurone. This reaction is catalysed by the enzyme choline acetyltransferase (Figure 1.3). Once ACh has combined with the receptor site, it must be rapidly removed from the synapse for repolarisation to occur. It is therefore catalyzed by the enzyme acetylcholinesterase to produce choline and acetate. As previously mentioned the choline is then recycled back into the terminal to produce new molecules of ACh.

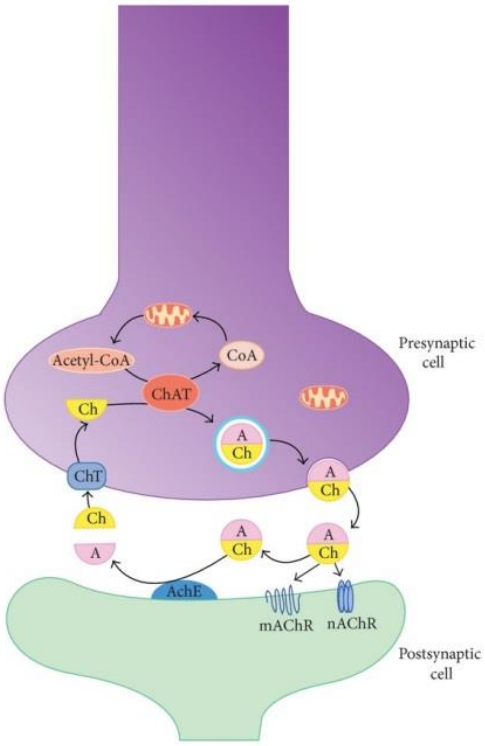

Figure 1.3: Eschematic Ach cycle representation in a synapsis.

Cortical ACh plays an important role in cortical awakening, attention, learning and memory, and BF cholinergic neurons are the main source of Ach to the cerebral cortex (Rasmusson, 2000; Semab 2000). Cholinergic innervation of the neocortex derives primarily from BF and has been proposed to play a key role in cognitive functions in humans.

This function seems to require a diffuse organized innervation to integrate the activity on different regions of the neocortex. Although this innervation rich in AchE has a diffuse distribution, several observations suggest that individual neurons in BF must interact with a relatively limited population of cortical neurons. Proximal clusters, intranuclear axonal collaterals exhibiting BF neurons must be particularly relevant in this regard (Donald A et al 1985).

In the CNS, Ach transmission is mainly guaranteed by dense innervation of select cortical and subcortical regions from disperse groups of cholinergic neurons within the basal forebrain (BF) and the pontine-mesencephalic nuclei, respectively. The BF contains a diverse population of neurons, including cortically projecting cholinergic and non-cholinergic neurons as well as various interneurons (Zaborszky et al., 2012). The BF includes the medial septum, horizontal and vertical limbs of the diagonal band of Broca (HDB and VDB, respectively), the substantia innominata (SI), as well as the nucleus basalis magnocellularis (B), which provide the majority of the cholinergic innervation to the sensory, motor and prefrontal cortices and to the hippocampus (Semba and Fibiger, 1989, Zaborszky et al., 2012, Eckenstein et al., 1988, Lysakowski et al., 1989). However, newer evidence concerning the BF system indicates the existence of a highly structured and topographic organization of efferent projections to sensory cortices (Zaborszky, 2002, Golmayo et al., 2003, Zaborszky et al., 2005, Zaborszky et al., 2013). The above mentioned authors propose that cholinergic and non-cholinergic projections to the neocortex are not diffuse, but instead, are organized into segregated or overlapping neuronal groups (Zaborszky et al., 2013). Consequently, previous results suggest a refined anatomical and functional topographical organization of the BF corticopetal projection system that may control cortical sensory processing in a specific manner. Studies measuring cortical ACh level have demonstrated that visual stimulation causes much greater ACh release in visual cortex than in non-visual cortical areas (Collier and Mitchell, 1966; Fournier et al., 2004; Laplante et al., 2005). Anatomical tracing methods have not revealed any extensive projections from sensory relay nuclei to the BF (Semba et al., 1988; Záborszky et al., 1991). Thus, it has been proposed that sensory information arrives to the BF through cortico-cortical projections from primary cortical

sensory areas via the prefrontal cortex (Záborszky et al., 1997). Results from either electrophysiological recordings (Golmayo et al. 2003) or inactivation of the prefrontal cortex (Rasmusson et al., 2007) have demonstrated that the prefrontal cortex is necessary for sensory-evoked cortical ACh release. These results strongly support the proposed specific circuit –sensory cortex to prefrontal cortex to basal forebrain –for each sensory modality.

1.3 Alzheimer Desease

Alzheimer's disease (AD) is considered a progressive neurodegenerative disorder with an estimated 5.3 million patients of all ages in the United States of America (Hebert et al 2013). AD is acknowledged as the most common leading cause of dementia in late adult life. It is associated with cerebral cortical atrophy and neuropathology hallmark of the disease are neurofibrillary tangles and amyloid protein deposits contributing to plaques. The senile plaques are composed of insoluble aggregates of Aβ peptides, which are derived from the amyloid precursor protein (APP) via cleavage by the protease, β- and γ-secretase (De Strooper 2010; Rajendran and Annaert 2012). Two different forms are established, based on the onset of first symptoms and presumed pathogenesis. Early-onset AD is a term used for uncommon, accounting for only 2-5% of all Alzheimer's cases and is diagnosed before the age of 65. Approximately 15% of the early-onset cases are familial, where a genetic predisposition leads to the disease (Mendez 2012). In contrast, most cases of AD do not exhibit genetic inheritance and are termed sporadic AD. The pathophysiology of late-onset AD remains only partly understood, but some environmental and genetic differences may be associated as risk factors.

Given its prominent role in regulating attention and memory circuits, cholinergic signaling is a key player in mediating cognitive performance. The cholinergic hypothesis of AD emerged from evidences of loss of cholinergic markers in the cortex (Geula and Mesulam, 1989), loss of the number of neurons in the BF (Whitehouse *et al*., 1982), and the recent report of a volume loss in the nucleus basalis of Meynert (Cantero et al., 2016). Although AD is most classically

associated with memory deficits, these deficits are typically conflated with attention issues (Romberg et al., 2013). Nevertheless, both, the sensory-motor deficits and arousal decline, also appear later in AD patients. This progression in AD symptoms may be due to the heterogeneity of the BF nuclei and their specific projections. As we will describe, some BF areas are involved in the sensory processing that is required for attention, memory and learning processes, sensory-motor coordination, or promotion of arousal. Thus, heterogenic cholinergic neuronal loss may also occur in different BF structures in the course of the disease and our understanding of these structures requires much work.

1.4 IGF1

The insulin-like growth factor 1 (IGF-1) receptor is a protein found on the surface of human cells (Figure 1.5). It is a transmembrane receptor that is activated by a hormone called insulin-like growth factor 1 (IGF-1) (Figure 1.4) and by a related hormone called IGF-2. It belongs to the large class of tyrosine kinase receptors. This receptor mediates the effects of IGF-1, which is a polypeptide protein hormone similar in molecular structure to insulin. IGF-1 plays an important role in growth and continues to have anabolic effects in adults – meaning that it can induce hypertrophy of skeletal muscle and other target tissues. Mice lacking the IGF-1 receptor die late in development, and show a dramatic reduction in body mass, testifying to the strong growth-promoting effect of this receptor. Mice carrying only one functional copy of IGF-1R are normal, but exhibit a ~15% decrease in body mass.

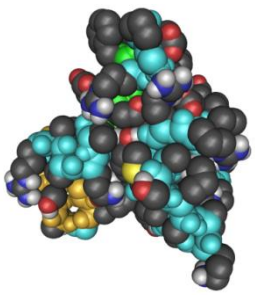

Figure 1.4: Molecular structure of IGF1 protein.

Two alpha subunits and two beta subunits make up the IGF-1 receptor. Both the α and β subunits are synthesized from a single mRNA precursor. The precursor is then glycosylated, proteolytically cleaved, and crosslinked by cysteine bonds to form a functional transmembrane αβ chain (Gregory et al 2001). The α chains are located extracellularly, while the β subunit spans the membrane and is responsible for intracellular signal transduction upon ligand stimulation. The mature IGF-1R has a molecular weight of approximately 320 kDa. The receptor is a member of a family which consists of the insulin receptor and the IGF-2R (and their respective ligands IGF-1 and IGF-2), along with several IGF-binding proteins.

The IGF-1R and the insulin receptor both have a binding site for ATP, which is used to provide the phosphates for auto phosphorylation. There is a 60% homology between IGF-1R and the insulin receptor.

In response to ligand binding, the α chains induce the tyrosine auto phosphorylation of the β chains. This event triggers a cascade of intracellular signaling that, while cell type-specific, often promotes cell survival and cell proliferation (Jones and Clemmons 1995) (LeRoith et al 1995). The structures of the auto phosphorylation complexes of tyrosine residues 1165 and 1166 have been identified within crystals of the IGF1R kinase domain (Xu et al 2015).

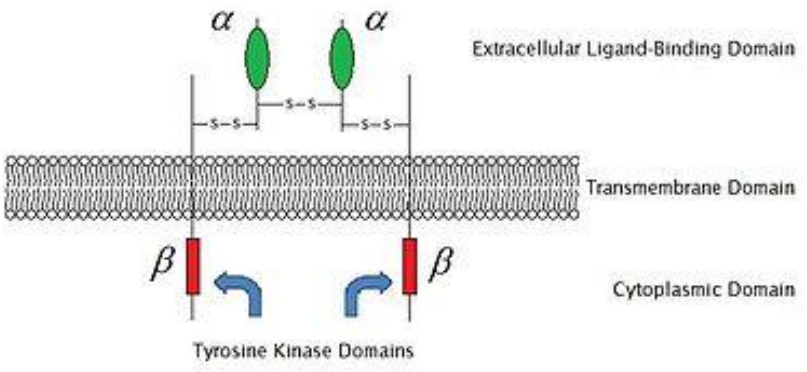

Figure 1.5: Schematic diagram of the IGF-1R structure.

Studies in female mice have shown that both supraoptic nucleus and paraventricular nucleus lose approximately one-third of IGF-1R immunoreactive cells with normal aging. Also, old calorically restricted (CR) mice lost higher numbers of IGF-1R non-immunoreactive cells while maintaining similar counts of IGF-1R immunoreactive cells in comparison to old-Al mice. Consequently, old-CR mice show a higher percentage of IGF-1R immunoreactive cells, reflecting increased hypothalamic sensitivity to IGF-1 in comparison to normally aging mice (Saeed et al 2007) (Yaghmaie et al 2006).

It is now clear that the pleiotropic neurotrophic factor IGF-I also modulates cognition and mood (Fernandez and Torres-Aleman 2012).

Cholinergic neurons in BF, which exert wide modulatory actions on mood and cognition (Lin et al 2015), are profusely connected to mPfC (Bloem et al 2014) neurons. The BF receives connections form the prefrontal cortex and sends projections to the entire cortex (Semba 2000). Cholinergic innervation of the cerebral cortex plays a fundamental role in attention, learning, memory and sensory information processing. Loss of this cholinergic projection in AD provokes severe disorders in learning, memory, and sensory processing, which are major causes of disability in the patients, showing all of them extensive neuronal loss (Bondareff et al 1982; Whitehouse et al 1982).

Multidirectional relationships between IGF-I and neurotransmitter systems such as Ach are hinted by many observations. IGF-I is also known to modulate cholinergic function (Knusel et al 1990). Other indirect evidence adds further support to the notion that IGF-I and Ach may work in concert. IGF-I facilitates sensory processing in the cortex and enhances EEG activity (Trueba et al 2013; Nishijima et al 2010), and BF cholinergic neurons induce cortical activation and facilitates sensory processing (Oldford and Castro-Alamancos 2003; Sarter et al 2009).

Indeed, profound cholinergic disturbances are a hallmark of AD (Whitehouse et al 1982), while recent data hint to also a disturbed IGF-I function (Carro and Torres-Aleman 2004; Talbot et al 2012) in AD pathology.

1.5 TDP-43. Cell culture experiments.

Recently, the role of TDP43 in AD has become intensively studied. The TARDBP gene provides instructions for making a protein called transactive response DNA binding protein 43 kDa (TDP-43). This protein is found within the cell nucleus in most tissues and is involved in many of the steps of protein production. It is cytogenetic located at 1p36.22, which is the short (p) arm of chromosome 1 at position 36.22 and its molecular location is: base pairs 11,012,622 to 11,030,528 on chromosome 1 (Homo sapiens Annotation Release 108, GRCh38.p7) (Figure 1.4).

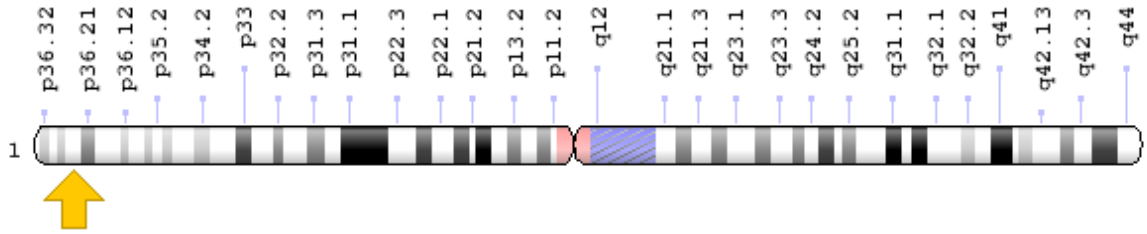

Figure 1.4: TDP-43 gene location.

The *TARDBP* gene is expressed during early development before birth when new tissues are forming. Many of the proteins whose production is influenced by the TDP-43 protein are involved in nervous system and organ development.

TDP43 was initially desribed as a transcriptional repressor that binds to chromosomally integrated TAR DNA. In particular, TDP-43 is a splicing factor binding to the intron2/exon3 region of the apoA-II gene (Kuo et al 2009). TDP-43 has been shown to bind both DNA and RNA and have multiple functions in transcriptional repression. Further roles has been included recently, such as regulator of splicing, pre-mRNA splicing, mRNA stability, microRNA processing, translational regulation, mRNA transport and translation (Ayala 2011; Buratti 2010; Kawahara and Mieda-Sato 2012).

Recent work has characterized the transcriptome-wide binding sites revealing that thousands of RNAs are bound by TDP-43 in neurons (Sephton et al 2011).

Dysregulation of many of these processes might precede the abberant aggregation and modification of TDP43 in affected cells. A hyper-phosphorylated, ubiquitinated and cleaved form of TDP-43—known as pathologic TDP43—is the major disease protein in ubiquitin-positive, tau-, and alpha-synuclein-negative frontotemporal dementia (Mackenzie et al 2011) and in Amyotrophic lateral sclerosis(ALS) (Neumann et al 2006). Elevated levels of the TDP-43 protein have also been identified in individuals diagnosed with chronic traumatic encephalopathy a condition that often mimics ALS and that has been associated with athletes who have experienced multiple concussions and other types of head injury (Schwarz et al 2011). Abnormalities of TDP-43 also occur in an important subset of AD patients, correlating with clinical and neuropathologic features indexes (Tremblay et al 2011). Moreover, TDP-43 pathology has been detected in 25-50% of all AD cases, especially those with severe clinical phenotype, and the presence of TDP-43 neuronal and glial inclusions is estimated to be approximately 25-30% (Uryu et al 2008).

Mutations in the *TARDBP* gene are associated with neurodegenerative disorders. TDP43 is the major component of neuronal inclusions in ALS and frontotemporal lobar degeneration (FTLD). Cytoplasmic TDP-43 pathology is the dominant histopathological feature of multisystem proteinopathy (Kim et al 2013). The N-terminal domain, which contributes importantly to the aggregation of the C-terminal region, has a novel structure with two negatively charged loops (Mompean et al 2016).

For all the mentioned above, including the lack of unanimity in the agreement of an unique BF classification between the different authors, the fact of historically / classically description assuming that the projections, to and from the BF, are diffuse and ipsilateral to the cortices, and the importance of the functions in which BF is implicated, also its cholinergic neurons, which are implicated in diverse neurodegenerative diseases, we decided to study the connection patterns between different nuclei of the BF and the A1, V1, S1 and mPfC circuits, both in

control animals (rats and mice) as in an Alzheimer's Disease model such as the APP/PS1 mouse. On the other hand, we were interested in studying the possible involvement of IGF1 and TDP-43 in the AD in terms of neuronal toxicity, since we hypothesized whether some of the AD symptoms could be a consequence of the neuronal loss occurring in BF nuclei or if they may be a gain of neuronal toxicity which leads to a loss of function in the circuits.

Hypotheses & Objectives

2. HYPOTHESIS AND OBJECTIVES

2.1 MAIN HYPOTHESIS

The BF has been classically characterized as a diffuse structure since no neuronal groups have been well defined, and numerous projecting and passing-by fibers run across it. Moreover, the BF is a heterogeneous structure and its neuronal components display a wide variety of biochemical phenotypes. Across the scientific literature, authors have described different constitutive structures of this region. Many functions had been attributed to the BF nuclei such as attention, cognition, learning and memory, sleep-wake cycle, motivational states and, language skills. However, there is not yet a consensus on how authors characterize and classify this heterogeneous region and their connections to other brain structures.

Despite many studies on the relationship between the location of different BF nuclei and their cortical projection, the question of how specific these projections are and how precisely different nuclei are in the BF map on their cortical targets are still unanswered.

Our hypothesis is: the specificity of anatomical pathways linking the BF nuclei with the cerebral cortex, as well as their functional roles may play an important role since it has been hypothesized that AD symptoms may be a consequence of either neuronal loss or impairment of BF neurons functionality due to toxicity.

2.2 GENERAL AND SPECIFIC AIMS

- **Aim 1: To anatomically trace the potential projecting pathways linking different BF nuclei and distinct cerebral cortices.**

  1.1 To delineate the potential specific neuronal groups in the BF involved in the control of specific sensory cortices. For this aim, fluorescent retrograde neuronal tracers were injected/deposited in the sensory cortices of rats, and in C57 control and transgenic mice in order to identify the BF neurons

projecting to these cortices. Optogenetic stimulation methods were used in the transgenic mice in order to validate the anatomical findings.

1.2 To determine the existence and characteristic features of the neural networks linking different sensory cortices with the BF nuclei. For this aim, fluorescent neuronal tracers and viral vectors were injected in the BF nuclei of rat and mice, in order to detect the projections from these cortices to the BF nuclei. Optogenetic stimulation methods were used in order to validate the anatomical results.

1.3 To investigate the involvement of motor and prefrontal cortices in these networks. For this aim, retrograde fluorescent neuronal tracers were injected in both motor and prefrontal cortices in rat and mice.

1.4 To compare the projection pathway of these BF-cortical networks in control and APP/PS1 mice. For this aim, two different fluorescent neuronal tracers were injected the BF nuclei and cortices of APP/PS1 mice.

- **Aim 2: To analyze the biochemical features of the BF neurons that give rise to these pathways. For this aim, different immunohistochemistry methods and optogenetic techniques were used in C57 control and transgenic mice.**

- **Aim 3: To identify the location of IGF-1 receptors in the BF nuclei of C57 control and of APP/PS1 Alzheimer mice model to investigate its possible implication in the pathogenesis of AD. For this aim immunohistochemistry methods were used.**

- **Aim 4: To study the effect of TDP-43 knockout in BV2 cells and primary microglia and its potential role in processes involved in Alzheimer's**

disease. This study may help to understand the differential role of TDP-43 in the cytoplasm and in the nucleus cytoplasm, as well as its potential impact on the acquired toxicity or loss of cell function that may be crucial in clarifying the pathogenesis of TDP-43 proteinopathy.

Materials & Methods

3. MATERIALS AND METHODS

Two broad different approaches depending of the goal have been used for this study. We performed *in vivo* experiments to achieve the Aims 1, 2 and 3, related to the characterization of the anatomical neuronal circuits and their physiological implications and biochemical features. Experiments to achieve Aim 4 were performed *in vitro*, as an approach for complete this aim which could not be carried out using the whole animal.

3.1 *IN VIVO* PROCEDURES

3.1.1 BIOLOGICAL MATERIAL USED FOR THE EXPERIMENTS

All animal procedures were performed in rodents and were approved by the Ethical Committee of the Autonomous University of Madrid in accordance with the European Community Council directive 2010/63/UE. Efforts were made to minimize animal suffering as well as to reduce the number of animals used.

Animals were kept in the veterinary office provided by the Autónoma University of Madrid at the Medical School (Manager in charged D. David Muñoz Valverde). Animals were placed in a 12 hours' light/darkness cycle room with controlled temperature and water and food provided *at libitum*. Animals inhabit in cages in accordance to the dimensions needed for each species. Transgenic mice were kept in a separate room and in cages were air is purified by HEPA filters. Before any surgeries or manipulation animals shared cages by living in community with other rats or other mice in each case. After surgical procedures, animals were placed in individual cages and placed in a special post-surgery room.

Most experiments were performed both in rats and mice in order to assess if there were any differences in the projection pathways between the two species. Transgenic mice models were essential to investigate specific biochemical characteristics of the BF neurons and for studying the neuronal pathways in disease stages.

Different species of rodents of both sexes have been used as follows:

a) Adult Sprague-Dawley rats weighting from 220-280g. This group of animals was used for characterizing the anatomical pathways linking the BF nuclei to different cortices as well as for optogenetic experiments (Aim 1 and 2).

b) Control mice C57 from 3 months to 2 years of age range and weighting from 25-40g. These animals were used for studying the anatomical pathways linking the BF nuclei and different cortices and for the study related to the identification and location of IGF1 receptor (Aims 1, 2 and 3).

c) B6.Cg-Tg (Chat-COP_4*H_{134}R/EYFP,$Slc_1 8a_3$)5^{Gfng}/J (B6.Cg Tg) transgenic mice labelled for cholinergic neurons. These animals were used for studying the anatomical pathways linking the BF nuclei to different cortices. They were also used for optogenetic experiments and for assessing the location and functionality of the cholinergic neuronal population (Aims 1 and 2).

d) Transgenic mice modeling the Alzheimer disease, APP/PS1. These animals were used for studying the anatomical pathways linking the BF nuclei and different cortices (Aim 1).

e) APP/PS1 transgenic mice with a double mutation (NIH, USA). These animals were used to study of the expression and location of IGF1 receptor (Aim 3).

3.1.2 NEURONAL TRACERS AND INJECTING MATERIAL

Fluorescent neuronal tracers were chosen based on their excitation and emission spectra so we could combine them and still being able to differentiate between them in a same sample under fluorescence and confocal microscope (Table 3.1). We also selected the tracers that could be combined with inmunohistichemical methods.

In a first step, we tested different concentration and volume injections of tracers to standardize the optimal procedures. Moreover, we tested different

surgical approaches by using both, glass pipette injection (pressure and electrical) and Hamilton syringes injections using syringes of different volumes sizes. Concerning the neuronal tracers, we also tested their consistency and reliability by changing their injection sites to assess that we obtain the same results no matter which tracer was employed. Once we had established the parameters and materials that worked best for our proposal, we define the working protocol. Rather than pipettes, Hamilton syringes (1 µl volume size, gauge 32) were chosen as the best instrument for injections.

The neuronal tracers selected were the following:

a. Fluoro-Gold (FlGo: injection; Fluorochromes, Llc. Denver, USA) is a neuroanatomical fluorescent tracer that retrograde labels the neuronal cell bodies. It is visualized in yellow color under fluorescence and confocal microscope (Table 3.1)

b. Fast Blue (FB: deposit; Polysciences, Inc. Warrington, PA) is employed as a retrograde neuronal tracer, labelling the somas of the neurons. It is visualized in blue color under fluorescence and confocal microscope (Table 3.1).

c. Cholera Toxin subunit B (TxCh) is a retrograde and anterograde tracer visualized after an immunocytochemical DAB reaction as a black color under light microscope.

d. Biotinylated Dextran Amine (BDA) is an anterograde neuronal tracer visualized after an immunocytochemistry 3,3´-Diaminobenzidine (DAB) reaction as a dark brown color under light microscope.

e. Adeno-associated viral vector AAV5-CaMKIIα::ChR2(H134R)-eYFP.WPRE.hGH (Addgene26969P, Penn Vector Core, University of North Carolina) (AAV5-ChR2), is employed as an anterograde neuronal tracer tagged with a yellow fluorescent protein (eYFP). This signal is converted to

a DAB immunocytochemistry-permanent reaction and observed as a dark brown color under light microscope.

f. Sindbis virus is employed as an anterograde neuronal tracer. We used two different variations, one was JK57M Sindbis mutant that expresses mCherry, so we can visualize the labelled-neurons in red color under a fluorescent microscope; the second Sindbis virus we used was JK100L2M, this is the regular Sindbis virus which expresses eGFP, so labelled-neurons can be visualized in green color under a fluorescent microscope (Table 3.1).

	Excitation max	**Emission max**
FlGo	350-385 nm	530-600 nm
FB	365 nm	420 nm
GFP	488 nm	510 nm
mCherry	587 nm	610 nm

Table 3.1: Spectra excitation/emission wavelength of the different neuronal tracers used.

3.1.3 STEREOTAXIC COORDINATES FOR BF AND CEREBRAL CORTEX

Coordinates were calculated according to the Paxinos and Watson Atlas (2007) to target the structures of interest for each case. All injection sites coordinates were measured from Bregma and the bone surface was taken as zero for the dorso-ventral coordinate. All injection stereotaxic coordinates are indicated in the following table.

Stereotaxic coordenates		Target structure	Stereotaxic coordenates	
Rat	AP: -2.3 mm L: 5.5 mm DV: 1 mm	S1	AP: -1.70 mm L: 3 mm DV: 1.5 mm	Mice
	AP: -5.8 mm L: 7.0 mm DV: 1 mm	A1	AP: -2.46 mm L: 4 mm DV: 2.2 mm	
	AP: -6.3 mm L: 3.5 mm DV: 0.5 mm	V1		
	AP: 0.0 mm L: 1.5 mm DV: 7.5 mm	VDB/HDB	AP: 0.74 mm L: 0.2 mm DV: 5 mm	
	AP: 0.24 mm L: 1.5 mm DV: 8.8 mm	HDB	AP: 0.14 mm L: 1.2 mm DV: 5.7 mm	
	AP: -1.32 mm L: 2.8 mm DV: 7.2 mm	B nucleus	AP: -0.58 mm L: 2 mm DV: 4.2 mm	
	AP: -3.24 mm L: 3 mm DV: 2 mm	mPfC		
	AP: 3.72 mm L: 3 mm DV: 2 mm	M		

Table 3.2: Stereotaxic coordinates and target structures in rat and mice.

AP: antero-posterior; L: lateral; DV: dorso-ventral.

3.1.4 SURGICAL PROCEDURES

All surgeries in rats and mice were performed using the same common procedures. All injection sites were planed previously to the surgical procedure.

Animals were anesthetized with an intraperitoneal injection of a mixture of ketamine (70mg/kg) and xylazine (5mg/kg) in NaCl saline solution. When all reflexes were abolished, animals were shaved from the head and then immediately placed in the stereotaxic frame (David Kopf Instruments, Tujunga, California) using ear bars or check bars to keep the head fixed in the appropriated position. The excess hair from the head after shaving was removed and the skin was cut to expose the skull. We also administrate to the animals the analgesic Metacam (meloxicam 1 mg/Kg sc) before they were placed in the stereotaxic frame. In some cases animals were maintained with inhalation anesthetic isofluorane (0.5%, maintenance doses). In the cases were isofluorane could not be used due to the procedure, and the animal displayed any reflex or movement, supplementary doses of ketamine (35 mg/Kg) and xylacine (2.5 mg/Kg) intraperitoneally were given. The protocol used is described as follows: A point of origin "the zero" is established in the stereotaxic frame for the all three stereotaxic coordinates (antero-posterior, lateral and dorso-ventral). A Hamilton Syringe (1μl volume size) is fixed to the stereotaxic tower and its tip is placed above Bregma in the skull of the animal that has been previously fixed to the stereotaxic frame. Bregma was determined by using the tip of a Hamilton syringe fixed to a holder in the stereotaxic tower, and was used as the "zero" from where all coordinates were calculated (Figure 3.1). Once the desire stereotaxic coordinates were calculated for each target area, a small hole was drilled using a drill of appropriate diameter depending on the species. The dura mater was pierced by using a syringe tip in order to allow an easy penetration of the Hamilton syringe tip. After this, the Hamilton syringe is loaded with the fluorescent neuronal tracer or substrate used for each experiment. To confirm the syringe is fully loaded and functional, we ejected a small amount of the content before entering the brain to reach the dorso-ventral coordinate previously established. When entering the brain, we allow for 10 minutes for the tissue to stabilize around the Hamilton syringe tip. After the injection of 20 to 80 nl, depending of the experiment, we allowed the tracer to diffuse for another 10 minutes. After this time, the Hamilton syringe was removed

and its functionality was again tested as described above. Afterwards, the incision was sutured and the animals were housed in the post-surgery room. Animals were treated with Dalsy oral administrated in drinking water (ibuprofen 20mg/cc; 15 mg/Kg diluted in drinking water) during 2-5 days post-surgery; additional doses of Metacam (1 mg/Kg sc) were also administered when necessary. It was important that the animal had a full and quick recovery period after the surgery for both, the animal wellbeing and for the appropriate transportation of the neuronal tracers.

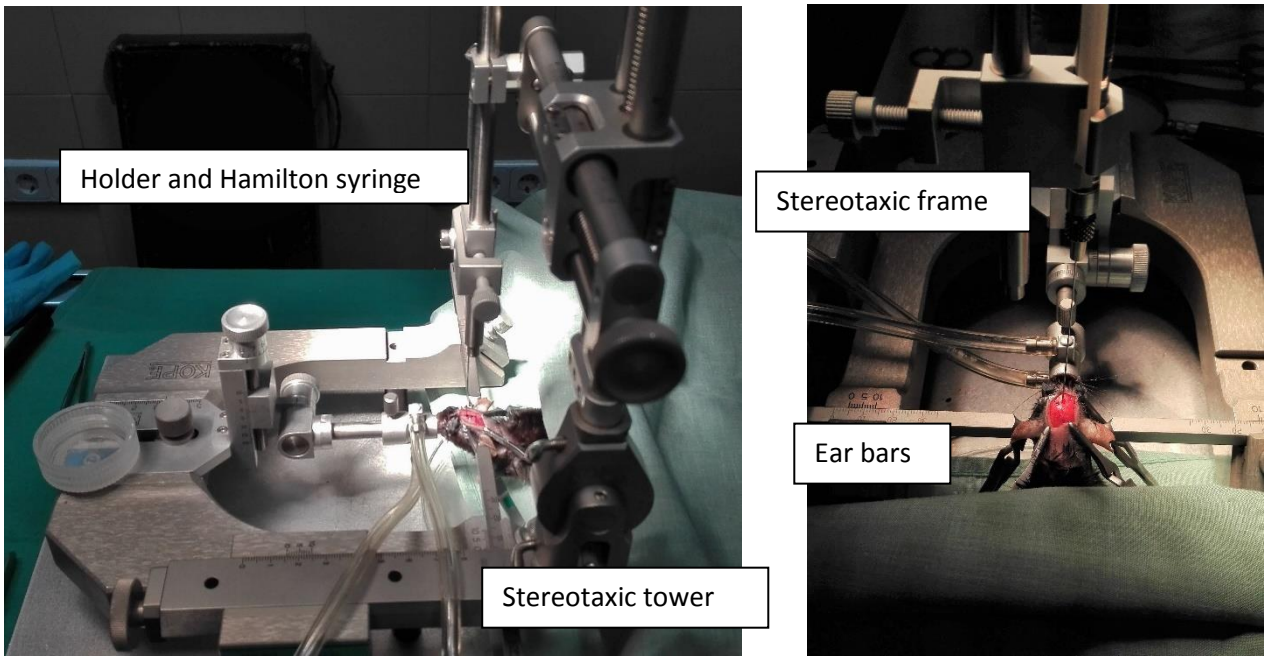

Figure 3.1: Photographs of the surgical device in lateral (A) and posterior (B) views.

3.1.5 EXPERIMENTAL INJECTIONS GROUPS IN RAT AND MICE

Animals were divided in four different experimental groups in order to achieve the Aims 1 and 2: Anatomical potential projecting pathways and biochemical features of BF neurons, listed in Section 2.

a. Animals (rat and mice) injected in S1/A1 cortices:

Rat: Anatomical experiments were performed in 11 adult Sprague-Dawley rats (RA-1 to RA11). The anatomical neuronal projections from the BF nuclei to these sensory cortices were studied by injecting (FlGo) or depositing (FB) the

neuroanatomical fluorescent retrograde tracers in the S1 and A1 cortices respectively.

After appropriate craniotomy, 40 nl of 4% saline solution of FlGo was injected in S1 cortex in the 11 rats using a 1µl Hamilton syringe using the stereotaxic coordinates indicated above. Deposits of 2 mm^2 of absorbable gelatin "Spongostan" embedded in 1% saline solution of FB were also placed for 20 minutes in A1 using the stereotaxic coordinates specified in Table 3.2.

Mice: Anatomical experiments were performed in 18 B6.Cg-Tg transgenic mice. For a better understanding of the biochemical characteristics of the cortical afferent connections from the BF, FlGo injections in the S1 cortex and FB deposits in the A1 cortex of the animals were made. After appropriate craniotomy, 100 nl of a 4% saline dilution of FlGo was injected in S1 with a 10 µl Hamilton syringe using the stereotaxic coordinates specified in Table 3.2. Deposits of 0.5-1 mm^2 pieces of absorbable gelatin "Spongostan" soaked in a 1% saline solution of FB were placed on the appropriate cortex in the animals, for 15 min.

b. Animals (rat and mice) injected in S1/V1 a1:

Rat: Anatomical experiments were performed in 11 adult Sprague-Dawley rats (RA-12 to RA21). The anatomical neuronal projections from the BF nuclei to these sensory cortices were studied by injecting the fluorescent retrograde tracers FlGo and FB in the S1 and V1 cortices, respectively. After appropriate craniotomy, 40 nl of 4% saline solution of FlGo was injected in the S1 cortex in 10 rats using a 1µl Hamilton syringe following the stereotaxic coordinates indicated above. Similarly, 40 nl of FB were injected in the A1 cortex following the stereotaxic coordinates listed in Table 3.2.

Mice: Anatomical experiments were performed in 15 B6.Cg-Tg transgenic mice. For a better understanding of the characteristics of the cortical afferent connections from BF, FlGo injections in the S1 cortex and FB deposits in the V1 cortex were made. After appropriate craniotomy, 100 nl of a 4% saline dilution of FlGo was injected in the S1 cortex with a 10 µl Hamilton syringe at the specific stereotaxic coordinates (Table 3.2). Deposits of 0.5-1 mm^2 pieces of absorbable gelatin "Spongostan" soaked in a 1% saline solution of FB were also placed on the V1 cortex for 15 min.

c. Animals (rat and mice) injected in basal forebrain structures:

For this set of experiments different anatomical tracing techniques were used.

Since we were interested in the BF nuclei projections to specific targets and the possible reconstruction of neuronal networks with novel tracing techniques, I spent some time to Dr. Laszlo Zaborszky´s Laboratory in the Centre for Molecular and Behavioral Neuroscience at Rutgers University (New Jersey, USA). Here, we worked together to implement a technique to inject in the BF of rats and mice two modified Sindbis vector viruses (Cold Spring Harbor Laboratories) used for neuronal tracing: 1) A variant modified virus labelled with mCherry, and 2) A variant modified virus labelled with GFP.

Once back in Spain, fluorescent retrograde tracers (FlGo and FB) and another similar viral vector: adeno-associated viral vector AAV5-ChR2, were injected in the BF nuclei of rat. We chose this particular vector to drive the expression of the light-activated cation channel, channelrhodopsin-2, tagged with a fluorescent protein (ChR2-eYFP) that is specific to Ca^{2+}/calmodulin-dependent protein kinase II α (CaMKIIα)-expressing neurons, ensuring that BF neurons anterogradely transport the virus to the cortex (Tye et al., 2011).
Injections of the retrograde fluorescents tracers and the Sindbis virus were used for anatomical studies while injections of the AAV5-ChR2 were used for functional studies employing optogenetic techniques.

Rat: Anatomical experiments were performed in 8 Sprague-Dawley rats. To ascertain the presence of reciprocal connections between the HDB and B nucleus and the different cortices, two different approaches were used: 1) for anatomical studies 11 animals received 30 nl of FlGo in HDB as well as 30 nl of FB in the B nucleus (Table 3.2); 2) for physiological studies 15 Sprague-Dawley rats were injected with the adeno-associated viral vector AAV5-ChR2 into the HDB (n= 8) or the B nucleus (n= 7) using a 0.5 ml Hamilton syringe. Animals were allowed to recover for at least 3 weeks before optogenetic experiments were performed in order to allow the virus be transduced and transported to its target areas.

Mice: 6 mice were injected with Sindbis virus (100 nl) using a glass pipettes attached to a picosplitzer device under a laminar flow chain in an isolated white surgical room. Also, 4 mice were injected with a 1µl Hamilton syringe 20nl of fluorescent retrograde tracers, FlGo and FB, in VDB/HDB and B.

d. Animals (rats) injected in the prefrontal cortex:

In order to assess the implication of mPfC in the BF projecting pathways, injections of 30 nl of FlGo were performed in mPfC (Table 3.3) in 9 Sprague-Dawley rats.

		Injection sites					
Neuronal tracers		S1	A1	V1	mPfC	VDB/HDB	B
	FlGo	11 S-D 18 C57			9 S-D	11 S-D	
	FB		11 S-D 18 C57	10 S-D 15 C57			11 S-D
	AAV					8 S-D	7 S-D
	Sindbis mCherry					4 S-D 4 mice	
	Sindbis GFP						4 S-D 4 mice

Table 3.3: Summary of the animals injected with the different neuronal tracers in the distinct structures. S-D: Sprague-Dawley rats; C57: control mice; APP: APP/PSI transgenic mice.

3.1.6 PHYSIOLOGICAL PROCEDURES. OPTOGENETIC STIMULATION

(Aims 1 and 2: anatomical potential projecting pathways and biochemical features of BF neurons):

Optogenetic experiments were performed to study the possible functional implications of the neuronal circuits.

Optogenetic technology takes advantage of genetically encoded light-sensitive proteins, such as microbial opsins, that are introduced in intact living mammalian neurons, allowing manipulation of neuronal activity in vivo and in vitro (Boyden et al 2005; Deisseroth, 2010). The technique is characterized by the ability to modulate neuronal firing on a millisecond timescale with great cell-type specificity in awake, freely moving animals (Gradinaru et al 2007). A widly used depolarizing opsin is Channelrhodopsin-2 (ChR2; and genetically modified variants), a cation channel that induces action potential firing upon illumination with pulses of blue light (Mattis et al 2012) (Riga et al 2014).

Rat: We used 15 Sprague-Dawley rats injected with the viral vector for physiological experiments.

- Sensory stimulation**:** Whisker deflections were performed by brief air puffs using a pneumatic pressure pump (Picospritzer) that delivers an air pulse through a 1 mm inner diameter polyethylene tube (1-2 kg/cm^2, 20 ms duration, resulting in whisker deflections of ≈15º). To avoid complex responses due to deflections of multiple whiskers, these were trimmed to 5 mm in length so that reproducible responses could be evoked. The experimental protocol consisted of pulses delivered to the principal whisker (whisker that gives the highest spike response) at 1 Hz. We applied 120 whisker stimuli (control period; 2 minutes). Similar pulses were applied after blue light stimulation of the BF during 4 minutes (240 stimuli).

- Optogenetic stimulation: rats were anesthetized with a mixture of ketamine (100 mg/kg) plus xylazine (3 mg/kg) and stereotaxically injected with the adeno-associated viral vector AAV5-ChR2 into the HDB or the B nucleus (coordinates indicated in table 3.1). We choose this particular vector to drive expression of the light-activated cation channel, channelrhodopsin-2, tagged with a fluorescent protein (ChR2-eYFP) that is specific to Ca^{2+}/calmodulin-dependent protein kinase II α (CaMKIIα)-expressing neurons, ensuring that BF neurons anterogradely transport the virus to the cortex (Tye et al., 2011). The coordinates were the same as above. Animals were allowed to recover for at least 3 weeks before electrophysiology experiments were performed. Optical stimulation of

ChR2-expressing neurons was achieved with light-emitting diodes (LED; 473 nm; Thomas Recording, Germany) delivered from an optical fiber (core diameter 120 μm) positioned directly above the HDB or B nucleus. The LED was triggered with a square-step voltage command. Stimulation was applied by a single long-lasting pulse (1 s). Illumination intensity was <30 mW/mm^2 at the BF, which is below the damage threshold of ~100 mW/mm^2 for blue light (Cardin et al., 2010).

To study the effect on cortical responses of optogenetic stimulation of BF neurons, young adult rats were anesthetized with urethane (1.5 g/kg, i/p). The depth of anesthesia was sufficient to eliminate pinch withdrawal, palpebral reflex and whisker movements and was assessed periodically during the experiment. Local anesthetic (Lidocaine 1%) was applied to all skin incisions and supplemental doses of urethane were given to maintain areflexia. Animals were placed in a Kopf stereotaxic device (David Kopf Instruments, Tujunga, CA) in which surgical procedures and recordings were performed. The body temperature was maintained at 37 °C. An incision was made exposing the skull and small holes were drilled in the bone over the barrel and prefrontal cortices (Table 3.2). Field potential recordings were made with tungsten macroelectrodes (<1 MΩ, World Precision Instruments, WPI, Sarasota, FL). Field potentials were filtered between 0.3 -100 Hz, amplified and sampled at 500 Hz. Signals were fed into a personal computer with the temporal references of the stimuli for off-line analysis with Spike 2 software (Cambridge Electronic Design, Cambridge, UK).

- Data analysis: The average of the cortical evoked potentials triggered by tactile stimuli were calculated every 1 minute (60 stimuli), using Spike 2 software. The area of the evoked potential was measured from the negative slope beginning with the first negative wave up to the same voltage level with a positive slope. The evoked potentials were recorded two minutes before blue light stimulation (control period) and four minutes after the light stimulation.

Statistical analysis was performed using Graph Pad Prism 7 software (San Diego, CA, USA). Results are reported as means ± SEMs. Data were normally distributed, according to the Shapiro–Wilk normality test and analyzed using a Student's paired t-test. Statistical significance was set at a 95% confidence level (two-tailed).

Mice: We used C57 mice injected with AAV5 virus and transgenic mice expressing the light-activated cation channel, channelrhodopsin-2, tagged with a fluorescent protein (ChR2-YFP) under the control of the choline-acetyl transferase promoter (ChAT). B6.Cg-Tg (Chat-COP$_4$*H$_{134}$R/EYFP,Slc$_1$8a$_3$)5^{Gfng}/J mice; The Jackson Laboratory) were used for optogenetic stimulation of the BF. Young adult mice (3-6 months old) were anesthetized with urethane (1.5 g/kg, i/p). The depth of anesthesia was sufficient to eliminate pinch withdrawal, palpebral reflex and whisker movements and was assessed periodically during the experiment. A local anesthetic (Lidocaine 1%) was applied to all skin incisions and supplemental doses of urethane were given to maintain areflexia. Animals were placed in a Kopf stereotaxic device (David Kopf Instruments, Tujunga, CA) in which surgical procedures and recordings were performed. The body temperature was maintained at 37 °C. An incision was made exposing the skull and small holes were drilled in the bone over the barrel and auditory cortices (AP 1-3 mm, L 5-7 mm, DV 0.2-1 mm, and AP -2.5 mm, L 4 mm, DV 2.5 mm from Bregma, respectively) as well as on the BF, HDB (AP 0.14 mm, L 2 mm, DV 4 mm) and B nucleus (AP -0.7, L 2, DV 4). Single-unit recordings were performed with tungsten microelectrodes (2-5 MΩ, World Precision Instruments, WPI, Sarasota, FL) and the cortical field potential was recorded through tungsten macroelectrodes (<1 MΩ). Unit recordings in the BF were also performed by an optrode (see below). Unit firing was filtered (0.3-3 kHz), amplified via an AC preamplifier (P15, Grass Instruments) and sampled at 10 KHz while field potentials were filtered between 0.3 -100 Hz, amplified and sampled at 500 Hz. Signals were fed into a personal computer with the temporal references of the stimuli for off-line analysis with Spike 2 software (Cambridge Electronic Design, Cambridge, UK).

- Sensory stimulation: Whisker deflections were performed by brief air puffs using a pneumatic pressure pump (Picospritzer) that delivers an air pulse through a 1 mm inner diameter polyethylene tube (1-2 kg/cm^2, 20 ms duration, resulting in whisker deflections of ≈15º). To avoid complex responses due to deflections of multiple whiskers, these were trimmed to 5 mm in length, so that reproducible responses were evoked. The experimental protocol consisted of 30

pulses delivered to the principal whisker (whisker that gives the highest spike response) at 0.5 Hz (control period). Whisker stimulation was also applied after blue light stimulation of the BF during 30 minutes. Auditory click stimulation was performed by application of a brief (1 ms duration) square voltage pulse to Sony earphones. The stimuli were presented at a rate of 0.5 Hz at the level 50 dB. Following the baseline recording, stimulation was also applied after blue light stimulation of the BF during 30 minutes.

- Optogenetic stimulation: Optical stimulation of ChR2-expressing neurons was achieved with light-emitting diodes (LED; 473 nm; Thomas Recording, Germany) delivered from an optical fiber (core diameter 120 µm) or through an optrode (microelectrode 1-2 M + optical fiber) positioned directly above BF area. The LED was triggered with a square-step voltage command. Illumination intensity was <30 mW/mm^2 at the BF, which is below the damage threshold of ~100 mW/mm^2 for blue light (Cardin et al., 2010). Stimulation was applied by 20 ms pulse trains of 473 nm light at 5 Hz or by a single long-lasting pulse (200 ms). The stimulation area was very restricted since total transmitted light power was reduced by 50%, after passing through 100 µm of neuronal tissue, and by 90% at 1 mm (Aravanis et al., 2007).

- Data analysis: The somatosensory or auditory evoked potentials were calculated every 1 minute (30 stimuli). The amplitude of the evoked potential was measured from the baseline to the first negative peak. The mean tactile response was measured from the peristimulus time histogram (PSTH) as the number of spikes evoked in the 0-50 ms time window after the stimulus onset divided by the number of stimuli. Also, the power spectrum and wavelet transform were calculated from cortical field potentials. Statistical analyses were performed using GraphPad Prism 5 software (San Diego, CA, USA) and consisted of paired comparisons between the same cells before and after BF optogenetic stimulation. If the data were considered normally distributed, according to the Shapiro–Wilk normality test, we used parametric statistics. For two groups, we used the t test (paired). For multiple comparisons we used one-way ANOVA analysis of variance followed by Bonferroni post-hoc test. Data are presented as mean ± standard error

of the mean (SEM). The threshold level of significance was set at $P < 0.05$ (*) and $P < 0.01$ (**) are indicated in results.

3.1.7 ANIMALS PERFUSION

After a survival period of one week animals were anesthetized with an overdose of ketamine and xylacine and perfused transcardially. Animals devoted to optogenetic procedure were perfused at the end of the experiment. The perfusion system consisted of a peristaltic bomb (Masterflex L/S) with an adjustable speed flux, which distributes the perfusion liquids throw the arterial system of the animal. The animal was placed lying on its back and a longitudinal incision was made from the pre-sternum to the abdominal region; once the skin and muscles were opened, the ribs were cut at both sides of the sternum so we had full access to the heart. Once the heart was exposed, an incision was made in the left ventricle and the cannula fixed to the perfusion system, was immediately inserted into the left ventricle so the perfusion liquids start circulating through the arterial system of the animal. In the case of rat perfusion, the cannula stayed placed in the aorta clamp with a gastrointestinal tweezers. In the case of mice this was not needed. Then, we made an incision in the right auricle, so the lasting blood and perfusion liquids could exit by the return-broad-stream. The composition, volumes and order of the perfusion liquids were as follows:

1º) 0.9% saline was perfused at low speed to clear out the blood of the circulatory system. 1 cc of heparin is added to the saline to help in the washing step. Saline is perfused until the liquid exiting the right auricle looked clear, meaning the circulatory systems must be clean at that point. The approximate volume used was 0.5 L for rat perfusion and 300 ml for mice.

2º) A 4% paraformaldehyde fixative solution in phosphate buffer 0.1 M, pH 7.4 (500 ml for rats and 200 ml for mice), was perfused over 50 minutes for rats and 30 minutes for mice.

3º) Finally, increasing concentrations of sucrose in 0.1 M phosphate buffer were perfused. (0.5 liters in rats and 300 ml in mice 5% sucrose solution; 250 ml for rats and 150 ml for mice of 10% sucrose solution; 250 ml for rats and 100 ml for mice of 20% sucrose solution).

Once the perfusion finished, the skull was opened and the brain was extracted. Brains were immersed in 4% PFA for 24 hours (post-fixation process) and stored in 30% sucrose for at least three days for tissue cryopreservation. The sucrose role in the cryopreservation process was to create an extracellular hyperosmotic medium that avoids the intracellular-microglass formation that may cause a potential damage to the cells when the tissue was frozen.

3.1.8 TISSUE PROCESSING

The brain tissue was fixed to the microtome plate using Tissue Teck, a special solution which acts as a glue. Brains were sectioned in a frozen microtome (Leica cryostat) at -15º C on the coronal plane at 40 μm.

Sections were collected in three consecutive ordered series devoted to Nissl staining, fluorescent visualization and storage series. Series processed for Nissl staining were used for delimiting structures; fluorochrome series were devoted to the neuronal tracers labelled results and were studied both under a Nikon Axioskop fluorescent microscope and under a confocal microscope (Leica TSC SP5) using a Tile Scan tool of LAS AF software. Once sectioned, slices were mounted and process for histology. They were dehydrated in ethanol for 15 seconds', followed by a six-increasing concentration of xylol solutions for a total of 30 minutes. Then the sections were covered using DePeX as mounting medium and they were allowed to dry at room temperature. Once the mounting media was dry, the slides were kept in the fridge to protect the fluorochromes integrity. The third series of sections were kept for further analysis and immunohistochemically techniques described in the next subsection 3.1.9. These sections were kept in the freezer in an anti-freezing solution at -20º C.

3.1.9 INMUNOHISTOCHEMICAL AND STAINNING TECHNIQUES

a) Nissl staining:

- Leave sections overnight in 70º ethanol for tissue dehydration and adipose tissue removal.
- 2 x rinsing in distillate water
- Cresil violet stainning (5g cresil violet in 500 cc distillate wáter + 0,25 cc glacial acetic acid), 2 to 6 minutes in 45º C in a shaking bath
- 2 short wash in distillate wáter to wash the excess of dye
- 1 minute dehydratation in 70% etanol
- 1 minute in 96% etanol to remove the lipids and the unspecific dye
- 10 minutes in 100% clorophorm, shaking
- Quick step in 96% etanol
- Differentiation in acetic-ethanol (960 cc od 96% etanol + 17 cc of glacial acetic acid)
- 1 minute dehydratation in 100% etanol
- Dehydratation and rinsing in a 6 x 10 minutes' steps in increasing concentration solutions of xylol
- Mounting and covering with DePeX of the slides
- Let dry at room temperature

b) ChAT inmunohistochemistry:

- Wash in 0.1 M Phosphate Buffer (PB) 4 x 10 minutes
- Wash in saline phosphate buffer (PBS) 3 x 5 minutes
- Prepare incubation medium:
    - 8000 µl 0.5% Triton in PBS solution
    - 2000 µl normal horse serum
    - 0.5 g bobine serum albumina (BSA)
- Preincubation of the tissue in the medium: 2 hours, shaking
- Primary antibody incubation, 36-48 hours, shaking, room temperature
    - Goat anti ChAt (1:150). Chemicon AB 144-P
- Wash in PBS 0.1 M, 4 x 5 minutes, room temperatura
- Secondary antibody incubation, 2 hours, shaking, on ice
    - Alexa Fluor 546 Donkey Anti-goat IgG (H+L) (1:200). Life technologies
- Wash in PBS 2 x 5 minutes
- Mounting slides and cover

c) Glucose oxidase inmunohistochemistry:

- Rinsing in PB 0.1 M 2 x 5 minutes
- Endogenous peroxidase inactivation, 20 minutes
    - PB 0.1 M + H_2O_2 2%
- Rinse in PB 0.1 M, 5 x 3 minutes
- ABC kit (1 drop reagent A + 1 drop reagent B in each 5 ml of PB) in PB 0.1 M + Triton X-100 1%, 2 hours of incubation
- Rinse in PB 0.1 M, 2 x 5 minutes
- Rinse in Acetate buffer (TAS) 0.1 M pH 6, 3 x 3 minutes
    - For 200 ml of TAS 0.2 M preparation:
        - 5.88 g 3-hydrato sodic acetate
        - 2.5 ml H_2O bi-distillate
- Reaction development
    - Solution A
        - 50 ml TAS 0.2 M pH 6
        - 1.23 g nickel sulphate (Nickel (II) Sulphate 6-Hydrato®. PAnreac 131445.1209
        - 0.2 g D-Glucose®. Panreac 131341. 1 kg
        - 0.02 g amonium cloride®. Sigma A-4514. 100 g
        - Add 0.003 g Glucose oxidase (Sigma G-2133, 10.000 units)
    - Solution B
        - 50 ml H_2O bi-destillaste
        - 0.03 d Diaminobenzidine (DAB). Sigma D5637 5 g

  Mix the solutions A and B and add the glucose oxidase in shaking conditions
  just before developing the reaction.
  Allow the reaction to develop by visual control until desire dye of the tissue.
- Rinse in TAS 0.1 M, 2 x 5 minutes
- Rinse in PB 0.1 M, 2 x 5 minutes
- Mount the slices and cover the slides

d) FlGo immunohistochemistry

- Wash in 0.1 M Phosphate Buffer (PB) 4 x 10 minutes
- Wash in saline phosphate buffer (PBS) 3 x 5 minutesGoat
- Prepare incubation medium:
    - 8000 µl 0.5% Triton in PBS solution
    - 2000 µl normal horse serum
    - 0.5 g bovine albumin serum (BSA)
- Preincubation of the tissue in the medium: 2 hours, shaking
- Primary antibody incubation, 36-48 hours, shaking, room temperatura
    - Rabbit Anti Fluorescent-Gold antibody (1:150). Millipore
- Wash in PBS 0.1 M, 4 x 5 minutes, room temperature
- Secondary antibody incubation, 2 hours, shaking, on ice
    - Alexa Fluor 488 Donkey Anti.Rabbit IgG (1:200). Life technologies
- Wash in PBS 2 x 5 minutes
- Mounting slides and cover

e) Cholera toxine inmunnohistochemistry:

- Wash in 0.1 M Phosphate Buffer (PB) 4 x 10 minutes
- Wash in saline phosphate buffer (PBS) 3 x 5 minutes
- Prepare incubation medium:
  - 8000 □l 0.5% Triton in PBS solution
  - 2000 □l normal horse serum
  - 0.5 g bobine serum albumina
- Preincubation of the tissue in the medium: 2 hours, shaking
- Primary antibody incubation, 36-48 hours, shaking, room temperature
  - Goat anti-Cholera toxine antibody (1:200). List Biological Laboratories, INC.
- Wash in PBS 0.1 M, 4 x 5 minutes, room temperatura
- Secondary antibody incubation, 2 hours, shaking, on ice
  - Alexa Fluor 546 Donkey Anti-goat IgG (H+L) (1:100). Life technologies
- Wash in PB 2 x 5 minutes
- Mounting slides and cover

f) GFP immunohistochemistry:

- Wash in PB 0.1 M, 2 x 5 minutes
- Peroxidase endogenous innactivation (2% H_2O_2), 10 minutes
- Wash in PB 0.1 M, 3 x 10 minutes
- Preincubation, 2 hours, room temperatura
  - Normal goat serum (NGS) 10%
  - Bovine serum albumina (BSA) 1%
  - Triton X-100 "%
- Primary antibody incubation, overnight, room temperature
  - Normal goat serum 3%
  - BSA 1%
  - Triton X-100 1%
  - Rabbit anti GFP (1:500). Chemicon International
- Wash in PB 0.1 M, 5 x 10 minutes
- Secondary antibody incubation, 2 hours, room temperatura
  - NGS 3%
  - BSA 1%
  - Triton X-100 1%
  - Goat anti Rabbit IgG biotinylated (1:100). Chemicon International
- Wash in PB 0.1 M, 3 x 10 minutes
- Incubation ABC Elite 1:100 in PB 0.1 M + Triton X-100 1%, 1 hour
- Wash in TAS, 3 x 5 minutes
- DAB reaction: DAB 0,02% + H_2O_2 0.0001% in PB 0.1 M, pH 7.4
  Reaction time will vary from one immuno to another, visual control.
- Wash in TAS 0.1 M, 2 x 5 minutes
- Wash in PB 0.1 M, 2 x 5 minutes
- Mounting slices, counterstain with tionine and dehydratation

g) IGF1 Immunohistoichemistry

- Wash in PB 0.1 M, 3 x 5 minutes, shaking, room temperature
- Preincubation / blocking step in PBTBSA, at least 15 minutes, shaking, at room temperature
    - PB 0.1 M
    - Triton X-100 1%
    - BSA 1%
- Wash in PBTBSA, 3 x 5 minutes
- Rabbit anti IGF1 incubation, 1 hour, room temperature or overnight at 4º C, shaking (500 µl /well)
- Wash in PBTBSA, 3 x 5 minutes
- Alexa Fluor 546 Donkey Anti-goat IgG (H+L) (1:100). Life technologies incubation (1:1000) in PBTBSA, 1 hour, room temperature, shaking or overnight at 4º C.
- Wash in PB 0.1 M, 3 x 5 minutes
- DAPI staining
- Wash in PB 0.1 M, 2 x 5 minutes
- Mount in Gerbatol

Antibody	Host species	Reactivity	Dilution	Suplier
Anti-ChaT	Donkey	Goat	1:150	Chemicon
Alexa Fluor 546	Donkey	Goat	1:200	Life technologues
Alexa Fluor 488	Donkey	Rabbit	1:200	Life technologies
anti GFP	Rabbit	GFP	1:500	Chemicon
Biotinylated anti Goat	Rabbit	Goat	1:100	Chemicon
Anti Fluorescent-Gold	Rabbit	FlGo	1:150	Millipore
Anti IGF1	Rabbit	IGF1	1:200	Lifescience
Anti-cholera toxin B subunit	Goat	Cholera toxin B subunit	1:200	List Biological
Elite ABC kit	-------	-------	1 drop of each reagent/ 5 ml	Vector Laboratories

Table 3.4: Antibodies and reagents used for immunohistochemistry.

3.1.10 CONFOCAL STUDY

The study of the fluorochrome series was performed under the confocal microscope (Leica TCSSP5), using the LASAF software TileScan tool. Samples were analyzed using bio-mapping (maximal projections) under both lin405 mm UV and linAr488 mm using a 10x objective, for the quantification of neurons in each channel. Images are a stack of sections in maximal projection, but neurons were counted in each individual layer. Maximal projections of the images were analyzed in the two channels (UV and green) and the merged image was studied too. The procedure used was as follows: 1. For the neuronal counting each channel was selected in each section of the ROI (Region of Interest). We eliminated the nonspecific background, and convert the images to 8 bits; we then smoothed them out with the filter to apply the previous segmentation particle analyzer. In some cases it has been necessary to use the ROI from the BG subtraction plugin tool and the Watershed tool to separate and count particles correctly. In cases where the particle analyzer results were entirely satisfactory they were manually reviewed in the Cell Counter plugin. 2. To calculate the proportion of double labeled neurons, a manual multipoint tool was used on the merged image and separate channels were used as well to corroborate the results. In doubtful cases, a possible co-localization of channels was assessed in a merged image combining images of the resulting ROIs in the previous section, in both color channels.

3.2 IN VITRO EXPERIMENTS

In this Section we explain the materials and methods for achieving our Aim 4, which was to study the effect of TDP-43 knockout in BV2 cells and primary microglia and its potential role in processes involved in Alzheimer's disease.

3.2.1 BIOLOGICAL MATERIAL

- TDP43 oligomers
- Cellular cultures of BV2 cells
- Cellular cultures of microglia
- Transgenic model of Tardbp loxP/loxP mice

3.2.2 PROCEDURES

3.2.2.1 Experiment 1 (in vitro): BV2 cells

For this experiment BV2 cells were used. BV2 cell is the immortalised murine microglial cells line that has been frequently used as a substitute for primary microglia (PM):

- Step 1: Coating and seeding

We coated two 96 well plates with PDL 0.5ng/ml – one with coverslides and one without) per each student. In each well 2500 cells (32 wells for plate without coverslides and 24 with coverslides) were seeded in DMEM (Dulbecco's Modified Eagle's *medium)* with low glucose, 10% FCS (fetal calf serum) and without antibiotics and left in incubator on 37ºC. After 24 hours siRNA transfection was performed. siRNA protocol is shown below:

siRNA transfection mix per well:

- 50nM (1.75ul Optimem + 5.75ul siRNA)
- Lipofectamine2000 (0.27ul Lipofect + 7.23ul Optimem) and wait 5 minutes
- Mix and keep in the room temperature for 20 minutes
- Add 15ul of siRNA transfection mix to each well and incubate on 37ºC
- Change the medium the next day (about 14-16 hours, not toxic) to remove Lipofectamine with DMEM low glucose, 10% FCS, 1%PS (fosfatidyl serine)
- For siRNA transfection different oligomers were used – TDP pool, oligo1, oligo2, oligo3, oligo4 (divied into two plates) and GC as a control in both plates. In coverplates only TDP pool was used.

After 8 hours the medium was changed, either with full serum fresh medium (FED) or serum free (STARVED) in the plate and the coverslides. During the same day, HeLA SweAPP cells for Aβ production were seeded for uptake assay. Both BV2 plate/cover slides and HeLa SweAPP cells were left in the incubator on 37 ˚C for 12-15 hours. The medium was replaced with the medium from HeLa SweAPP, which was already taken out and incubated for 4 hours before transfer the medium from BV2 plate. This medium was then collected for further analysis, and Alamar Blue Assay was done to access viability of the cells. BV2 plate was incubated on 37 ˚C for last 15 hours. Consequently, medium from BV2 plate was collected into the empty plate and preceded for clearance assessment by MSD (Meso Scale Discovery).

- Step 2: Bicinchoninic acid (BCA) assay and Western Blot (WB)

BCA is a kit for measuring the protein amount. It is necessary to avoid mistakes by loading different amount of protein. Colorimetric detection and quantitation of total protein was analyzed. This method combines the well-known reduction of Cu^{+2} to Cu^{+1} by protein in an alkaline medium (the biuret reaction) with the highly sensitive and selective colorimetric detection of the Cu^{+1} using a unique reagent containing bicinchoninic acid. The purple-colored reaction product of this assay is formed by the chelation of two molecules of BCA with one cuprous ion. (Figure 3.1).

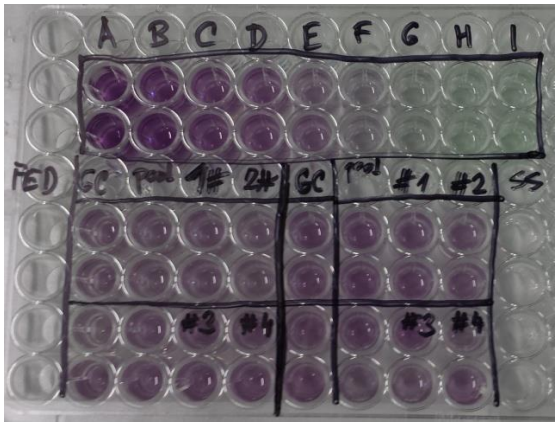

Figure 3.2: BCA analysis Chemiluminiscence Fuji LAS 4000.

Western Blot protocol

- Sample preparation – loading amount based on BCA results
- Electrophoresis – 200 V for 40 minutes
- Transfer – 10 minutes
- Labelling – 1° Ab 1:5000 Rb AntiTDP43 (rabbit) over night on 4 °C
- 3 times wash with PBS-T
    - 2° 1:10000 RbαTDP43 for 1 hour on room temperature
- 2 times wash with PBS-T and 1 time with PBS

Internal loading controls:

- β-actin 1:5000 (~37kDa)
- GAPDH 1:5000 (~45kDa)
- We incubated either GADPH or β-actin with 1° Ab -AntiTDP43 (Rabbit) 1:100 (5ml 5% milk, 5ul TDP43 Ab, 1ul of β-actin/GAPDH) for 1 hour, room temperature.
- 3 times wash with PBS-T
- with 2° Ab –αRb 1:100 (5ml 5% milk, 5ul TDP43 Ab, 1ul of β-actin/GAPDH) for 1 hour, room temperature.

- Step 3: MSD analysis

MSD is a unique technology that offers an ultra-low detection of biomarkers in single or multiple formats. The quantification of biomarkers is performed by electrochemical stimulation. We focused on detection of Aβ, APP using 96 well 4-spot array to measure the clearence of these markers from the BV2 medium.

- Step 4: Alamar Blue Assay

Alamar Blue Assay is designed to measure quantitatively the proliferation of various human and animal cell lines, bacteria and fungi. Alamar Blue Assay incorporates an oxidation-reduction indicator that fluoresces based on metabolic activity and at the same time changes color in response to chemical reduction of growth medium resulting from cell growth.

Alamar Blue procedure:

- Pipette 0.4 ml of Alamar Blue into a test tube.
- Dilute to 10 mls with phosphate buffer.
- Mix well.
- Pipette 100 µl into each well.

- Step 5: Confocal Microscopy

BV2 coverslides were used for phagocytic assay on BV2 cells. Fluorescently labelled Aβ in two time intervals (1 hour and 15 minutes) and lysotracker 561(75 minutes) were applied for the phagocytic assay. Samples were analysed by 2-photon confocal microscopy.

3.2.2.2 Experiment 2 (*ex vivo*): Primary microglia

- Step 1: Fagocitic assay

Primary microglia preparation from pups P5 (litter 5) was obtained from Tardbp loxP/loxP mice, flanking exon 3. (Figure 3.3)

Primary Microglia Primary Cultures protocol:

- Remove the brain, remove the meninges, dissect the cortex
- Place in HBSS 4ºC
- Cut the cortical tissues with scissors in small pieces
- Place in 15ml tubes, containing 3 ml of TripleX, incubate 37ºC for 20 min
- Resuspend with 5 ml pippete up-down 10 times
- Dissociate mechanically the tissues re-suspending with 1 ml pippete slowly 10 times
- Spin down the cells suspension at 400g for 4 min
- Remove the supernatant and re-suspend in 10 ml of DMEM 4.5g glucose (without sodium pyruvate), 10% FCS, 1% PS
- Count cells and plate $1x10^6$ in T75 flask

Primary Microglia Purification Protocol:

- Changed to a fresh medium after 2-4 days.
- Change the medium twice a week, exchanging about 50% of the medium.
- After 2-3 weeks, microglia can be harvested by shaking (shake vigorously the flask for at least 5-10 min and check at the microscope.

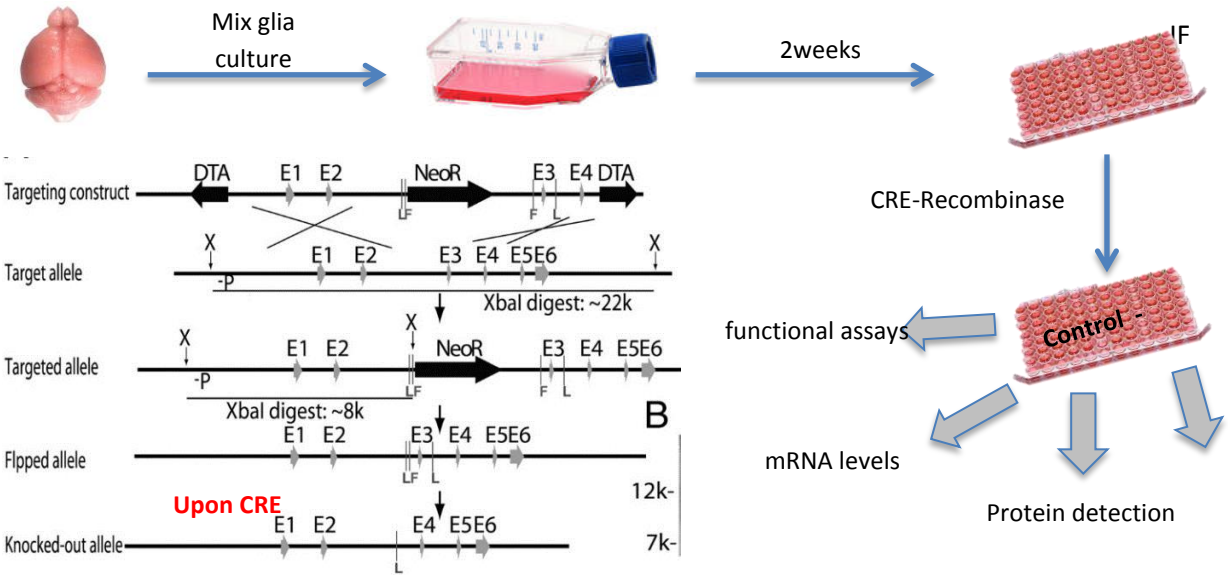

Figure 3.3: Primary microglia culture and transgenic model of Tardbp loxP/loxP mice.

Once the primary microglia was purified, we seeded the microglia cells in a 96 well plate, and after 3 days we started the fagocitic assay.

We had two different situations: control and TAT-CRE (knockout). In each situation we had four conditions: different TDP43 agregates concentration (100nM and 500nM) and uptake time line (2 hours and 30 minutes).

Preparation of dilutions:

- Stock: 20uM; For 20.000 nM.
- For TDP43 100nM dilution 1:200 (1ml: 5ul of oligo + 995ul of serum free médium).
- For TDP43 500nM 1:40 (1ml: 25ul of oligos + 975 serum free medium)

Our phagocitic assay on primary microglia (3 days post-treatment) was as folows: we coated two 96 well plates with astrocite medium where we have previosly placed one coverslides per well. In line 1 (GC) and 3 (TDP43 knockout) we added a medium containing TDP43 agregates in a 100nM concentration, while in lines 2 and 4 we added on top of the cells medium containing TDP43 agregates in 500nM concentration and we incubated them at 37ºC for different time points. We also had some wells with just medium inside (labelled X and Y in the plate photograph). Medium from line 1 and 2 was removed in two hours and medium in lines 3 and 4 was removed in 30 minutes. After this, the cells were fixed with PFA 4% during 20 minutes, followed by washes with PBS. After fixation we added DAPI tostain the cells nuclei. Then we mounted the coverslides in a slide for confocal microscope adquisition. We also collected the medium from the wells without cells (just medium) for further analysis (Figure 3.4).

Control	TAT-CRE	Treatment	Time
O O	O O	100 nM	2 hrs
O O	O O	500 nM	
O O	O O	100 nM	30 min
O O	O O	500 nM	
O O	O O	For IF use	
O O	O O		

Figure 3.4: Fagocitic assay of TDP43 agregates in microglia cells.

We monitored the plates under optic microscope after 1.5 hours and 24 hours and 3 days of treatment. We kept the cells to assess the possible uptake of the aggregates of TDP43 using immunofluorescent staining and we also collected the medium (Kept in -20ºC) for fractionation and Western Blot assays.

With these primary microglia cells in the cover-slides we performed immunofluorescence assay to detect the TDP43 aggregates uptake by the primary microglia cells.

Afterwards, we studied the mounted slides containing primary microglia under confocal microscope (Figure 3.6).

Protocol for Immunofluorescence:

- Fix in 4% PFA /10-15 min at room temperature
- Wash in PBS
- Block/permeabilize (10% Donkey Serum, 500ul + 0.1% TX100 /30 min at room temperature)
- 1º Antibody in blocking / 90 min at room temperature

12 wells: Ms α His 1:100
Rb α Iba1 1:500

- Wash in PBS
- 2º Antibody Alexa 1:1000; DAPI 1:10k / 45 min at room temperature
- Wash well in PBS
- Mount on slides in DAKO fluorescent mounting medium
- Leave over night at 4ºC for the mounting medium to polymerize

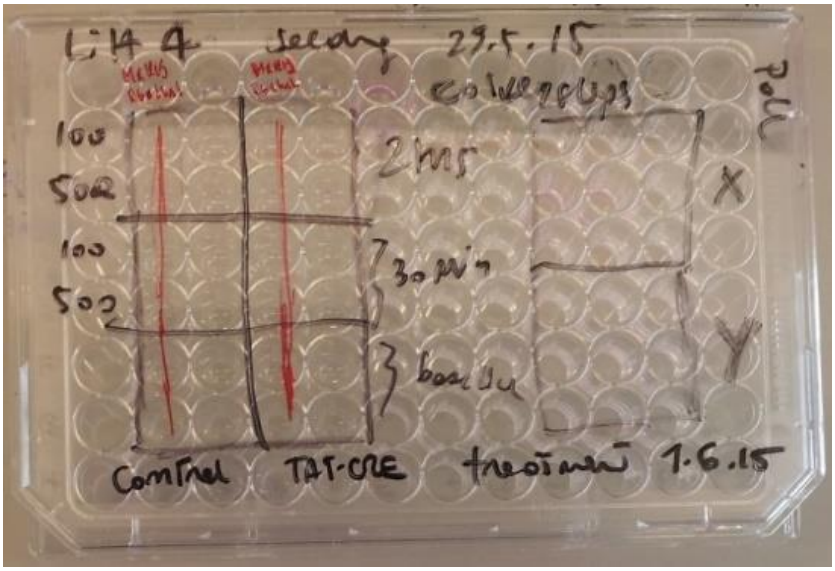

Figure 3.5: Fagocitic Primary Microglia assay plate.

Figure 3.6: Slide of primary microglia fagocitic assay**.**

APPENDIX:

Phosphate buffer 0.1 M protocol:

- 31.7 g phosphate di-hidrogen sodium 1-hidratated
- 113 g di-sodium phosphate anhidro
- Mix the previous substrates in 5 liters of distillated water
- Adjust pH to 7.4 (with acetic acid or sodium hydroxide)
- Add 0.2 M phosphate buffer and distillate water in the same proportion to obtain 0.1 M buffer.

Fixative solution protocol:

- Heat 0.5 liters of distillate water at 60º C
- Filter 500 ml of 0.2 phosphate buffer
- Add the 500 ml of phosphate buffer to the distillate water previously filtered
- Add 40 g of paraformaldehyde (PFA) to the previous solutions. To help the mixing add few drops of NaOH
- Keep the solution in the fridge

Anti-freezing solution for storage:

- 100 cc phosphate buffer (33.65 g monobasic sodic phosphate + 7.7 g sodic dihidroxide, in 1 liter of distillate water)
- 300 cc glycerin
- 300 cc etilen-glycol
- 300 cc distillate water

Results

4. RESULTS

The results are organized in five Sections (4.1-4.5) in order to answer our Aims. The results corresponding with Aims 1 and 2 concerning the anatomical neuronal circuits linking the BF and the different cortices and the biochemical features of the neurons of these pathways are explained in sections 4.1, 4.2, 4.3 and 4.4. The results concerning the location of the IGF1 receptors in control and APP/PS1 mice answering the Aim 3 are explained in the section 4.5. The Aim 4 results concerning the possible role of TDP43 in AD are listed in section 4.6.

4.1 BASAL FOREBRAIN-SENSORY CORTICES CONNECTION PATHWAYS

Our first Aim, 1.1, was to delineate the potential specific neuronal groups in the BF involved in the control of specific sensory cortices. To achieve this Aim 1.1, retrograde tracers were injected or deposit in the sensory cortices of mice (S1 and A1 cortices) and rat (S1, A1 and V1 cortices). Also, our Aim 2, to analyze the biochemical features of the BF neurons that give rise to these pathways is presented in this Section.

MICE: experiments were performed in C57 wild type mice to study the connections linking the different BF nuclei and the distinct sensory cortices (S1, A1).

The anatomical study of the BF efferent connections to the S1 and A1 cortices was performed on 18 cases. The locations of the FlGo injection site in the cortices as well as the FB deposit were confirmed using the sections devoted for fluorescence (Figure 4.1) and Nissl studies. Both injections and deposits were confined to the desired site without signals of diffusion in any case.

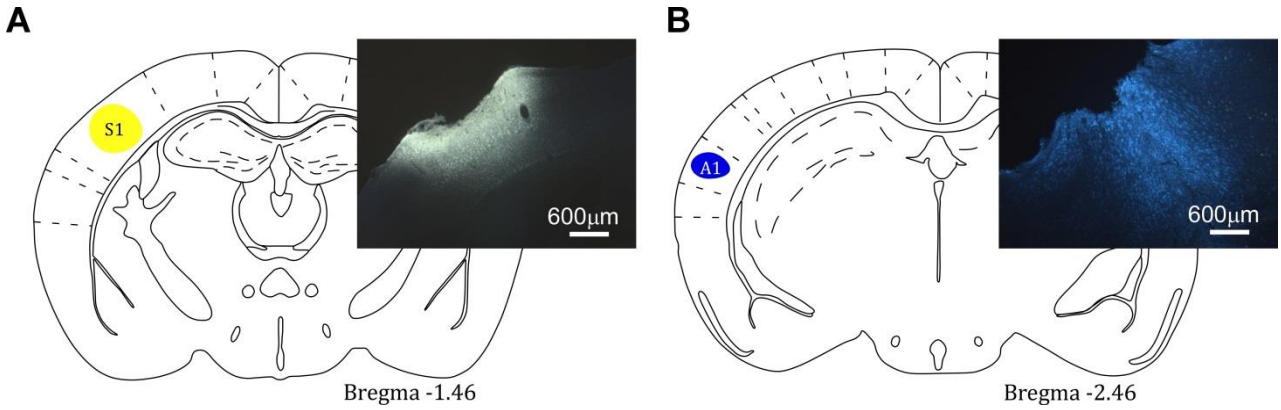

Figure 4.1: Location of the injection and deposit of fluorescent retrograde tracers.
Microphotographs of coronal brain sections and schematic drawings showing the injection sites of the retrograde tracers in a representative animal. A: FlGo injection in S1 cortex; B: FB, deposit in the A1 cortex;. Calibration toolbar 600 µm.

In all 18 cases, the study of the fluorescence series allowed us to detect numerous fluorescent retrograde single- or double-labeled neurons in the HDB, VDB (Figure 4.2) or in the SI and B nuclei (Figure 4.3).

Neurons in the SI and B nuclei were considered together because the two nuclei were difficult to delineate at caudal levels. Two different tracers (FlGo and FB) were injected/deposited in the two different sensory cortices (S1/A1 respectively) of the same hemisphere (n=10 mice). This experimental approach allowed us to establish whether the pathway of the BF cortical projecting neurons reaches A1, S1 or both cortices and if so in which proportion. The microscopy study of VDB/HDB nuclei revealed numerous intermingled neurons in these nuclei labeled by FlGo, FB or both tracers (Figure 4.2).

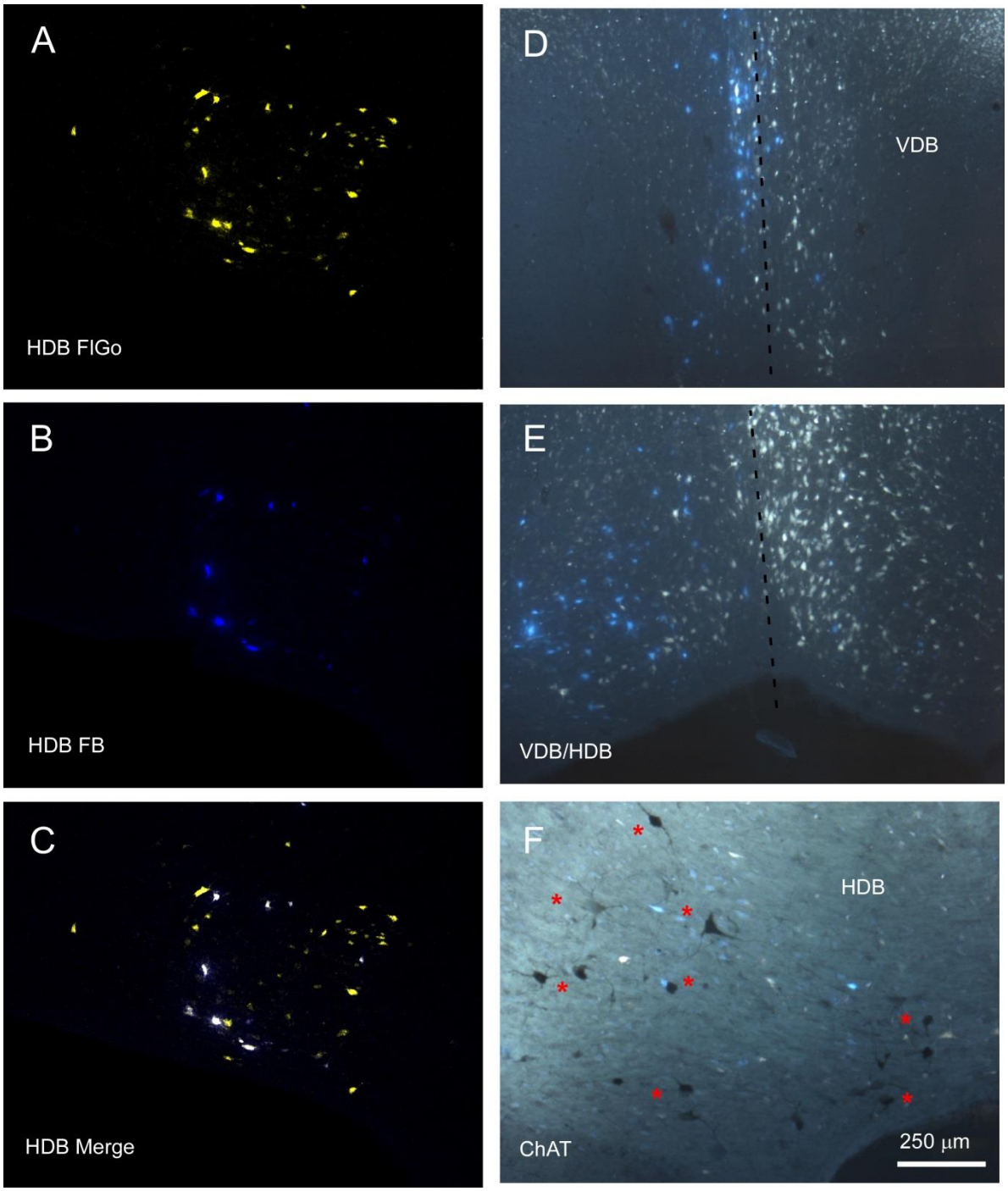

Figure 4.2: Distribution of labeled neurons in VDB/HDB

A-C: confocal microscope image of retrograde labeled neurons in VDB/ HDB; D, E: fluorescence microscope image of both FlGo and FB labeled neurons in the VDB and HDB. Dash line indicates the medial hemispheric line; F: Image combining fluorescent microscopy with ChAT immunocitochemistry techniques in HDB. Asterisk point to cholinergic neurons. Calibration toolbar 250 μm.

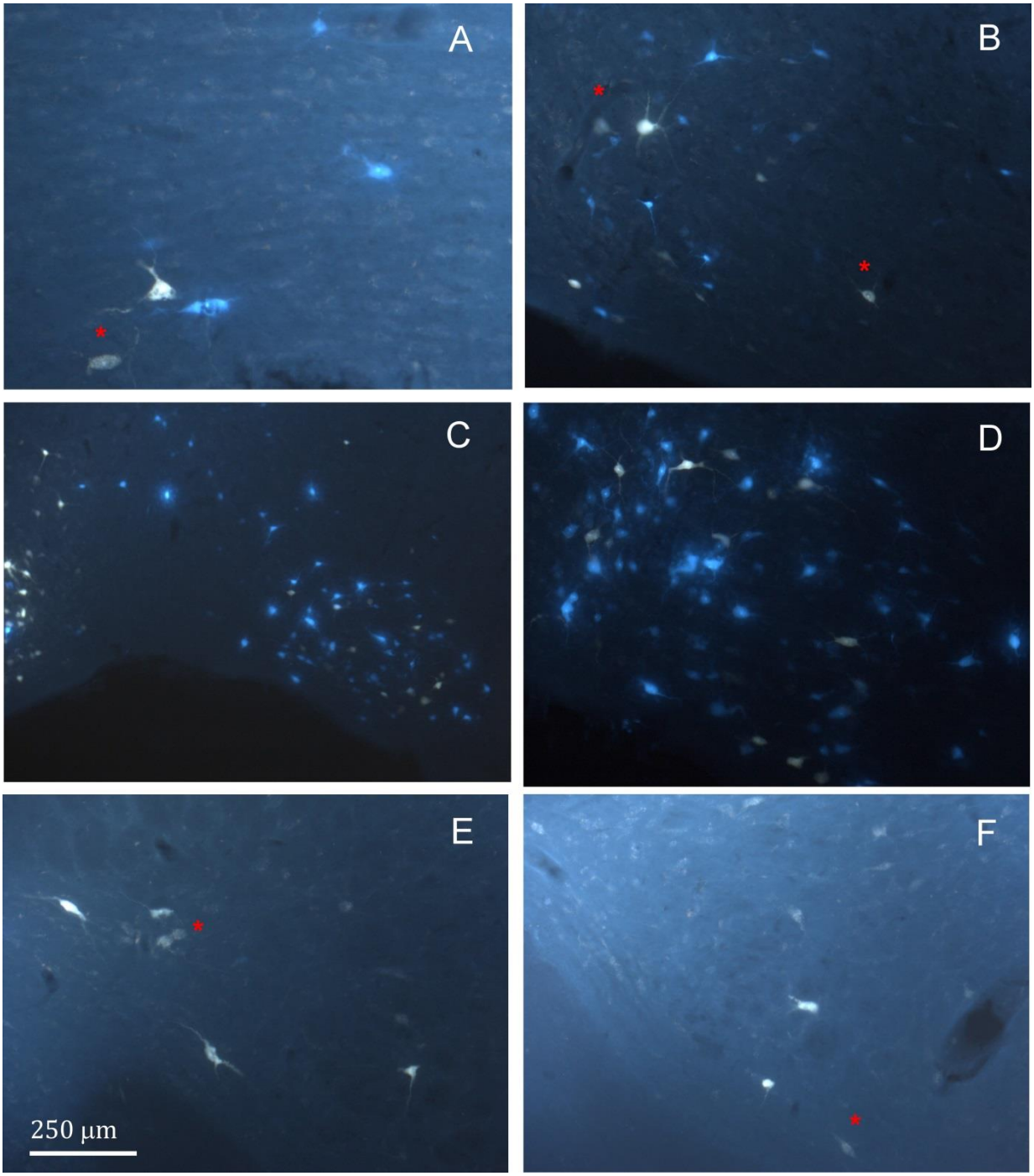

Figure 4.3: Distribution of labeled neurons in VDB/HDB.
A-F: Samples of fluorescent microscope images of single and double labeled neurons in HDB. G, H: Samples of fluorescent microscope images of single and double labeled neurons in SI/B nucleus. Red asterisks point double labeled neurons. Calibration toolbars: C, D, F-H: 230 µm, E: 530 µm.

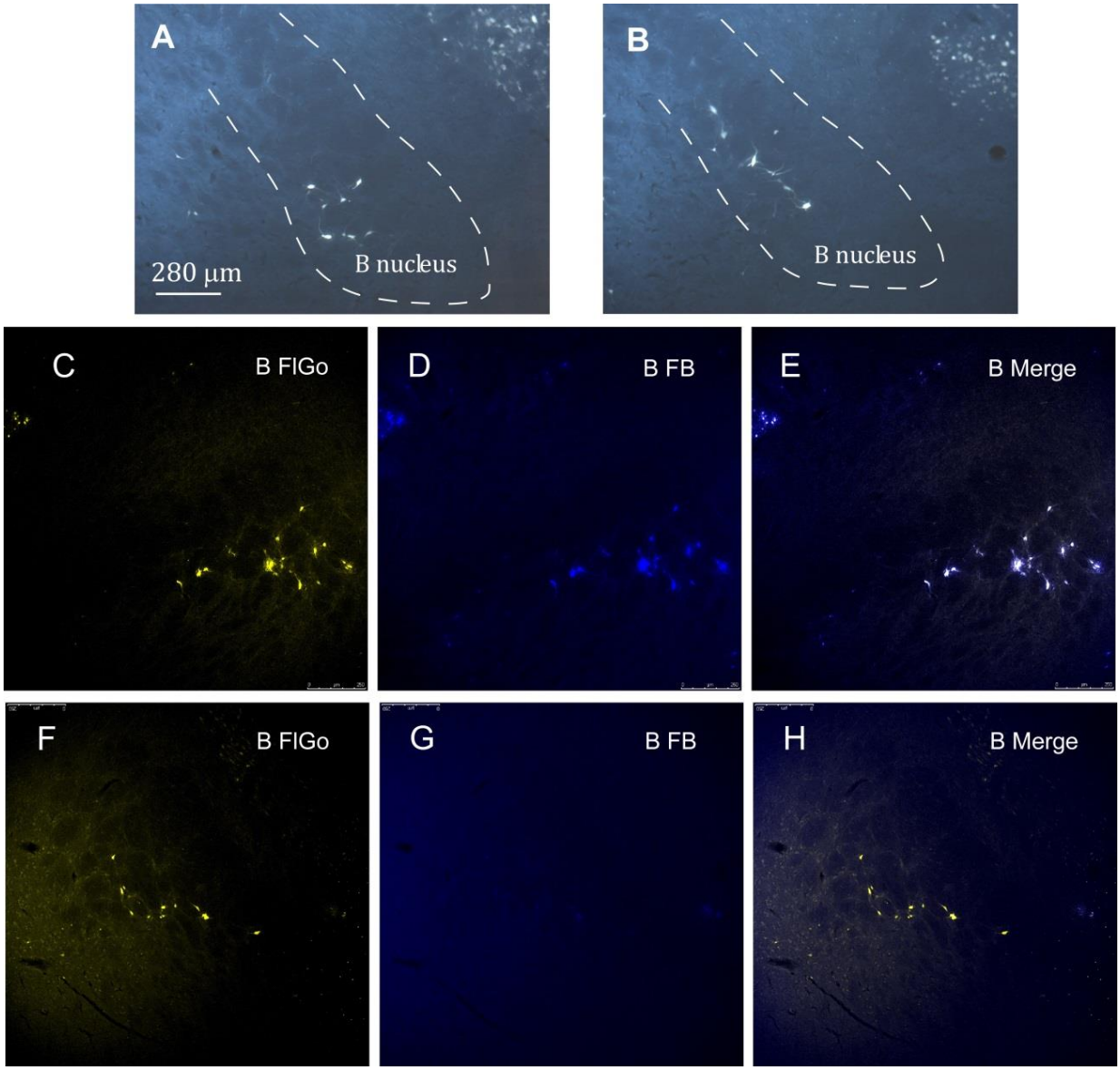

Figure 4.4: Distribution of labeled neurons in B nucleus.
A, B: Microphotographs of coronal sections showing retrogradely labeled neurons located in B nucleus of animals MCA-6 (top) and animal MCA-15 (bottom). Dash lines delimitate the B nucleus (B). C-G Confocal microscope detail of FlGo and FB labeled neurons in B nucleus. Calibration toolbar 280 µm.

The study of the distribution and percentages of these neurons showed that 34 ± 7.4 % of the neurons located in the VDB/HDB were labeled by both fluorescent tracers (neurons projecting to both the S1 and A1 cortices), while most of the VDB/HDB neurons (44.2 ± 7.4%) were single-labeled by FlGo injected into S1 cortex; only 21.8% of neurons were labeled by FB injected into A1 cortex. Conversely, the percentage of double-labeled neurons in B nucleus was lower than in VDB/HDB (22%)(Figures 4.2, 4.3 and 4.5), while the percentage of B neurons

single-labeled by either one or another tracer was roughly the same (40.6% from S1 and 37.4% from A1; Figures 4.4, C-H and 4.5). In addition, the immunochemical study revealed that fluorescent labeled neurons appeared to be scattered among the characteristic cholinergic neurons of the different BF nuclei and some of them were also positive for ChAT immunocytochemistry (Figure 4.2 F and 4.6). These percentage results have been normalized with the total number of labelled neurons in each region of interest (Figure 4.5).

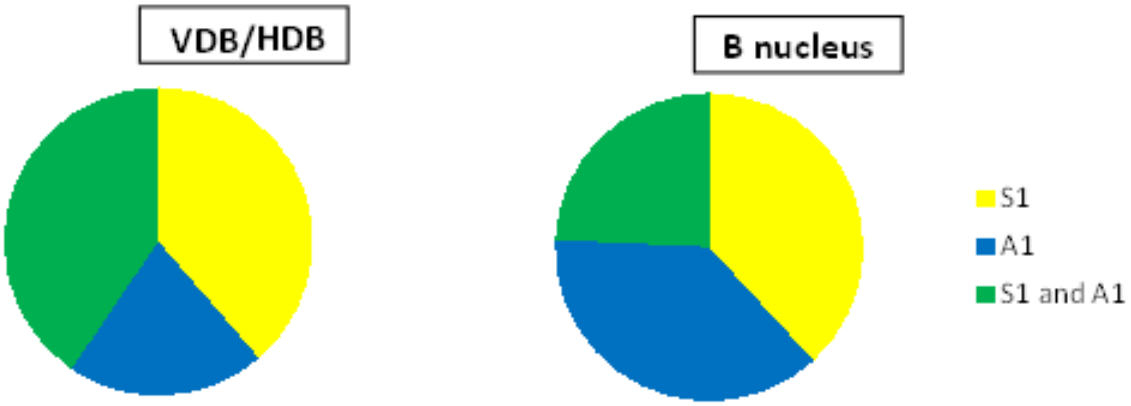

Figure 4.5: Graphic representation of number of labeled neurons in VDB/HDB and B nucleus after injection/deposit in S1, A1 or both cortices.

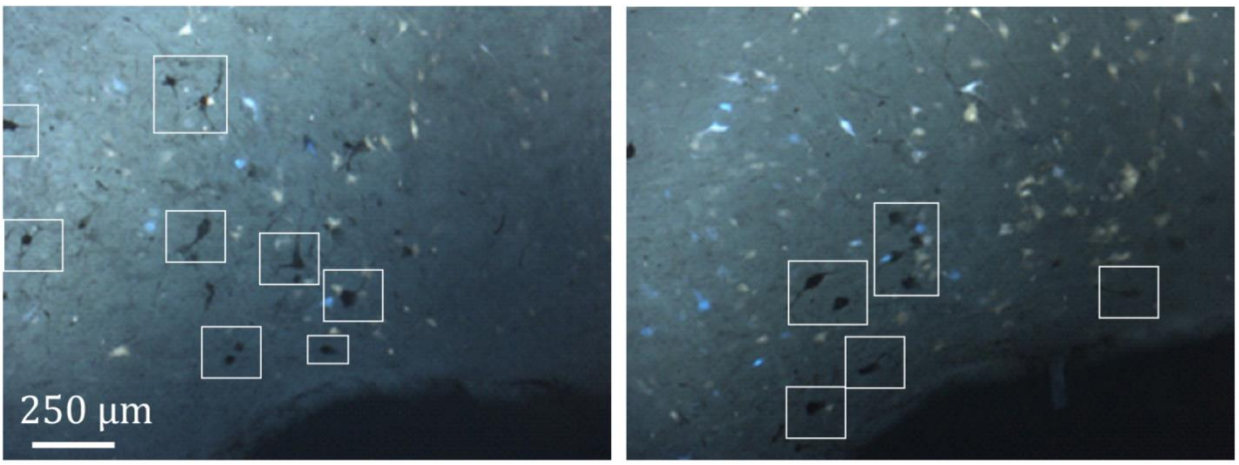

Figure 4.6: Microphotograps of ChAT inmmunostainning.
White squares indicates ChAT-possitive neurons in HDB. Toolbar 250 µm.

Our Aim 1.2 was to determine the existence and characteristic features of the neural networks linking different sensory cortices with the BF nuclei. Since we observed these preferential projecting pathways depending on the BF nuclei of study, we then wonder if these connections of the BF nuclei with the different sensory cortices were unidirectional or reciprocal. To achieve this purpose, we injected two retrograde tracers (FlGo and FB) at two different rostro-caudal levels of the BF, VDB/HDB and in B nucleus. We observed labelled neurons in the sensory cortices S1 and A1 confirming the reciprocity of these cortices with the BF.

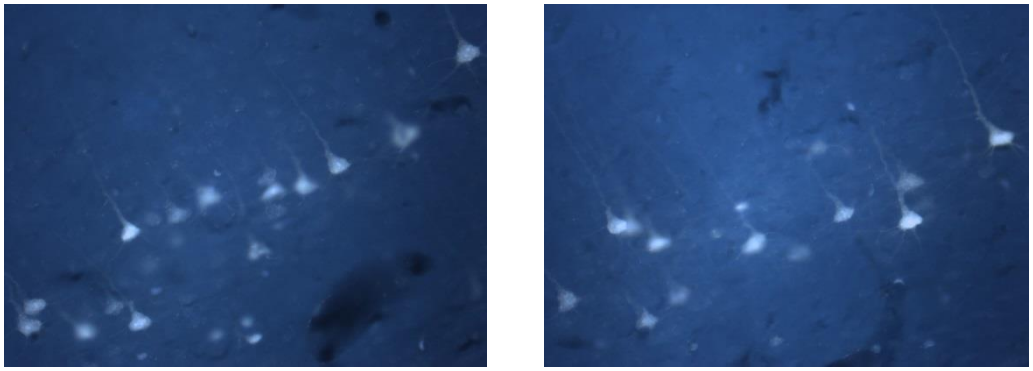

Figure 4.7: Labelled neurons in sensory cortex.
Left: labelled neurons in S1 cortex; Right: labelled neurons in A1 cortex. Both injections of the tracer were in B nucleus.

To elucidate if these anatomical results have a physiological correlation we asses these projecting pathways linking sensory cortices with the different BF nuclei by using a transgenic mice model B6.Cg-Tg (Chat-COP_4*H_{134}R/EYFP,$Slc_1 8a_3$)5^{Gfng}/J which has its chanelrhodopsin channels conjugated with a GFP protein so when stimulating optogenetically we are just exciting the cholinergic neurons.

Since the above results indicate that neurons in HDB mainly projected to the S1 whereas B neurons similarly projected to the S1 and A1 cortices. We used optogenetic methods for selective stimulation of cholinergic neurons in specific BF areas. To verify that blue LED stimuli induced spike firing of cholinergic neurons, we used an optrode to perform unit recordings in the BF simultaneously with optical stimulation in the same place. Short-lasting blue LED stimuli applied to the BF (HDB or B nucleus) induced spike firing in the BF neurons of ChAT-ChR2-YFP mice with a mean latency of 6.2 ± 1.1 ms (Figure 4.9). All light-responsive cells (n =

12 cells) had slow spontaneous firing rates (0.5 ± 0.3 spikes/s). Also, a train of stimuli (20 ms pulse duration; 5 Hz) or a single pulse lasting 200 ms induced spike firing of BF neurons and a desynchronization of the cortical field potential (Figure 4.9). During control conditions, the cortical field potential produced spontaneous slow oscillations reflecting a synchronized state induced by the anesthetic, which was reduced by blue light stimulation. Wavelet analysis showed that light stimulation induced an increase of fast cortical activity (>4Hz; Figure 4.8). The desynchronization in response to light stimulation lasted for only a few seconds, and could be evoked repeatedly.

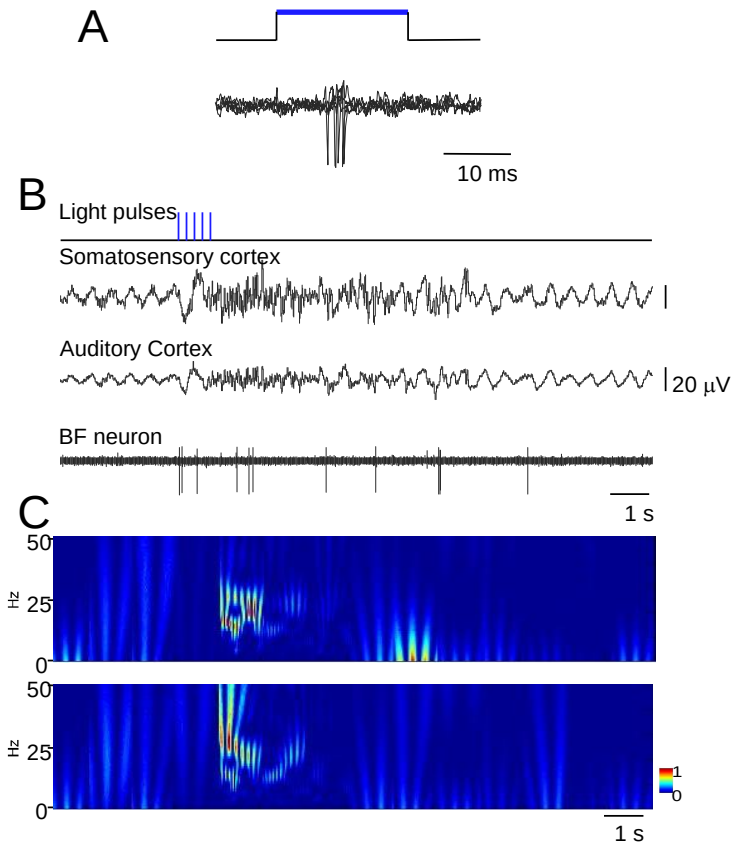

Figure 4.8: Blue light stimulation of BF neurons induces spike firing in the BF and desynchronization of the somatosensory and auditory field potentials.
A: a short-lasting blue LED stimuli induced spike firing in a representative B neuron (three superimposed traces are shown). B: a train of stimuli (20 ms pulse duration, 5 Hz) evoked spike firing increase in a HDB neuron and desynchronization of cortical field potentials simultaneously. The effect lasted less than 10 s. C: wavelet analysis of the same trace that in B showed a fast activity increase of cortical field potentials after the blue light stimulation.

To quantify desynchronization, we compared the power spectra of the cortical field potential before (30 s; control) and after the onset of blue light stimulation (a single pulse of 200 ms duration; 30 s). Figure 6 shows the percentage change with respect to the control values (100%) in the delta frequency band (0.5-4 Hz), in the theta frequency band (4- 10 Hz) and in a faster frequency band (10-30 Hz) that mainly correspond to beta frequencies. Data were calculated from 6 recordings in the S1 cortex and from 6 recordings in the A1 cortex). Blue light stimulation to the HDB reduced delta activity in the S1 and A1 cortices and increased theta frequencies and faster activities in the S1 and A1 cortices (Figure 4.9). The same result occurred when the blue light was applied to the B area (Figure 4.10). Although the differences were not statistically significant, HDB stimulation increased more theta frequencies in the S1 and A1 cortices than B stimulation. By contrast, B stimulation increased more beta frequencies in both cortices than HDB stimulation (Figures 4.10 and 4.11).

Blue light stimulation at the BF also increased the evoked potential amplitude elicited by whisker stimulation (somatosensory evoked potential) or by the application of clicks (auditory evoked potential). HDB optogenetic stimulation induced a long-lasting increase in either the somatosensory or auditory evoked potentials (Figure 4.9). The effect lasted at least 30 min and was larger for the somatosensory evoked potentials than the auditory evoked potentials (Figure 4.9). The mean amplitude increased rapidly from 6.6 ± 1.3 ?V in the control conditions to 11.4 ± 2.0 ?V, 5 min after optogenetic stimulation (ANOVA analysis, P = 0.002; n = 12) and remained 10.5 ± 1.9 ?V, 30 min after stimulation (ANOVA analysis, P = 0.0016; n = 12; Figure 7C). Auditory evoked potentials were less affected by the blue light when it was directed at the HDB. The mean amplitude changed from 3.9 ± 0.6 ?V in the control to 4.8 ± 1.1 ?V 5 min after optogenetic stimulation (ANOVA analysis, P = 0.101; n = 12). The increase reached statistical significance 10 min after blue light stimulation (6.0 ± 1.6 ?V; ANOVA analysis, P = 0.0109; n = 12) and remained facilitated 30 min after stimulation (5.2 ± 0.8 ?V; ANOVA analysis, P = 0.0207; n = 12; Figure 4.9).

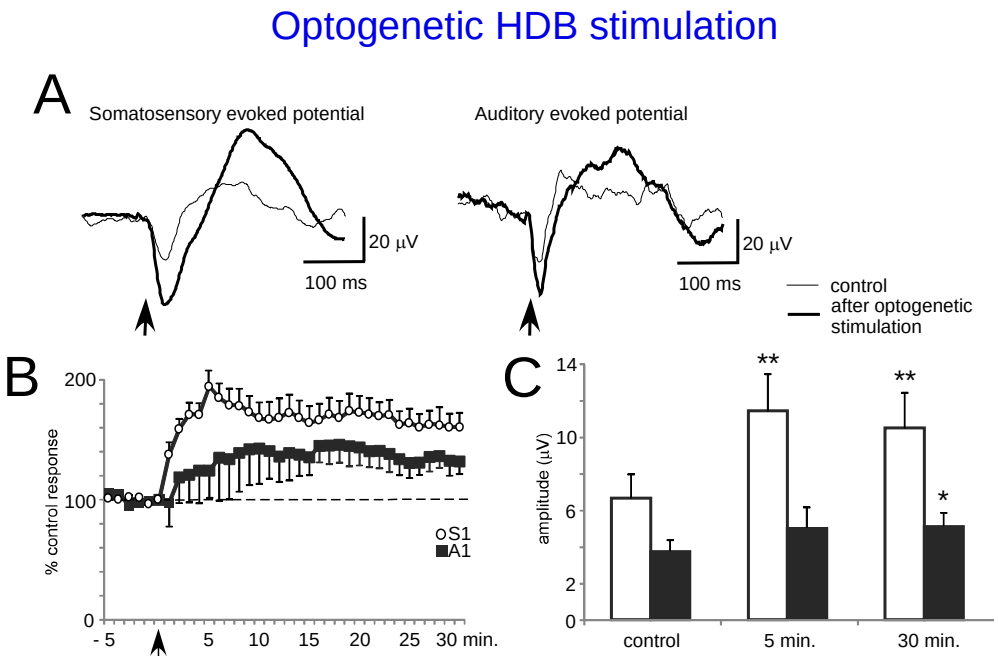

Figure 4.9: Blue light stimulation of HDB nucleus induces an increase of somatosensory and auditory evoked potentials.
A, raw data shows an important increase of the S1 evoked potentials (S1EP) and a modest increase of the A1 evoked potentials (A1EP) (control and 5 min. after blue light stimulation). B, the plot shows the time course in 12 cases. Note the larger increase in S1EP than in A1EP. C, plot of the mean amplitude measured in control and 5 or 30 min. after blue light stimulation at HDB nucleus. The amplitude increase was larger for S1 than A1 evoked potentials.

In contrast to the HDB stimulation, B optogenetic stimulation induced a lower increase of somatosensory evoked potentials at 5 min after the application of blue light in comparison with HDB stimulation (Figure 4.10). The mean amplitude of the somatosensory evoked potential increased from 5.5 ± 0.5 ?V in the control conditions to 8.6 ± 0.9 ?V, 5 min after optogenetic stimulation (ANOVA analysis, P = 0.0217; n= 12) and 7.9 ± 1.0 ?V, at 30 min after stimulation (ANOVA analysis, P = 0.072; n= 12; Figure 8C). Auditory evoked potentials were also less affected by the blue light in comparison with the effect on the somatosensory evoked potentials. The mean amplitude changed from 3.7 ± 1.0 ?V in the control to 4.4 ± 1.2 ?V, 5 min after blue light stimulation (ANOVA analysis, P = 0.1338; n= 12), reaching statistical significance 10 min after blue light stimulation (5.2 ± 1.4 ?V; ANOVA analysis, P = 0.0109; n = 12). However, the stimulation effect vanished 30 min after optogenetic stimulation (4.2 ± 1.2 ?V; ANOVA analysis, P = 0.072; n= 12; Figure 4.10).

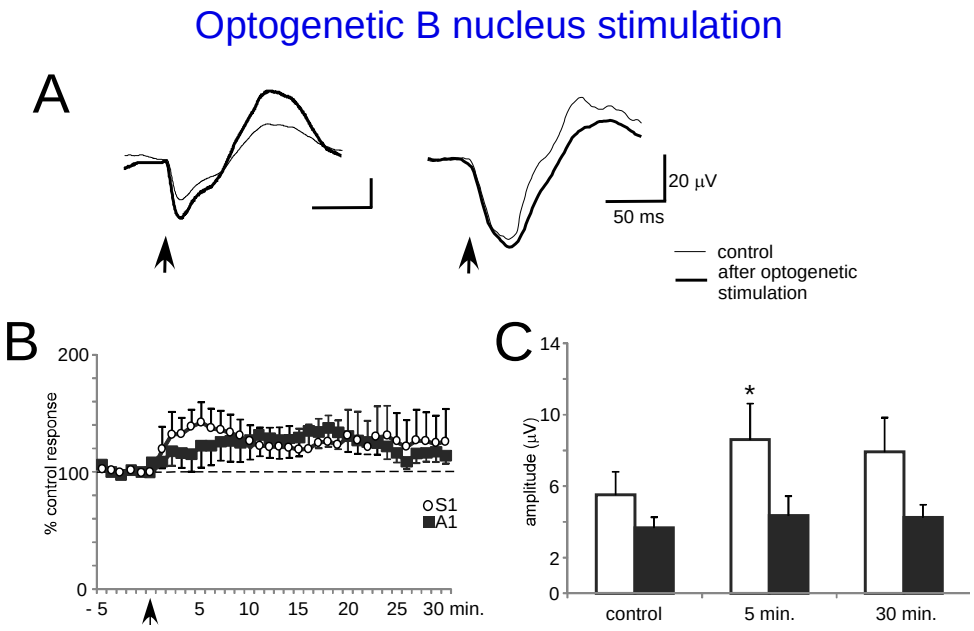

Figure 4.10: Blue light stimulation of B nucleus induces an increase of somatosensory11and auditory evoked potentials.
A, raw data shows that only somatosensory evoked potentials were affected by blue light stimulation at B nucleus (control and 5 min. after stimulation). B, the plot shows the time course in 12 cases. C, plot of the mean amplitude measured in control and 5 or 30 min. after blue light stimulation at B nucleus. The effect observed was smaller than in HDB stimulation.

Once we observed that different neuronal groups in the BF of mice display specific anatomical pathways to sensory cortices, we would like to study if these neuronal pathways linking sensory cortices with different BF nuclei were equivalent and conserved in rats.

RATS: Therefore, in order to detect the presence and characteristics of the pathways linking different sensory cortices with specific regions of the basal forebrain, simultaneous injections of FlGo and FB deposits were done in 21 animals; 11 animals received a FlGo injection in S1 and FB deposits in A1 (Figure 4.11) while in the remaining 10 animals FlGo and FB were respectively delivered in S1 and in V1 (Figure 4.11). In all cases, the FlGo injections were confined to the S1 layers and the FB deposits to A1 or V1.

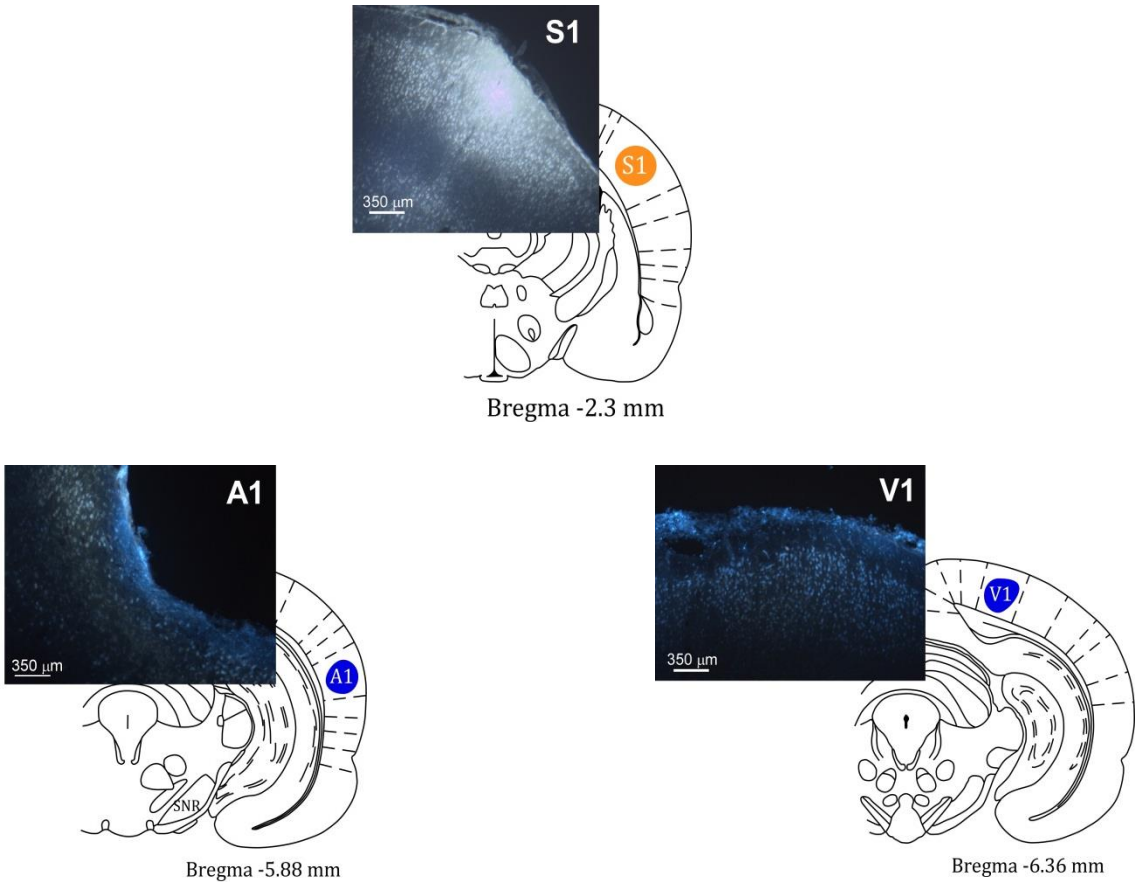

Figure 4.11: Injections/deposits of tracers in S1, A1 and V1 cortices of rats.
Schematic drawings and microphotographs of brain coronal sections showing the FlGo injection sites in the S1 cortex (A) and FB deposits in A1 (B) and V1 (C) cortices.

Neurons with retrograde labeling by FlGo, FB or both tracers were found in different BF regions in the 11 animals treated in the S1/A1 cortices. FlGo labeled-neurons were located in both VDB and HDB, in the SI, and at all rostro-caudal levels of the B nucleus including, at the most caudal levels, the zona incerta (ZI) (Figure 4.12). However, neurons showing FB fluorescence were found in neither the VDB nor the HDB although they were present at all levels of the B nucleus as well as in the ZI and SI. Double-labeled-neurons were found in both the B nucleus and ZI (Figure 4.12).

Quantification of these neurons allowed us to establish that more than 98% of the HDB neurons were FlGo single-labeled while the rest were double-labeled; in the B nucleus 50% of the neurons were single-labeled with FlGo, 15% single-labeled with FB and 35% double-labeled (Figure 4.14).

In the 10 animals with injection/deposits in the S1 (FlGo) and in V1 (FB) cortices, single FlGo, single FB and double-labeled neurons were found in HDB as well as at all levels of the B nucleus and in the ZI and SI. (Figure 4.13). Quantitative studies of labeling in the HDB showed 67.5% of neurons to be single-labeled with FlGo, 11% single-labeled with FB and 21.5% of the neurons to be double-labeled. In the B nucleus, 47.5% of the neurons were labeled with FlGo, 8% with FB and the 44.5% remaining of the neurons were double-labeled. The percentages of this quantitative analysis have been normalized since the relative number of neurons was higher in S1 / V1 injected animals (Figure 4.14). All together these data confirmed that BF project to the cortex heterogeneously.

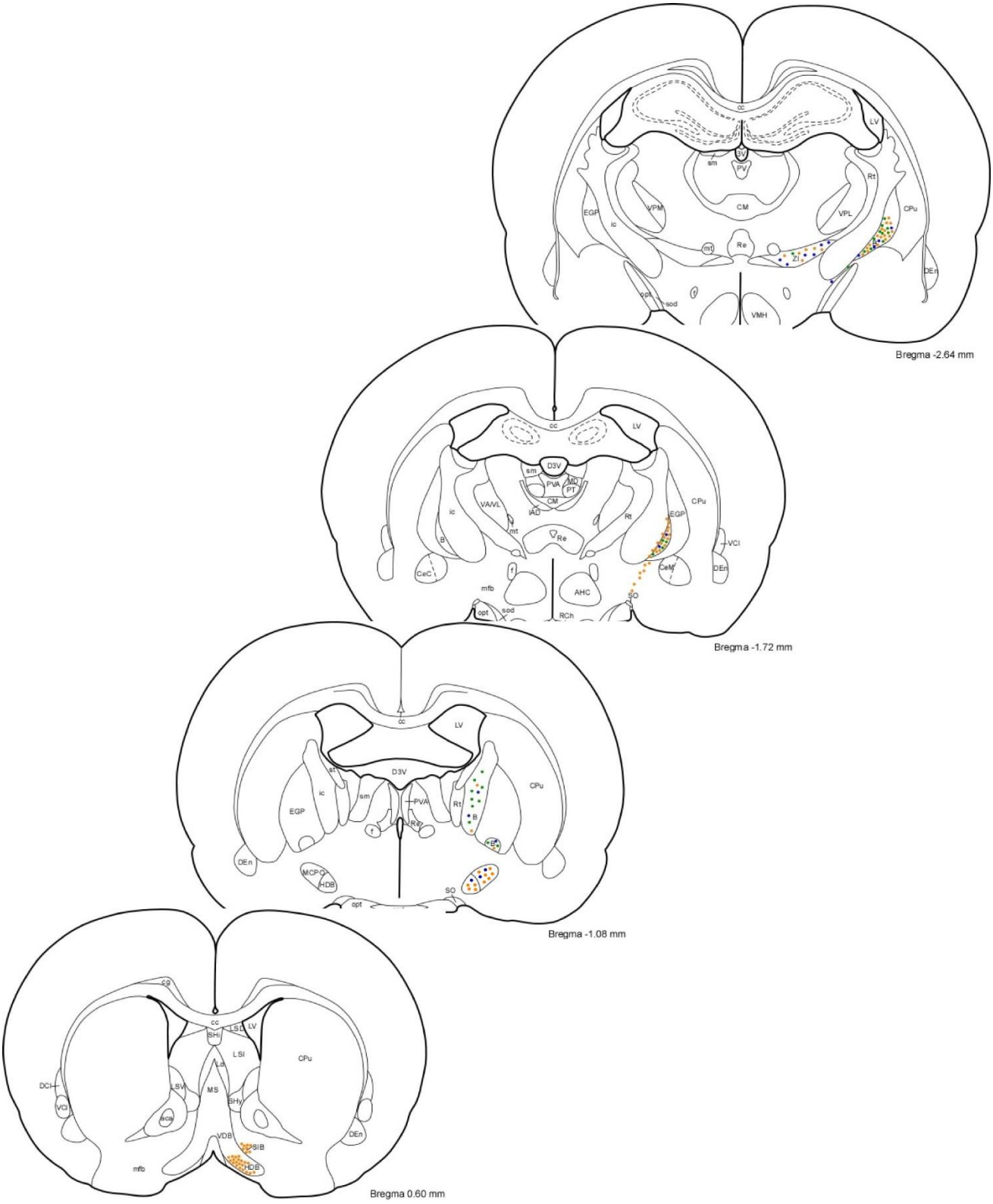

Figure 4.12: BF neurons projecting to S1, A1 cortices in the rat.
Rostral to caudal schematic drawing of brain coronal sections where the locations of single-FlGo (orange, injection in S1), single-FB (blue; injection in A1) and double-labeled neurons (green) were located.

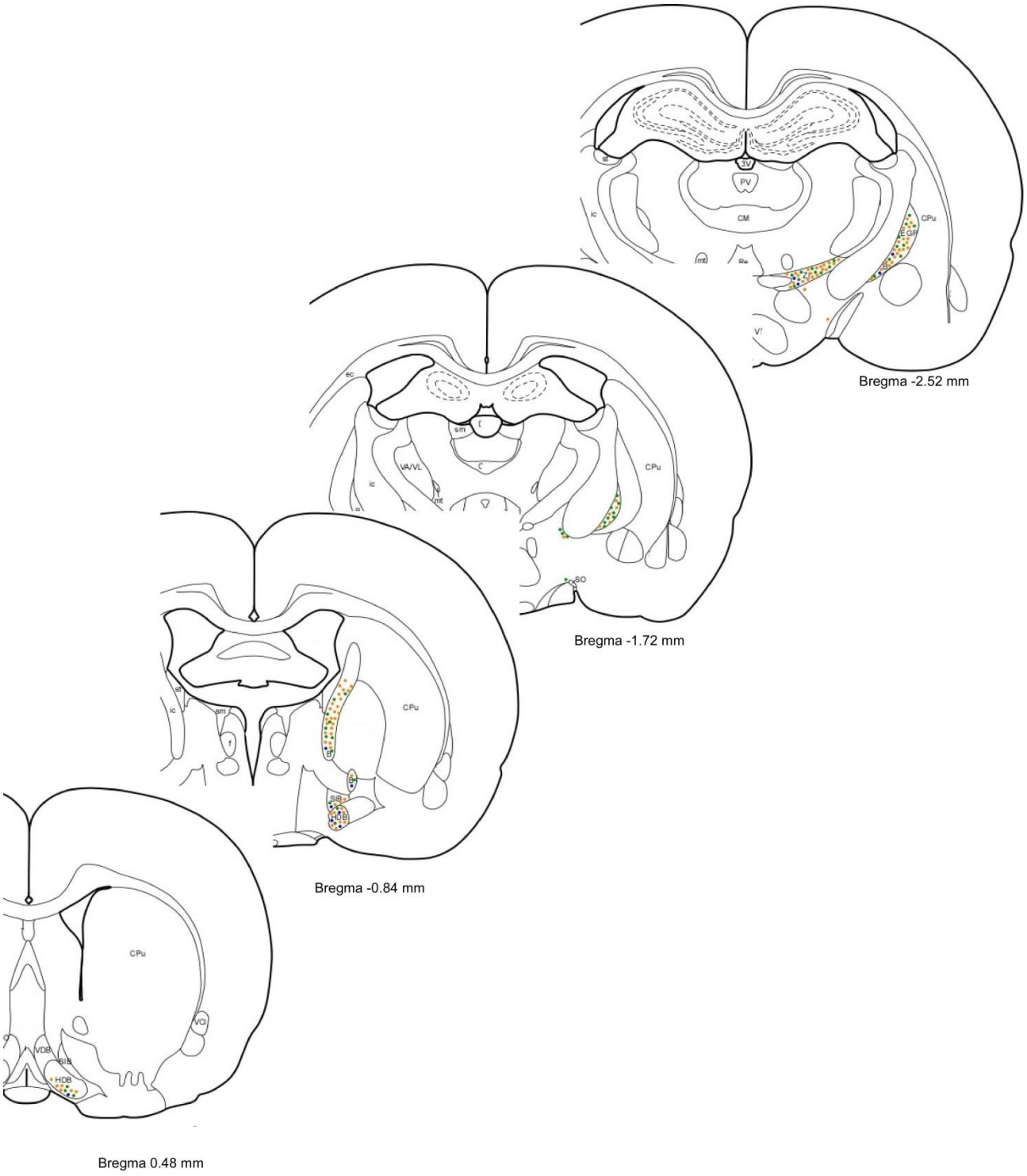

Figure 4.13: BF neurons projecting to S1, V1 cortices in the rat.
Rostral to caudal schematic drawing of brain coronal sections where the locations of single-FlGo (orange, injection in S1), single-FB (blue; injection in V1) and double-labeled neurons (green) were located.

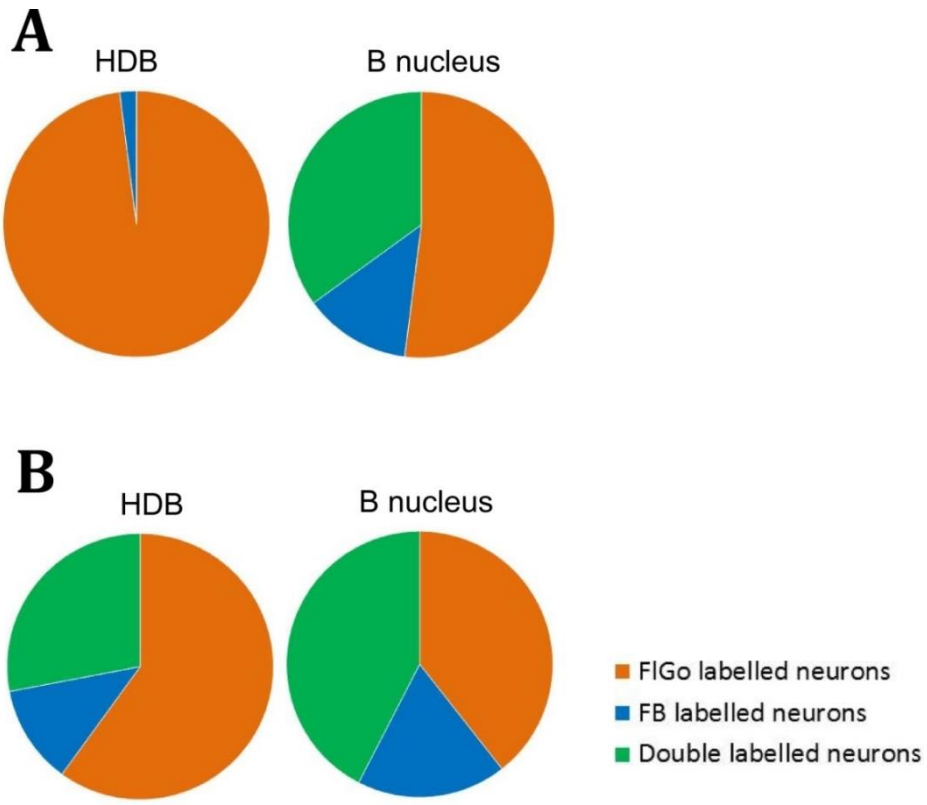

Figure 4.14: Normalized percentages of labelled neurons.
A. FlGo single labelled neurons (orange), FB single labelled neurons (blue) and double labelled neurons (green) in HDB. B. FlGo single labelled neurons (orange), FB single labelled neurons (blue) and double labelled neurons (green) in B nucleus.

Once we have the anatomical results, we would like to assess, as in the case of mice experiments, if these anatomical projecting pathways have a functional correlation. For that purpose, we used optogenetic methods for selective stimulation of virus-injected neurons in specific BF areas (Figure 4.15). The mean area of the earlier negative wave was calculated every 60 stimuli and the mean area of the control period were considered as 100 %. HDB optogenetic stimulation induced an increase of the sensory evoked potential (SEP) in S1 cortex (Fig. 4.16). The mean area increased rapidly reaching a maximum 2 minutes after blue light stimulation (172±25%, P = 0.018; n = 8) that was sustained until 4 minutes after stimulation (155±27%; P = 0.042; n = 8). In contrast, SEP potentials were inhibited in the mPfC by blue light stimulation when this was directed toward the HDB. The mean area decreased slowly, the decrease reaching statistical significance 3

minutes after blue light stimulation (78±8%, P= 0.004 and 83±9%, P<0.001, respectively; n=8; Figure 4.16).

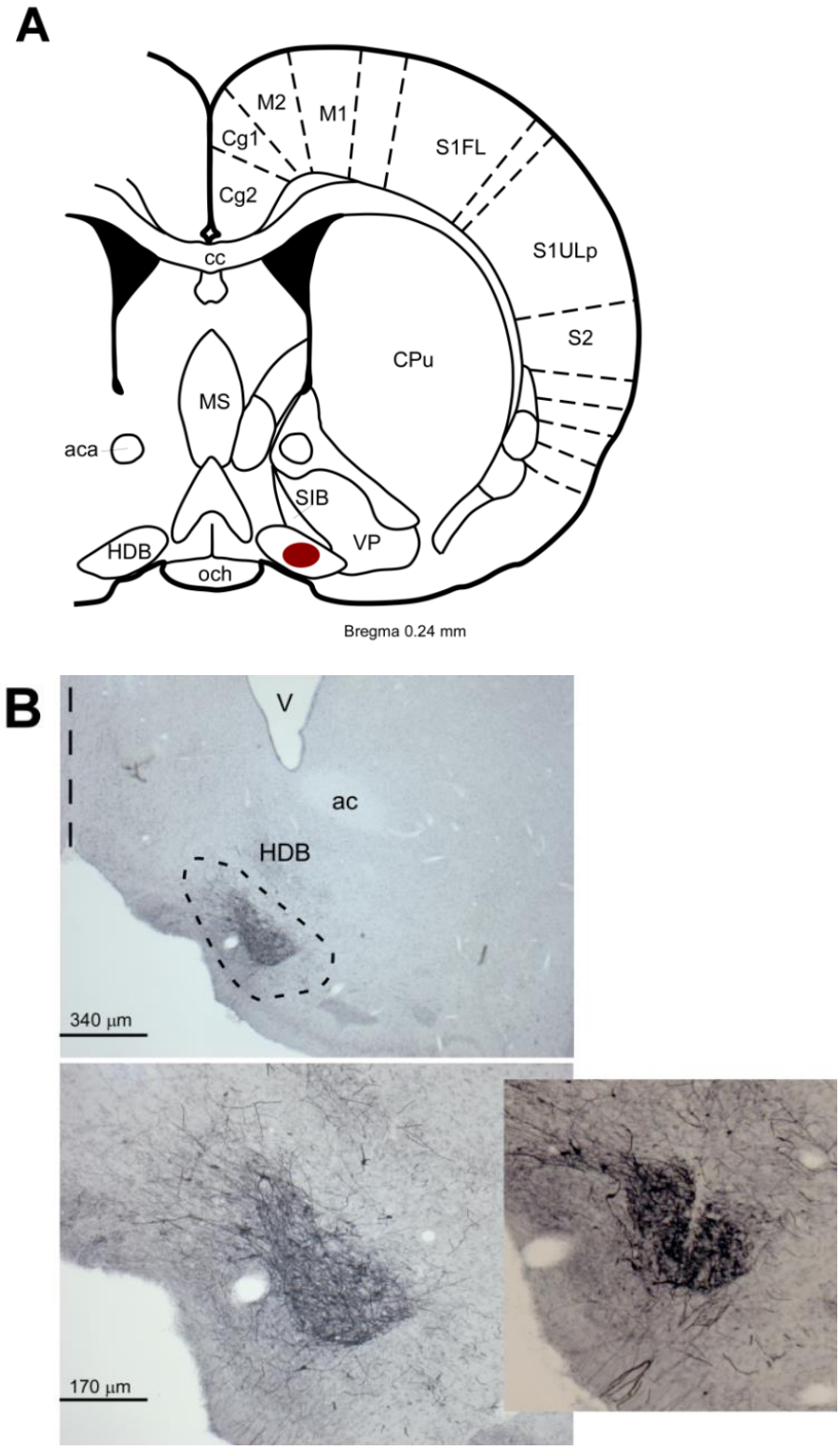

Figure 4.15: Virus injection in HDB.
A. Eschematic drawing of AVV5 virus injection site at HDB, Bregma 0.24mm. B. Microphotographs of AVV5 virus injection in the mice HDB.

B nucleus optogenetic stimulation induced a lower SEP increase, reaching statistical significance at 3 and 4 minutes after blue light stimulation (121±9%, P= 0.031 and 111±5%, P=0.048, respectively; n=10; Figure 4.16). B nucleus optogenetic stimulation also inhibited SEP in the mPfC (81±5%, P< 0.001; n=10)(Figure 4.16). However, the stimulation effect vanished 2 minutes after optogenetic stimulation. In summary, data indicate that BF stimulation also has heterogeneous effects on the cortex according to the stimulation location, supporting the above anatomical data.

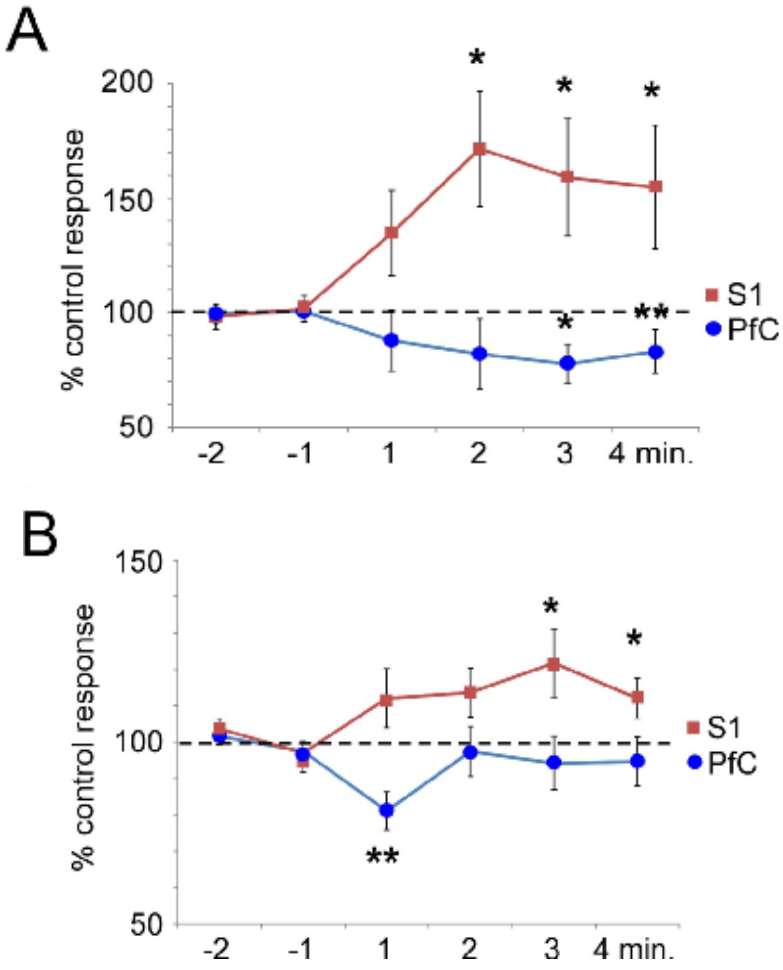

Figure 4.16: Optogenetic stimulation of BF induced cholinergic modulation of whisker responses in S1 and mPfC cortices.

A: plot of SEP responses in controls (2 minutes) and during the 4 minutes after HDB blue light stimulation (1 s pulse duration). Note that HDB stimulation induced different simultaneous responses in S1 and mPfC cortices. B: plot of SEP responses in control (2 minutes) and during the 4 minutes after blue light stimulation (1 s pulse duration) in the B nucleus. Note that B stimulation induced different responses in the S1 and mPfC cortices. The light induced inhibition in mPfC lasted less than when the light was applied to the HDB. In A and B the mean of the two control values was considered as 100%. *, p<0.05; **, p<0.001.

Once we observed this specificity in the projecting pathways concerning the sensory cortices and the BF, we then wanted to know if this differential and specific projecting manner from sensory cortex to VDB/HDB and B also was present in the BF nuclei concerning other modality cortices. This was our Aim 1.3: to investigate the involvement of motor and prefrontal cortices in these networks, which results are explained in the next Section 4.2.

4.2 BASAL FOREBRAIN CONNECTION PATHWAYS WITH OTHER CORTICES

RAT: Fluorescent retrograde tracers were injected in BF nuclei of 11 rats to study cortical projections to the BF. The locations of FlGo and FB deposits in animals injected in HDB and B nucleus, respectively, were confined to the corresponding structures as shown in Figure 4.17.

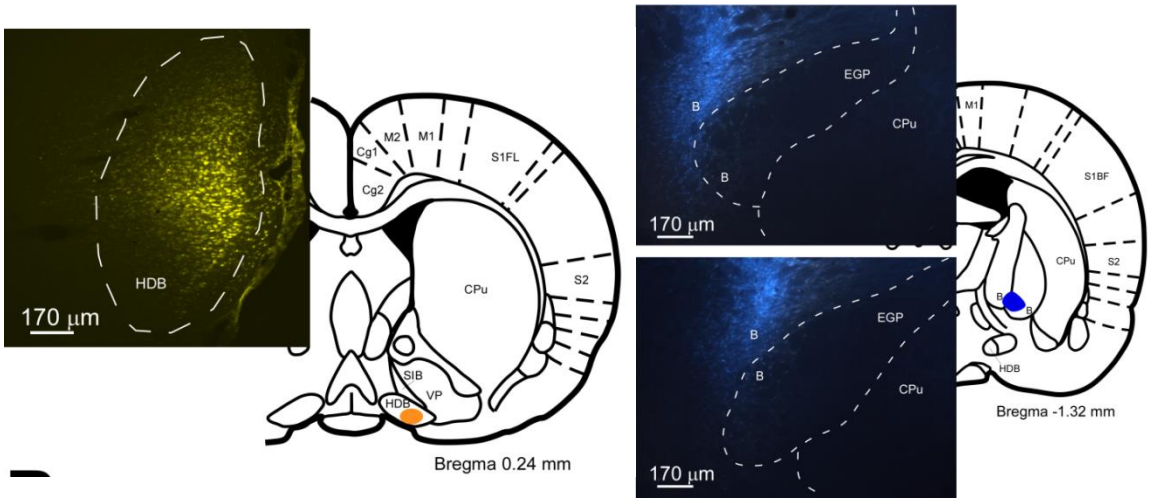

Figure 4.17: Fluorescent tracer injections in BF nuclei.
Micrographs of injection sites and squematic drawing of FB injection in B nucleus and FlGo injection inHDB.

Injections resulted in single FlGo retrograde labeled-neurons in the prelimbic/infralimbic, cingulate and motor cortices, while single FB retrograde-labeled neurons only appeared in the cingulate and motor cortices (Figure 4.18). Most of the neurons in the motor cortex were FB single-labeled although a few were FlGo single-labeled, indicating that motor cortex mainly projects to the B nucleus; practically all the neurons detected in prelimbic/infralimbic cortex were FlGo single-labeled, indicating that prelimbic/infralimbic cortex projects to the HDB. Only a few double-labeled neurons appeared and they were confined to motor cortex.

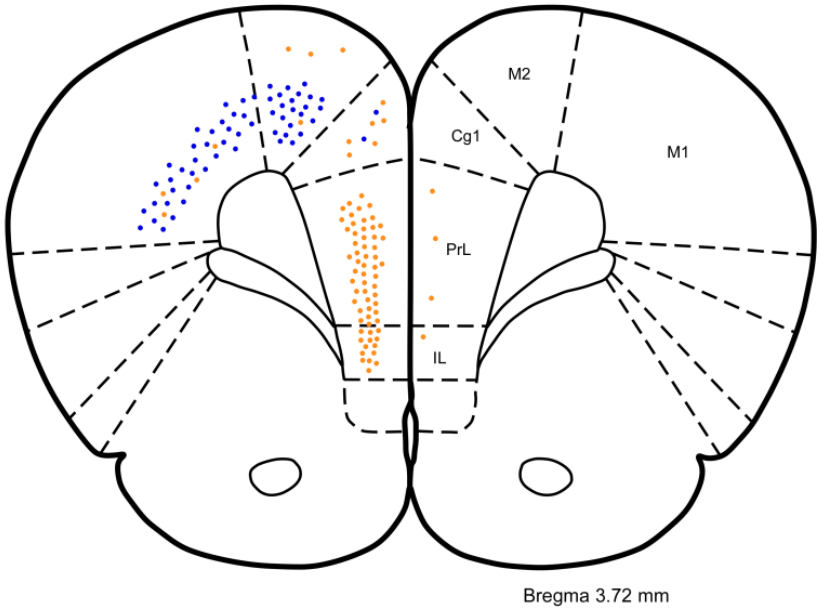

Figure 4.18: Labelled neurons projecting to BF nuclei.
Schematic drawing labelled neurons projecting HDB (orange dots) and B nucleus (blue dots).

To study if these circuits were reciprocal, we also injected in other animals the retrograde tracer FlGo in mPfC (Figure 4.19). Injections of the FlGo retrograde tracer in mPfC resulted in a great amount of neurons in all rostro-caudal levels of HDB (Figure 4.19) while a few neurons were located in B nucleus.

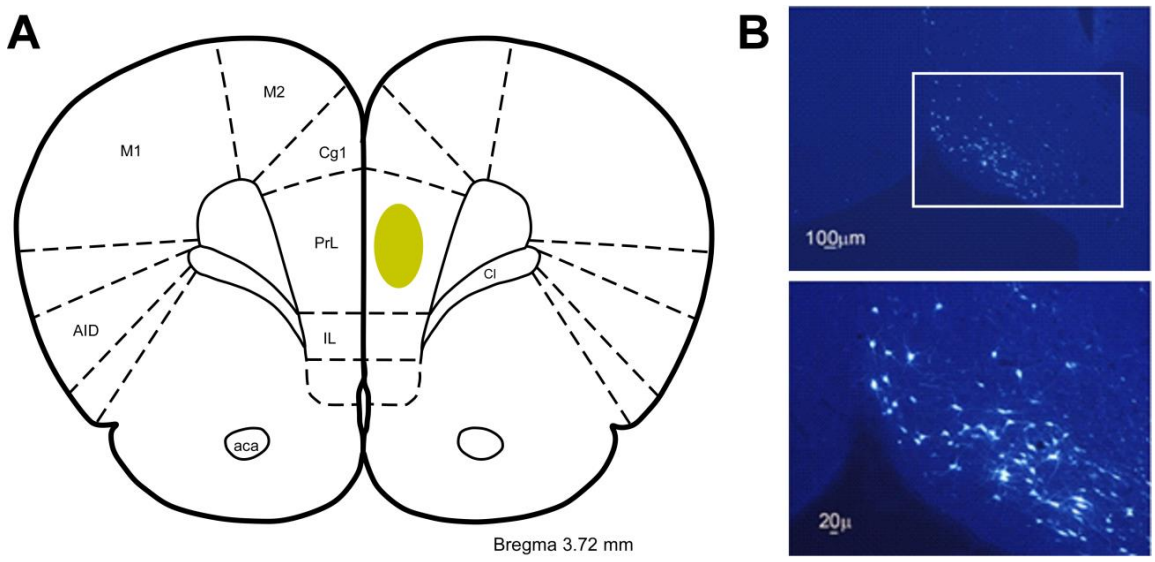

Figure 4.19: Injection in mPfC.
A. Schematic drawing of FlGo injection in mPfC. B. Microphotographs of labelled neurons in HDB.

4.3 CONTRALATERAL BASAL FOREBRAIN CONNECTIONS

MICE: The anatomical pathways linking BF with cortical areas with the BF were studied by injecting or depositing the neuroanatomical fluorescent retrograde tracers FlGo and FB in 18 B6.Cg-Tg (Chat-COP_4*H_{134}R/EYFP,Slc_18a_3)5^{Gfng}/J mice.

For a better understanding of the characteristics of the cortical afferent connections from BF, animals were divided into four groups of experimental procedures according to the injection side and the combination of both fluorochromes in the cortices. Group 2: FlGo injection in S1 of left hemisphere and FB deposit in S1 right hemisphere; Group 3: FlGo injection in A1 left hemisphere and FB deposit in A1 right hemisphere and Group 4: FlGo injection in V1 left hemisphere and FB deposit in V1 right hemisphere.

The distribution and relative percentage of these neurons was different depending of the experimental group, as described below.

In order to corroborate whether one given sensory cortex (somatosensory, auditory or visual) received projections from the ipsi- and/or contralateral BF, experimental Groups 2 (n = 3), Group 3 (n = 3) and Group 4 (n = 2) received a FlGo injection in the left hemisphere in the SI, A1 or V1cortex respectively, and a FB deposit in the right hemisphere of same cortices. Group 2 received the injection/deposit in S1 cortices of both hemispheres. Single labeled neurons were also found in the contralateral BF; these neurons were present in VDB, HDB and SI but not in B nucleus (<2%). A rostro-caudal gradient that differed in the number of contralateral neurons in VDB and HDB was observed; from rostral to caudal in VDB the gradient increased from 15.7% to 27.2%, while in HDB the gradient decreased from 11.3% to 5.6% Figure 4.20 A-C).

Group 3 received FlGo injection/FB deposit in A1 cortices of both hemispheres. In spite of the ipsilateral single labeled neurons found in VDB, HDB, B and SI nuclei, labeled neurons were also found in the contralateral BF (Figure 4.20 D-F). In VDB 24.5% of the contralateral labeled neurons were observed at rostral levels and 19.4% at caudal levels. In HDB, 30% of total labeled neurons were found in the contralateral side. In this case, differences were not observed in the rostro-caudal levels. In contralateral B nucleus, less than 2% of the total labeled neurons were observed.

Group 4 received the injection/deposit in V1 cortices of both hemispheres. Ipsilateral single labeled neurons were found in VDB, HDB, B and SI nuclei. Single labeled neurons were also found in contralateral BF (Fig. 4.20 G-I). In contralateral VDB 15.8% of labeled neurons were found at the rostral levels while 27.2% of labeled neurons were observed at the caudal levels. In HDB a rostro-caudal decreasing gradient was observed in the percentage of contralateral labeled neurons that ran from 15.7% to 3.8% respectively. In B no contralateral labeled neurons were observed. In B/SI nuclei less than 2% of labeled neurons were contralateral.

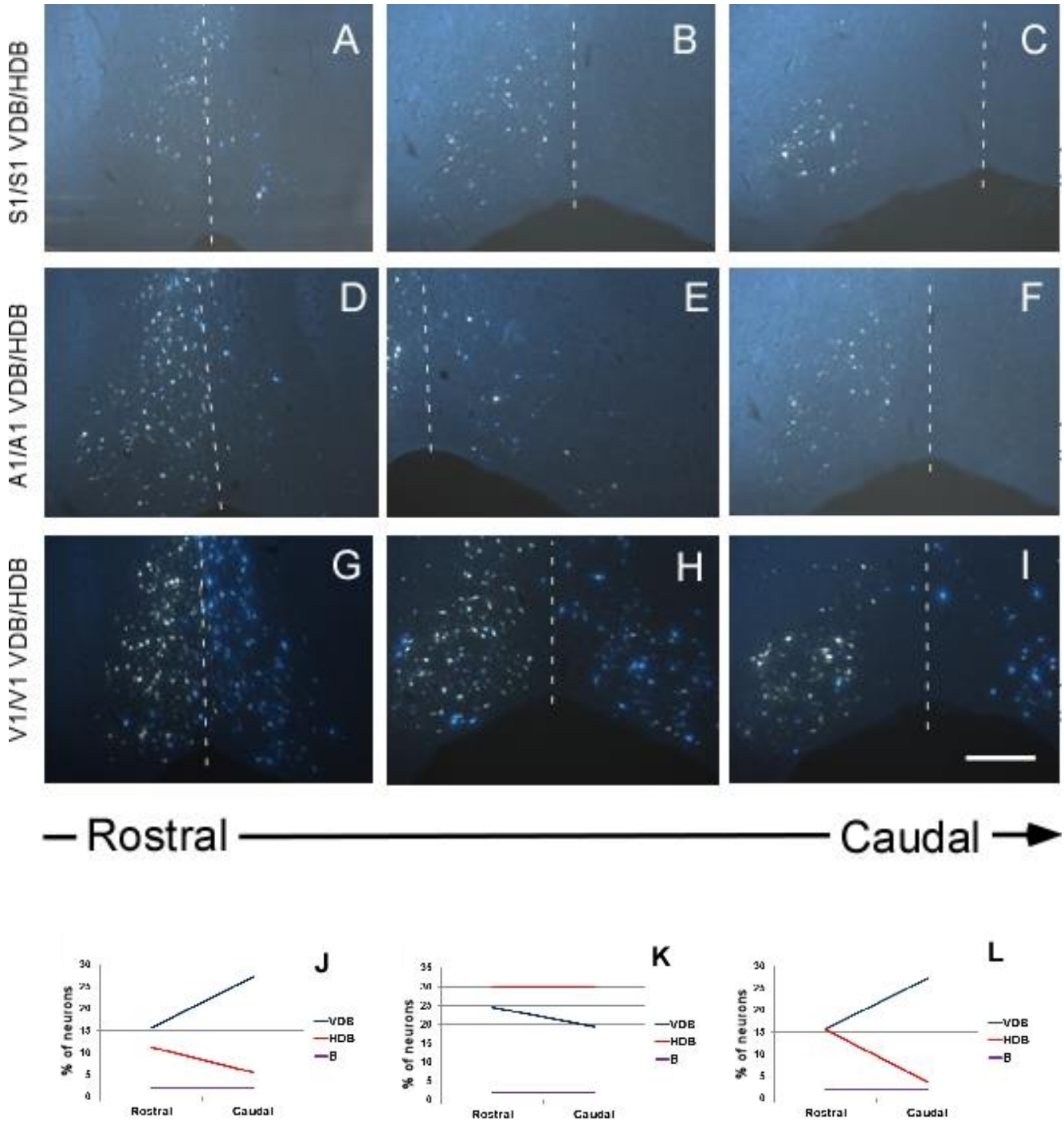

Figure 4.20: Fluorescent microscope images showing the rostro-caudal distribution of fluorescent labeled neurons.

A-C: Fluorescent microscope images from animals of group 2 (FlGo injection an FB deposit in S1); D-F: Fluorescent microscope images from animal of group 3 (FlGo injection and FB deposit in A1); G-I: Fluorescent microscope images from animal of group 4 (FlGo injection and FB deposit in V1). J-L: Graphic representation of rostro-caudal distribution of neurons in VDB, HDB and B nucleus in group 2 (J), group 3 (K) and group 4 (L). Calibration toolbar 600 µm.

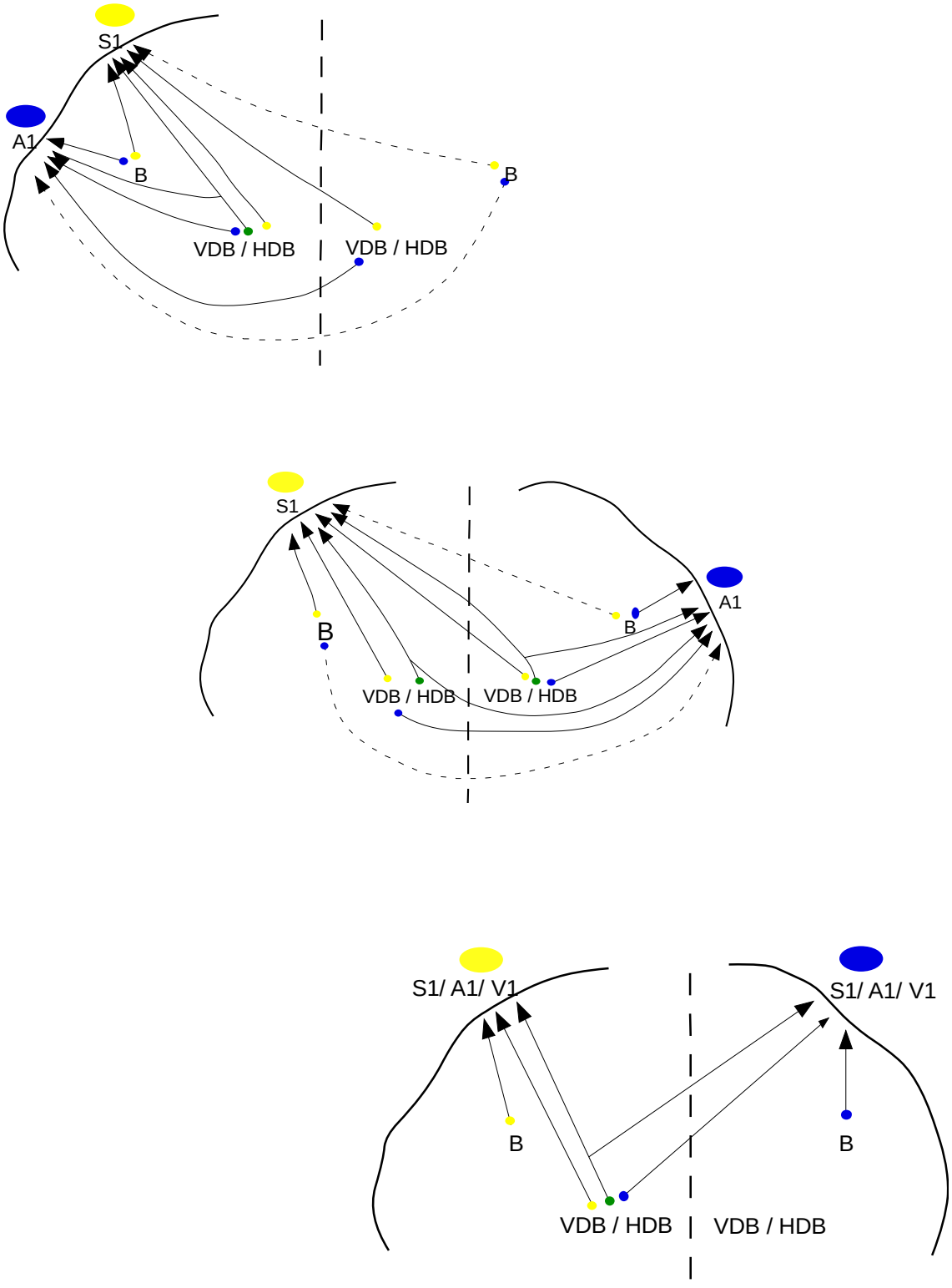

Figure 4.21: Schematic summary drawings of the projections from the BF to the sensory cortices and reciprocally in the different neuronal tracers injected groups.

4.4 BF-CORTICAL CIRCUITS IN APP/PS1 TRANSGENIC MICE

To achieve our Aim 1.4 in which we wanted to compare the projection pathways of these BF-cortical networks in control (above results) and APP/PS1 mice to study if the connections described in the above Sections display any changes in the AD model.

6 mice of 9 to 14 months of age were injected in the sensory cortices (A1 and V1) with retrograde tracers, FlGo and FB respectively. Fewer neurons seems to be projecting to S1 cortex from HDB comparing APP with control mice. However, further analysis should be done to establish the relevance and percentages of that suggested decrease in number.

We did also a ChAT immunohistochemistry to study if that decreased in neurons affected to the cholinergic ones. We observed a decrease in the number of cholinergic neurons in B nucleus both in males and females in APP/PS1 mice compared with controls. Moreover, in APP/PS1 females, the number of cholinergic neurons in HDB seems to be reduced compared with controls and APP male's mice (Figure 4.22).

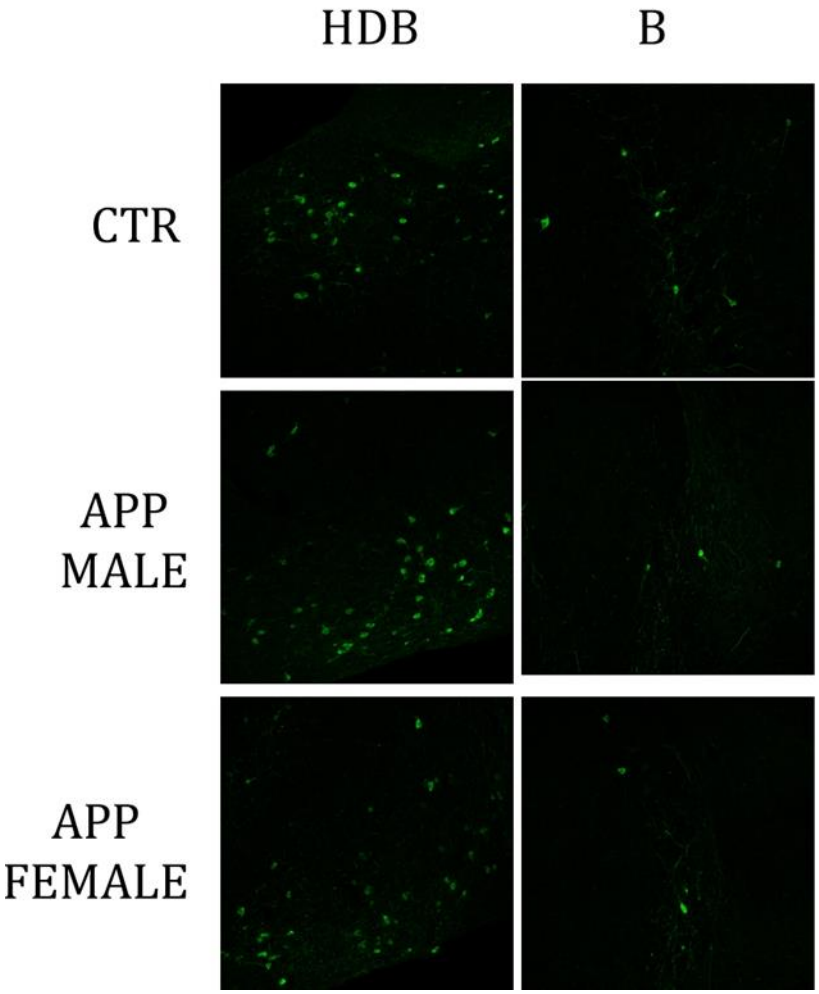

Figure 4.22: Cholinergic neuronal loss in APP/PS1 mice compared with controls.

Due to results shown in Section 4.4, we started the study of the possible toxicity leading to a lost in the neuronal function in AD mice models. This study was performed using two different approaches. The first one was englobes Aim 3, the study the location OF IGF1 receptors in the BF nuclei in control and APP/PS1 transgenic mice (Section 4.5). Our second toxicity approach, related with Aim 4, was the *in vitro* study in BB2 cells and microglia cultures (Section 4.6).

4.5 IGF-1 RECEPTOR LOCATION IN CONTROL AND APP/PS1 MICE

In this Section, we explain the results related with our Aim 3 where we wanted to identify the location of IGF-1 receptors in the BF nuclei of C57 control and of APP/PS1 Alzheimer mice model to investigate its possible implication in the pathogenesis of AD.

For these experiments, 6 C57 mice aging 9 to 12 months and 4 APP/PS1 mice of the same age were perfused and brains were sectioned for immunohistochemistry analysis for ChAT and IGF1 receptor. All brains sections were processed but we focused our study on the VDB/HDB and B nucleus containing-sections.

First of all we performed an experiment to establish if there was co-localization of Ach and IGF1 receptor in the BF neurons. We found positive double labelled neurons for ChaT and IFG1 both in the HDB and B nucleus (Figure 4.23)

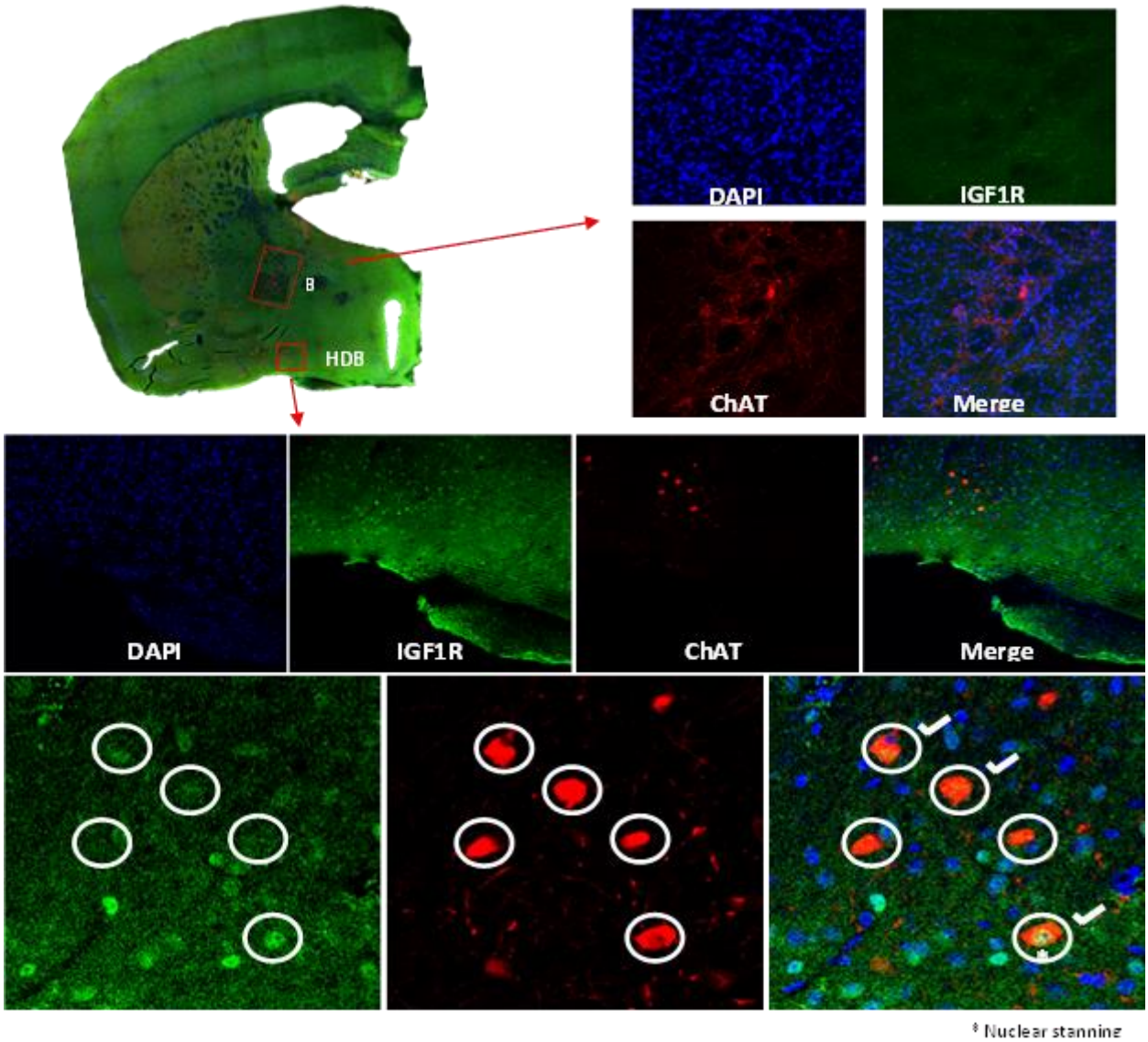

Figure 4.23: Co-localization of possitive neurons for ChaT and IGF1 in BF neurons

Once we have a positive co-localization of ChAT and IGF1 we did the same inmmunohistochemistry for comparing control and APP/PS1 mice BF structures. First, we observed an increased qualitative expression of IGF1 in APP/PS1 BF nuclei compared with the observed in controls (Figure 4.24).

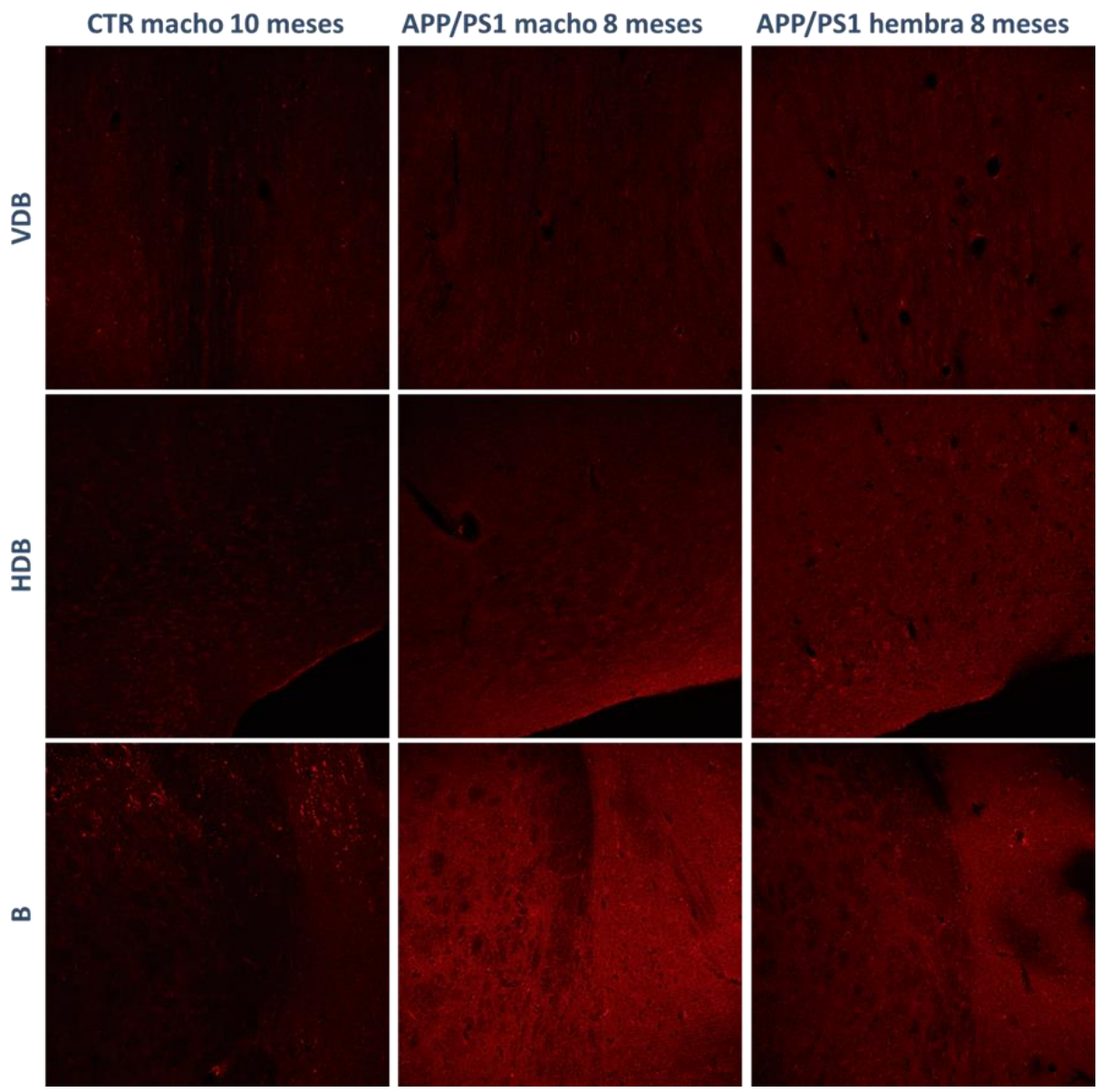

Figure 4.24: IGF1 receptor expression in BF nuclei of control and APP/PS1 mice. mice.

Moreover, we also observed an increased concentration of IGF1 receptors in VDB/HDB nuclei in the APP/PS1 mice compared with controls (Figure 4.25).

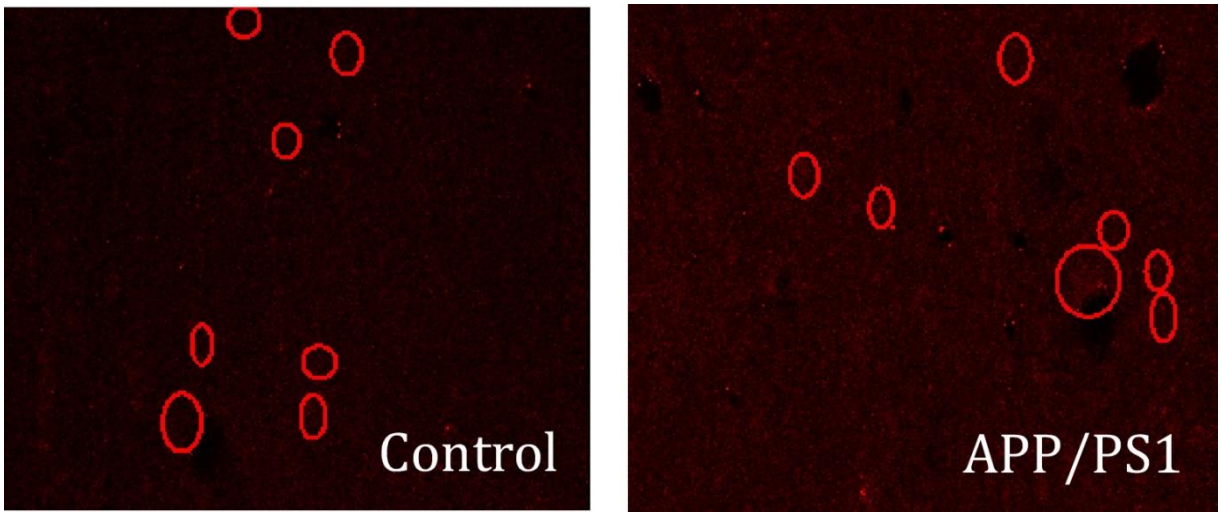

Figure 4.25: IGF1 receptor expression in VDB/HDB neurons.

4.6 *IN VITRO* EXPERIMENTS

In this Section we show the results for Aim 4, the study of the effect of TDP-43 knockout in BV2 cells and primary microglia, as part of the toxicity study.

4.6.1. EXPERIMENT 1 (IN VITRO): BV2 CELLS

First we would like to study if the TDP43 oli size was a main important factor in for the agregattion inside the cells both in starved and fed conditions in the culture.

4.6.1.1 Western Blot (WB)

siRNA transfection in BV2 cells was done to knockout TDP43. The oligo 1 and 2 result in reduction of TDP43 in both STARVED and FED condition. In contrast, oligo3 and oligo4 show no diference with control group in STARVED and FED conditions. TDP pool lead to reduction in all of the cases GAPDH and β-actin are equally distribuded in membrane. Thus, we can conclude that the loading amount of the protein was identical and the knockout effeciency is demonstrated in TDP pool, oligo1 and oligo2, but not in oligo3 and oligo4 (Figure 4.28).

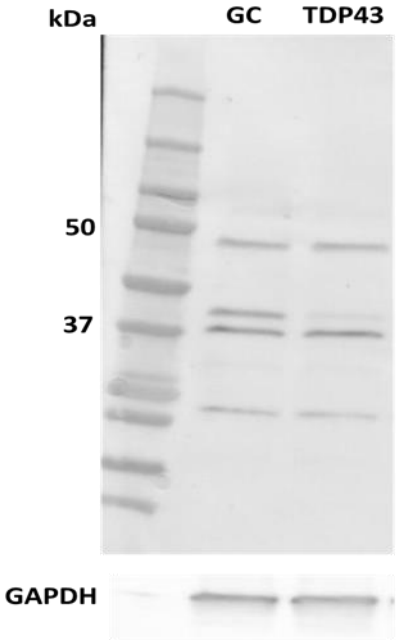

Figure 4.26 Western Blot in GS and TDP knockout and GAPDH.

4.6.1.2. MSD Assay

The MSD assay was analysed for the clearence of Aβ and sAPP from the BV2 medium. The level of sAPP do not change the concentration in the medium, whereas the levels of Aβ are decresed in all cases. The significant reduction of Aβ from the medium is detected in all cases of TDP43 knockdown (Figure 4.27).

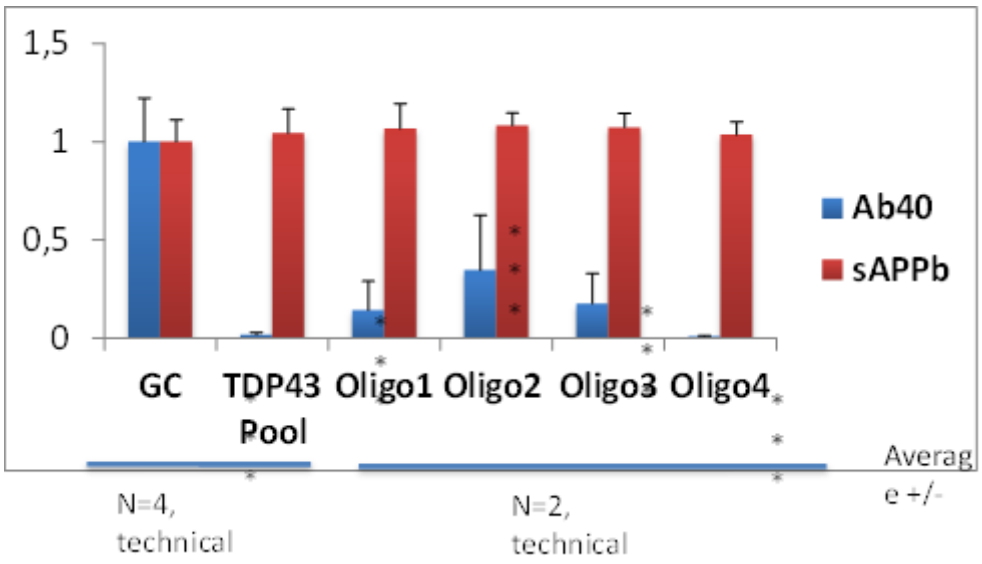

Figure 4.27: MSD assay in BV2 cells in GC controls and TDP knockout

4.6.1.3. Alamar Blue Assay

Positive colorimetric reaction was detected in all wells with BV2 cells. Specifically, during the 3 hours of incubation, blue color of the dye has changed to purple color. This reaction reflects the metabolic activity of the viable BV2 cells (Figure 4.28).

Figure 4.28: Alamar Blue Assay

4.6.1.4. Confocal microscopy ver si lo meto aquí o mejor en microglia

Phagocytic assay (on BV2 coverslides) was analysed using 2-photon confocal microscopy. Specifically, Lysotracker 561 and Aβ (1hour and 15 minutes interval) were studied. In general, lysotracker deposits were more distributed in the microglia cells in STARVED medium than FED medium in both GC controls and TDP pool knockout. Moreover, TDP pool knockout STARVED has shown the highest amount of lysotracker in the microglia (Figures 4.29 and 4.30).

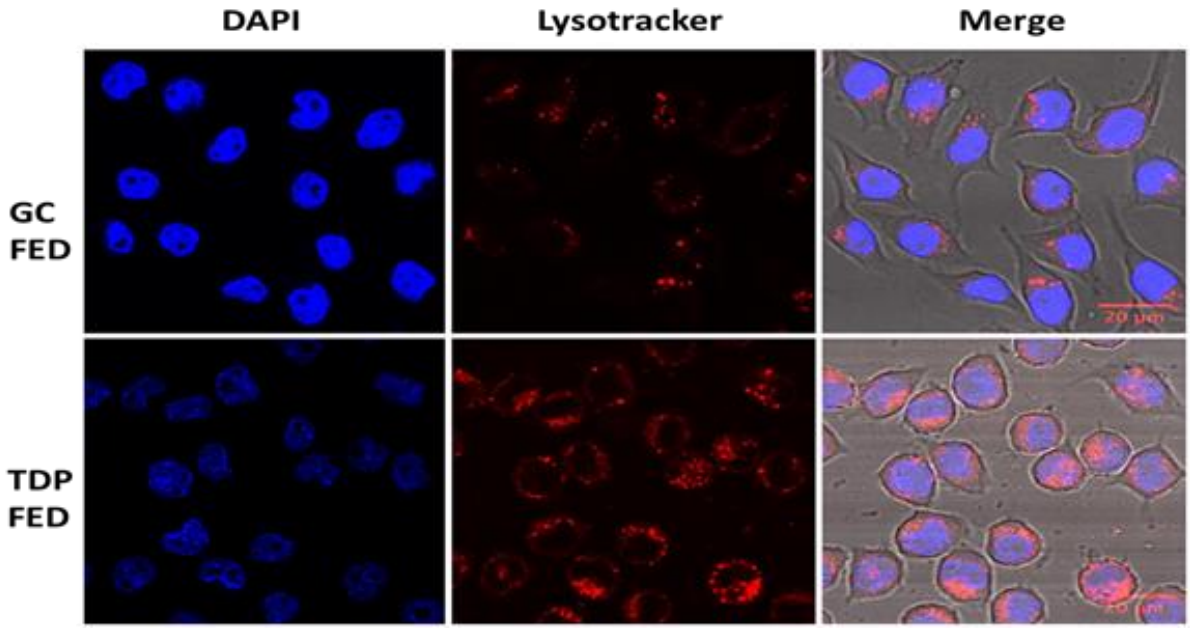

Figure 4.29: Aβ uptake in control (GC) and TDP43 after 1 hour.

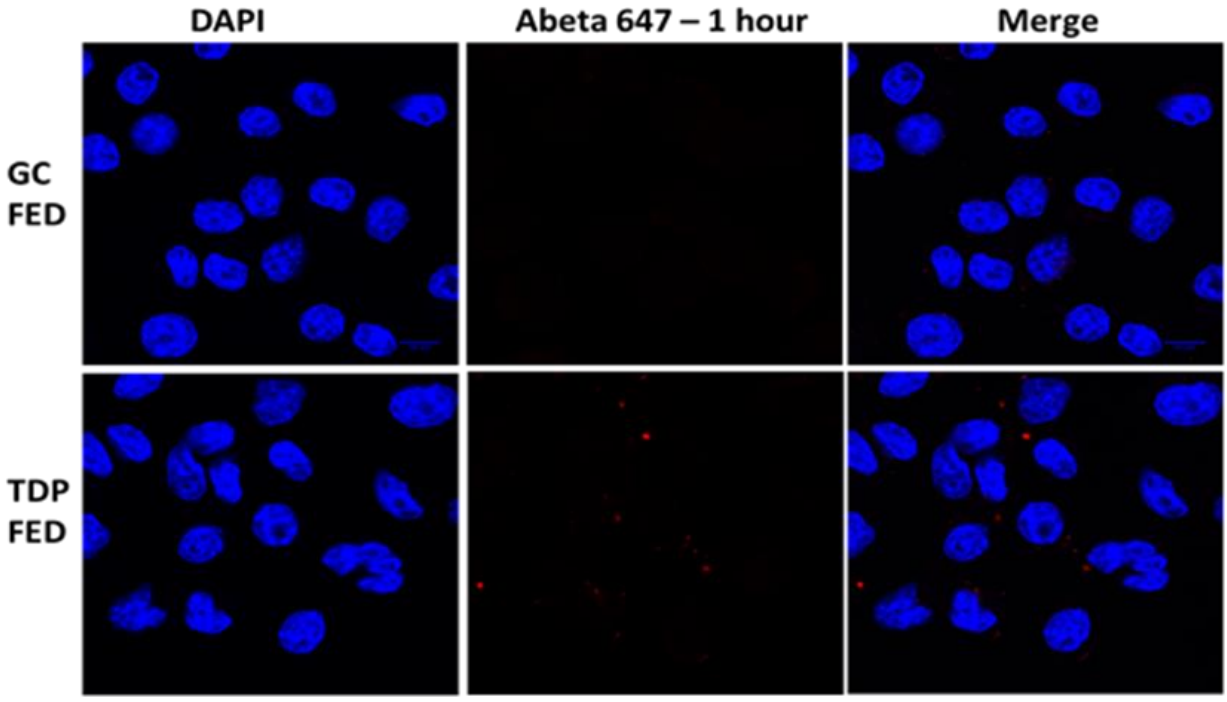

Figure 4.30: Lysotracer uptake in GC and TDP43 in FED conditions.

4.6.2. EXPERIMENT 2 (EX VIVO): PRIMARY MICROGLIA

IF

We monitored the plates under optic microscope after 1.5 hours, 24 hours (Figure 4.31) and 3 days (Figure 4.32) of treatment and we observed some morfological changes in the cells. Cre treatment rapidly affects microglia morphology. There were some vacuoles which disappear 3 days post treatment. We also observed thicker processes in the CRE cells comparing to the control.

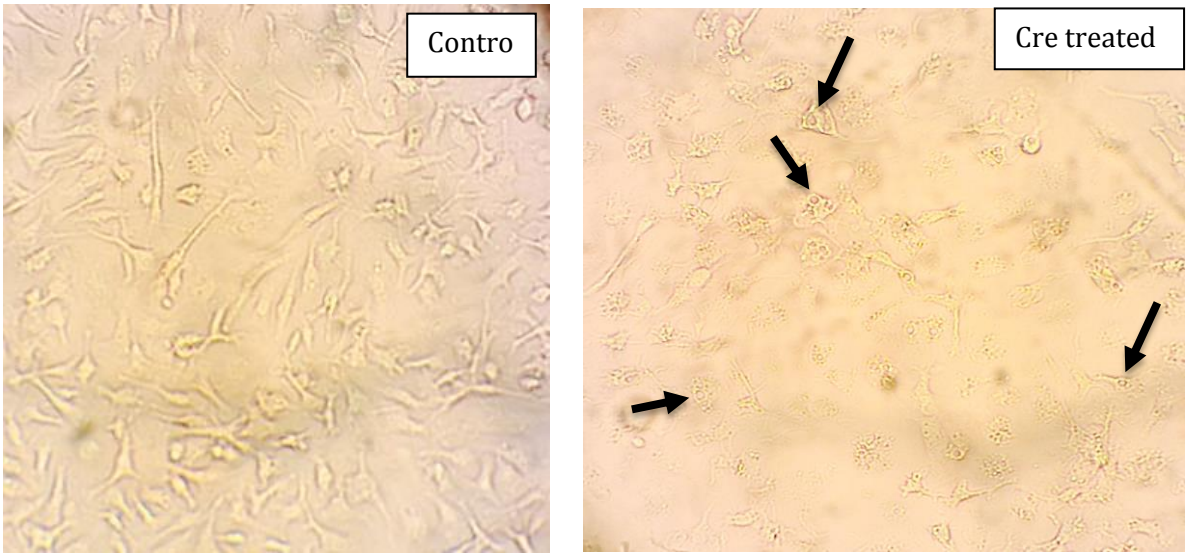

Figure 4.31: Vacuoles phenotype 24hrs after treatment.

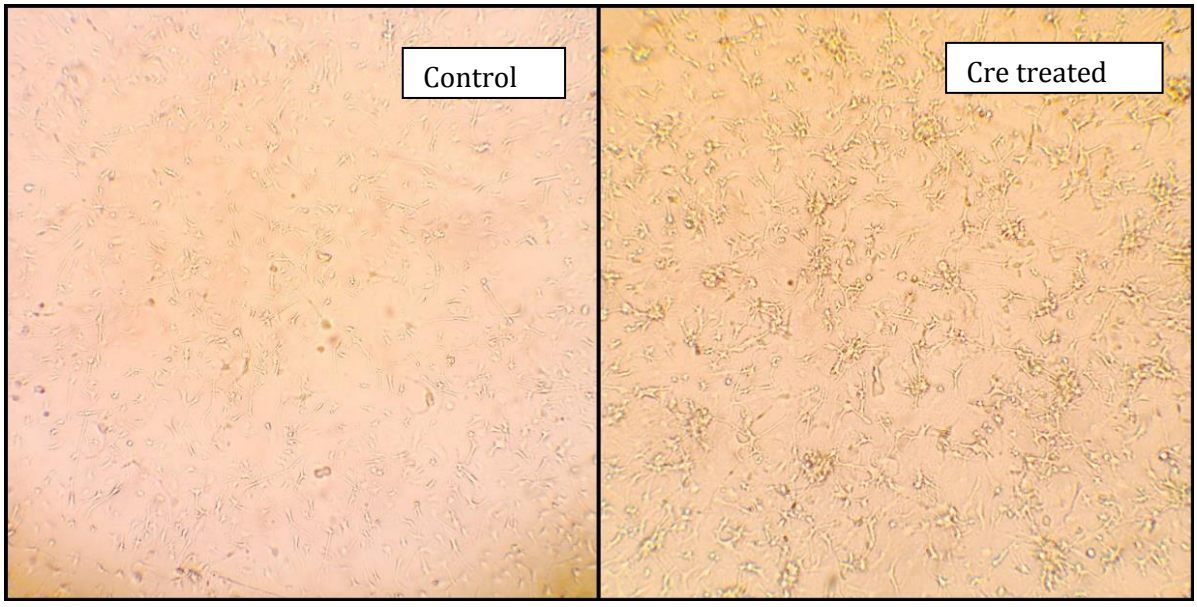

Figure 4.32: 3 days post treatment phenotype.

We keep the cells to assess the uptake of the aggregates of TDP43 using immunofluorescent staining and we also collected the medium (Kept in -20ºC) for fractionation and Western Blot assays.

With these primary microglia cells in the cover slides we performed an immunofluorescence assay in order to see the TDP43 aggregates uptake by the primary microglia cells. We then studied the slides under confocal microscope. We observed a higher uptake of TDP43 oligomers in the CRE treated cells than in the controls, and that higher uptake is correlated with the time of the treatment (more uptake in the 2 hours than in the 30 minutes) and we also see more uptake with the 500nM than with the 100nM concentration of aggregates (Figure 4.33).

There was not just a global increase in the uptake, but it seems that even if there are not more cells uptaking the TDP-43 oligos, once the cells uptake TDP43 they are uptake it more (they are full of them all over the cytoplasm). Also, the CRE treated cells seems to be bigger in size than the control ones.

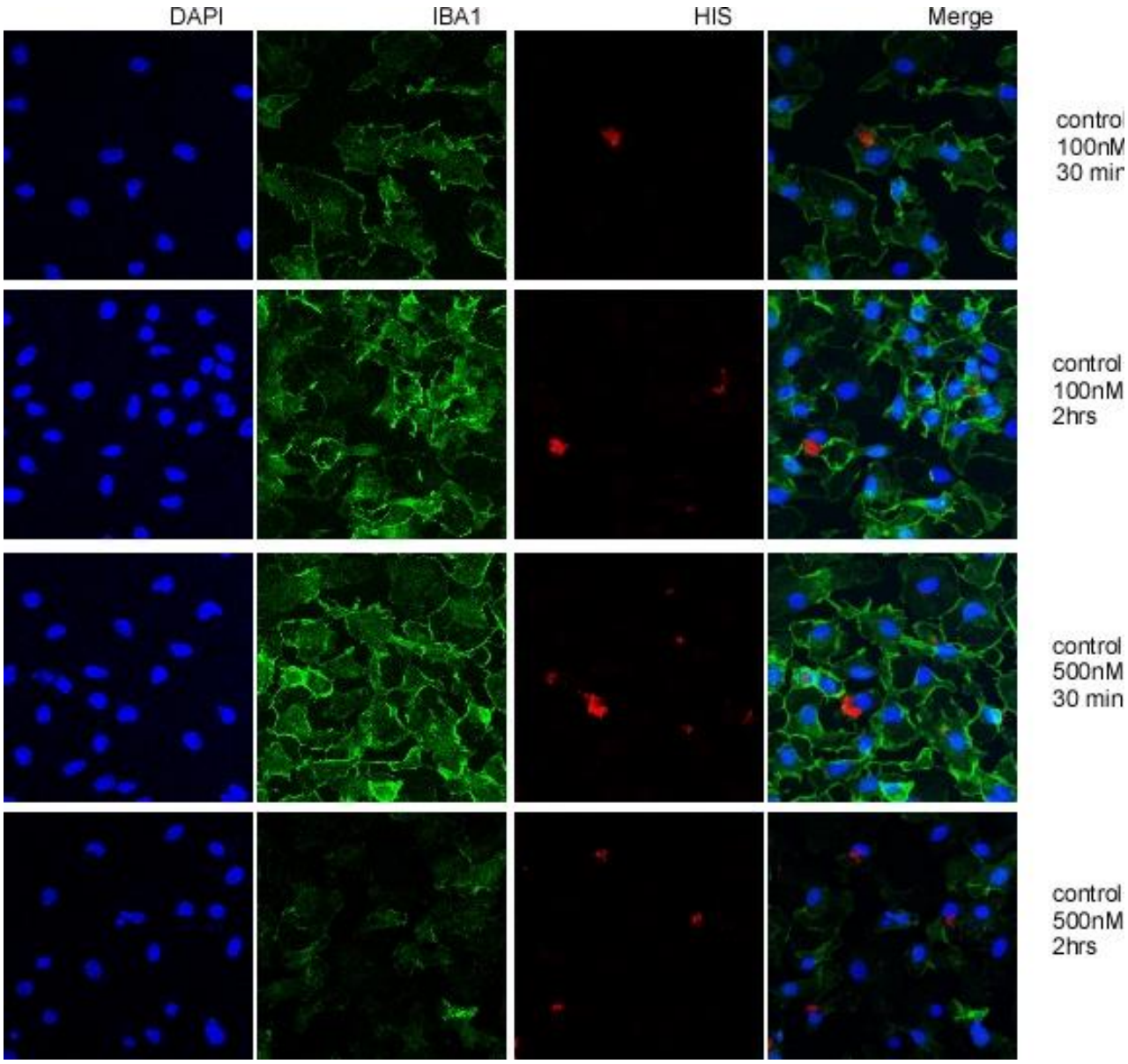

Figure 4.34: Confocal microscope images of primary microglia TDP43 agregated uptake in Cre treated conditions.in control conditions.

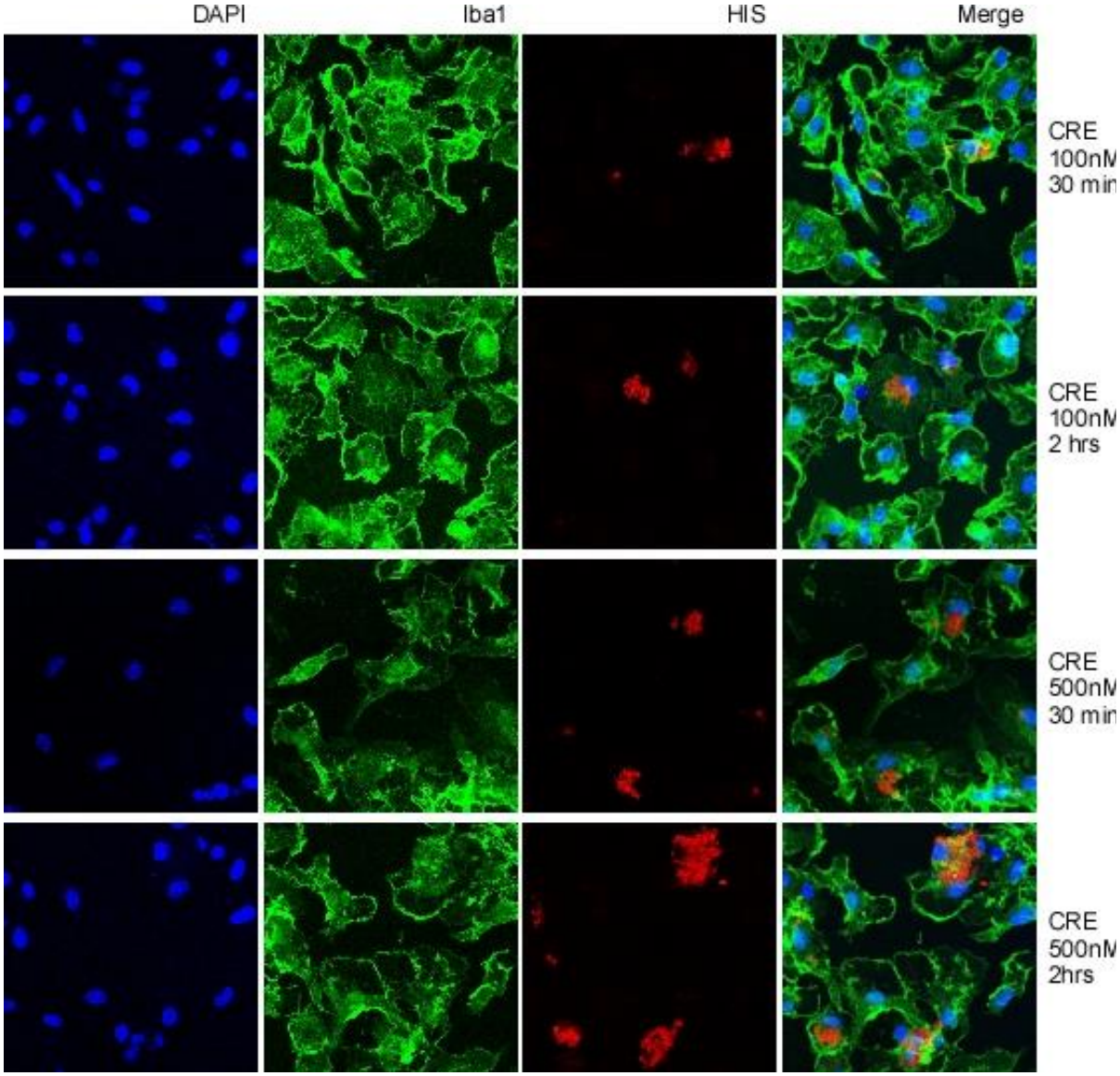

Figure 4.35: Confocal microscope images of primary microglia TDP43 agregated uptake in Cre treated conditions.

2.2.2 Fraccionation and 2.2.3 Western Blot

With the TDP43 aggregates medium we did a fractionation and a Western Blot for analyzing this media composition (Figure 4.36 and 4.37).

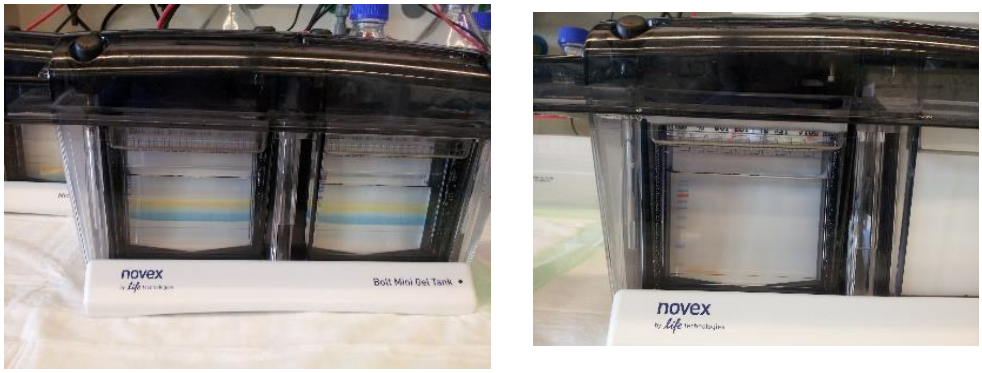

Figure 4.36: Electrophoresis setting.

These are the images we obtained from the Fiji LAS 4000. We have assessed that the aggregates we were using in the medium have two different sizes, corresponding to de 100nM and 500nM concentration. We can see in the membrane (Picture 13) that the 100nM TDP43 aggregates were smaller so they run better in the gel and the 500nM TDP43 aggregates were bigger and they got stacked on it.

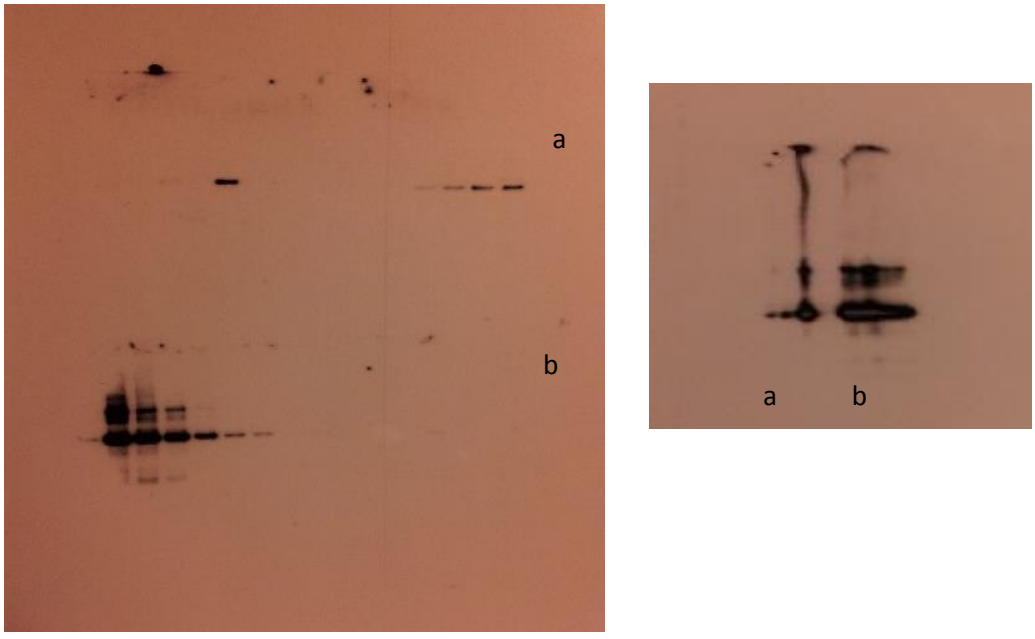

Figure 4.40: WB of TDP43 agregates medium in two different concentration.
a. Corresponds to 100nM, b. Corresponds to 500nM.

Discussion

5. DISCUSSION

In this Thesis, we tested the hypothesis that the specificity of anatomical pathways linking the BF nuclei with the cerebral cortex, as well as their functional roles may play an important role, since it has been hypothesized that AD symptoms may be a consequence of either neuronal loss or impairment of BF neurons functionality due to toxicity.

Our main findings showed that the different nuclei of the BF display specific projecting pathways to and from the different modalities cortices. The HDB may play an important role in the sensory stimuli discrimination due to its segregated projecting pathways to the different cortices and also due to a preferential circuit which shares with the mPfC. This is not the case of B nucleus which projects equally, with no preferential pathways, to all sensory cortices and do not have a B nuvleus-mPfC circuit. Moreover, HDB showed many contralateral projections which lead us to reinforce our idea of thinking of the HDB, not only as a relay station but, as a key point for filtering the sensory inputs. These different patterns identified in HDB and B nucleus, might be important in the AD developmental stages. We have observed a decrease in the number of cholinergic neurons in both HDB and B nucleus, most accused in the B nucleus as previously described also by other authors (Whitehouse *et al*., 1982), We hypothesized that the fact that the neuronal lost starts in B could be related with our findings of a higher concentration of IGF1 receptor in HDB cholinergic neurons than in B nucleus ones; therefore, IGF1 might be playing a protective neuronal role in HDB neurons, and these neurons might be compensating the B neuronal lost and masking the AD symptoms in first stages of the disease. This neuronal lost as well as symptoms in the late stages of AD, might be caused in our agreement of our results, among other causes, by the toxicity caused as a result of the aberrant function of TDP43, leading to a primary microglia massive activation trying to overcome the malfunction of the physiological neuronal metabolism which might be compensated in the first stages of AD but leads, when it is too acute, to the neuronal lost and so, to the

malfunction of these neuronal pathways causing the characteristic symptoms of AD.

A fundamental question at hand in the present study concerns whether the BF neuronal population operates more as a unified group, simultaneously activating all cortical areas, or instead operates as a set of distinct neuronal groups that differentially activate specific cortical regions.

Our results in rodents support the latter possibility since they reveal that the BF is a heterogeneous area in which neurons projecting to different cortical areas are segregated into different neuronal groups. In both rat and mice, most of the HDB has a large number of neurons that project to S1 cortex, indicating that this area is specialized in sensory processing of somatosensory stimuli. However, the B nucleus shows a similar number of cells projecting to S1 than to A1 and V1 cortices. Accordingly, optogenetic HDB stimulation induced more extensive facilitation of tactile evoked potentials than auditory evoked potentials, while optogenetic stimulation of B nucleus facilitated either tactile or auditory evoked potentials equally.

We have demonstrated that there is a topographical map linking neurons in different BF areas with their targets in primary sensory cortices and mPfC. B nucleus projections from the caudal BF to the S1, A1 and V1 cortices are similar in importance. In fact, this nucleus exhibits numerous double-labeled neurons, suggesting an absence of cortical specificity; however, the S1 and mPfC cortices receive major inputs from rostral BF areas, including the VDH and HDB (Figure 5.1).

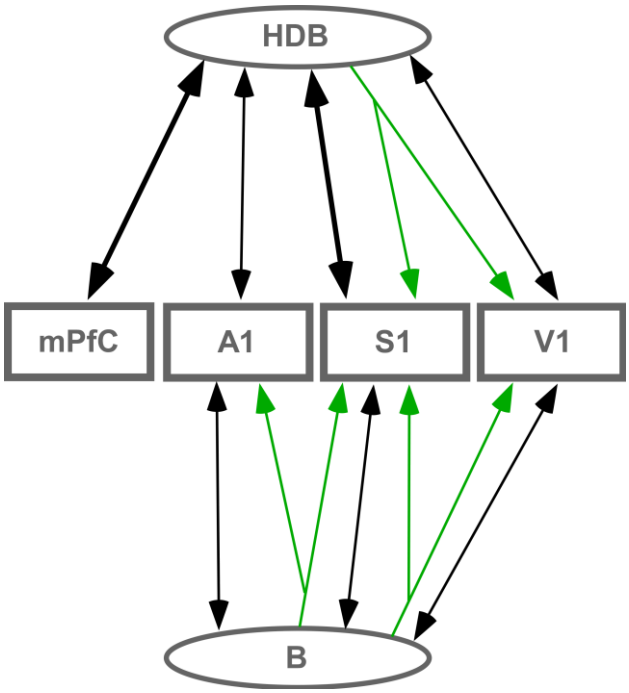

Figure 5.1: Summary diagram displaying anatomical connections of HDB and B nuclei. Results showed that HDB has preferential bidirectional projections (double arrows) to S1 and mPfC while the B nucleus projects to all sensory areas in general and does not project to mPfC. Green arrows represent double-labeled neurons. Black arrows represent single-labeled neurons.

Contralateral projections from the BF were mainly found in VDB and HDB areas while B nucleus displayed very few contralateral projecting neurons. These contralateral projections may serve to synchronize cortical related areas. The ipsi- or contralateral projection pattern also reveal that VDB or HDB areas have different cortical projections that B and SI areas (Figure 5.2).

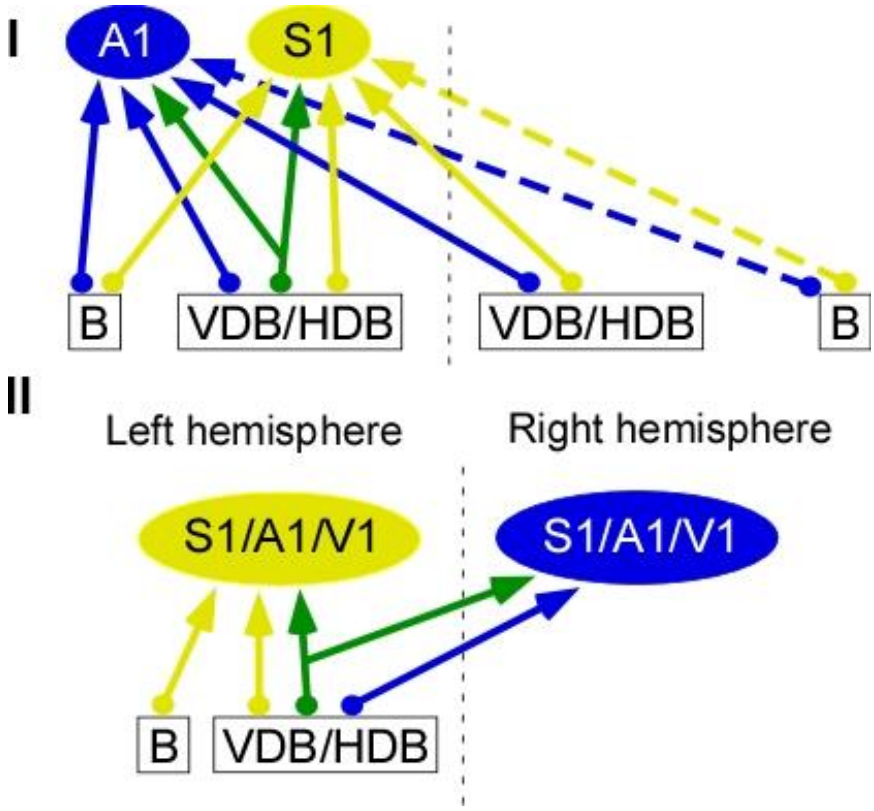

Figure 5.2: Summary of connections from BF neurons to sensory cortices.
Schematic diagram summarizes the cortical-BF connections. Yellow circles represent FlGo labeled neurons, blue circles represent FB labeled neurons and green circles represent double labeled neurons, found in each BF nucleus; colored arrows represent the corresponding sensory cortical projection. Yellow ellipsoids represent the injections of FlGo in A1, S1 or V1. Blue ellipsoids represent FB deposits in A1, S1 or V1. Dash line represents the middle line. Dashes arrows indicate a percentage less than 2% of labeled neurons.

Cortically projecting neurons in the BF were characterized as cholinergic, GABAergic or peptidergic neurons (Fisher et al., 1988, Zaborszky and Duque, 2000, Zaborszky et al., 2005, Mascagni and McDonald, 2009). Because cholinergic neurons in the BF are scattered among neurons with different neurochemical identities, we used optogenetic stimulation of cholinergic neurons in mice to study the specific cholinergic effects on sensory cortical responses of the BF-cortical circuits observed from the anatomical results. In contrast to the specific facilitation of sensory responses, blue light stimulation of either HDB or B nucleus cause similar desynchronization of S1 or A1 field potential. Likewise, illumination of neocortex desynchronizes the local field potential in the same transgenic, anesthetized mice, indicating that light evoked the release of ACh in the cortex

(Kalmbach et al., 2012). We have shown that optogenetic stimulation of cholinergic HDB neurons facilitated mostly tactile evoked potentials in S1 than auditory evoked potentials in A1 cortex. Thus, our results support a localized cortical effect of cholinergic projections. In contrast, optogenetic stimulation of B neurons facilitated auditory and tactile evoked potentials in the same proportion. In agreement with our data, optogenetic activation of BF cholinergic axons in visual cortex enhances performance of a visual discrimination task, while silencing BF cholinergic cells impaired performance (Pinto et al., 2013).

In the cases of rats experiments, using BF focal virus injections to express channel rhodopsin (ChR2), we confirming the results obtained in mice, that S1 whisker responses were mainly modulated by the HDB because optogenetic stimulation of HDB neurons induced important changes in whisker responses by S1 and mPfC neurons whereas the changes in cortical responses after optogenetic stimulation of the B nucleus were less evident. Most of these effects were due to activation of the cholinergic neurons since they were blocked by intraperitoneally injected nicotinic or muscarinic receptor antagonists. This BF-mPfC anatomical pathway seems to be very specific since projections to cortical areas mainly arise from specific neuronal groups, as supported by the observation that most of the HDB neurons were single-labeled after a cortical injection of retrograde tracer. Thus, it is reasonable to think that the pathway linking HDB-primary sensory cortices-mPfC and back to BF may be relevant in the specific sensory processing that is required for attention or learning processes. In contrast, using the same experimental protocol of retrograde tracer injection, the B nucleus showed a large proportion of double-labeled cortical neurons, showing that the B nucleus is non-specifically connected to sensory areas in general and is not directly related with mPfC. Moreover, the B nucleus also connected to the M1 cortex, suggesting that this pathway may be involved in sensory-motor coordination. Accordingly, the anatomical specificity described here has also been observed in the neuronal activation of prefrontal cortex-projecting vs. motor cortex-projecting BF neurons during task performance (Parikh et al., 2007). Thus, B nucleus neurons may integrate information necessary for sensory-motor modulation from the striatum

(Hu et al., 2016) given their significant projections to M1 and primary sensory cortices.

These findings suggest that a large population of cholinergic BF neurons is involved in cortical activation but, the cholinergic modulation of sensory responses is account from specific groups of neurons. In this process, might contribute ipsi- and contralateral projections cooperatively. In agreement with the existence of two functional roles of cholinergic BF pathways, micro dialysis studies in the medial prefrontal cortex have reported a tonic ACh increase during attention-related performance tasks (Passetti et al., 2000), that may promote a general state of cortical arousal (EEG desynchronization). Moreover, ACh can also be released briefly (phasic release) in concert with cue detection in a cued appetitive response task to facilitate specific information processing (Parikh et al., 2007). Thus, phasic release of ACh would support more rapid transitions of cortical states, consistent with cholinergic regulation of attention to relevant stimuli, while a sustained ACh release could promote a general state of cortical activation (see (Luchicchi et al., 2014, Sarter et al., 2014). Our results support these findings and suggest that different BF cholinergic neurons may play these different roles.

Based on these anatomical findings, the control of cortical processing by projections from given cholinergic areas in the BF could be much more specific than traditionally thought because our results reveal that the networks formed by BF-cortical bidirectional connections are specific to certain functions.

Different anatomical techniques have been used to map anatomical projections from the BF to different cortical areas (Bigl et al., 1982; Price and Stern, 1983; Zaborszky et al., 1986, 1999; Gritti et al., 1997, 2003; Zaborszky, 2002; Zaborszky et al., 2005, 2015; Nadasdy et al., 2010; Bloem et al., 2014). These studies have demonstrated the rostro-caudal distribution of neurons with different afferent and efferent inputs (also confirmed by present results). Furthermore, we provide novel information about the relationship between the location of BF neurons and their targets in the primary sensory and mPfC cortices. Present data also corroborate that these targets are integrated in distinct BF-cortical networks that may play different roles in sensory processing, motor control, or cortical arousal.

The bidirectional connectivity between mPfC and BF has attracted great interest as a circuit that is involved in modulating decision making, cortical arousal, and learning and memory (Groenewegen and Uylings, 2000; Miller and Cohen, 2001; Dalley et al., 2004; Henny and Jones 2008; Wise, 2008; Ramanathan et al., 2009; Martinowich et al., 2012; Paolone et al., 2012; Bloem et al., 2014; Zaborszky et al., 2015). The connections between the mPfC and other cortical areas that apparently contribute to information processing seem to be specific topographically organized (Hoover and Vertes, 2007; Bedwell et al., 2014; Bedwell et al., 2015; Zaborszky et al., 2015). The bidirectional projections between BF and mPfC described here are located so as to shape cortical activity (Schwierin et al., 1999; Massimini et al., 2004). In such processes, the cholinergic, GABAergic and glutamatergic BF neuronal groups or subgroups probably play diverse and complementary roles. Our results indicate that these projecting neurons are mainly concentrated in the rostral BF, including VDB and HDB. Their activation by optogenetic stimulation induced an important facilitation of whisker responses in S1. This response facilitation was due to activation of muscarinic receptors since it was blocked by the previous injection of atropine. However, the same projection inhibited whisker responses in mPfC though activation of nicotinic receptors since the inhibition could be abolished by mecamylamine.

The topography of BF projections to the cortex is an important issue because it might indicate in what manner the cholinergic BF system participates in cortical sensory processing. Probably, this finding is due to the importance of the whisker sensory system in rodents, giving greater evidence of the existence of neuronal clusters involved in the information processing of somatosensory stimuli. However, this pattern of projection could occur in other sensory systems although they were less evident. In fact, the cholinergic neurons that project to V1 are located in the BF, particularly the ventral pallidum, SI and the HDB (Gaykema et al., 1990, Laplante et al., 2005). Although the B nucleus is one of the main cholinergic nucleus of the BF, it projects weakly to V1 (Luiten et al., 1987, Vaucher and Hamel, 1995), as also occur in our experiments. In this regard, Záborszky et al. (2013) have demonstrated that the cholinergic and non-cholinergic pathways to the cortex are organized into segregated or overlapping pools of projection neurons.

The extent of overlap between BF populations projecting to the cortex depends on the degree of connectivity between the cortical targets of these projection populations.

Previous reports have indicated regional differences in the regulation of cortical ACh release. This has been demonstrated in a neurophysiological experiment wherein differential modulation of somatosensory and visual cortices to tactile and visual stimuli, respectively, resulted from activation of neighboring BF neurons (Golmayo et al., 2003). Moreover, they proposed that the BF could be an anatomical and functional relay between the prefrontal cortex and sensory cortical areas. Regionally specific activation of ACh release has been also demonstrated in V1 and S1 cortices following presentation of either visual or somatosensory stimuli (Fournier et al., 2004, Laplante et al., 2005). Taken together these results suggest that cortical ACh release is increased with regional specificity in response to a finely tuned sensory stimulus in urethane-anesthetized animals. This modality-specific activation is supported by the topographical projections from BF to sensory cortices (Zaborszky, 2002, Zaborszky et al., 2005, Zaborszky et al., 2013). Anatomical specificity has also been observed in the activation of prefrontal cortex-projecting vs. motor cortex-projecting BF cholinergic neurons during task performance (Parikh et al., 2007). These findings suggest the existence of different subpopulations of BF neurons involved in the modulation of specific tasks. Accordingly, clustering techniques applied to unit recordings of BF neurons during different attentional tasks have revealed many distinct categories of task-phase-specific activity patterns in the BF neurons (Tingley et al., 2014). Consequently, results strongly suggest the existence of neuronal populations in the BF that are involved in modulation of sensory cortical response, as has been published recently in the somatosensory cortex (Barros-Zulaica et al., 2014, Martin-Cortecero and Nuñez, 2014).

The BF is recognized as an important site of sleep-wake regulation (Koyama, 2012; Kalinchuk et al., 2015); actually, BF receives wide-spread input from hypothalamic nuclei, including the preoptic areas and lateral hypothalamic area, both of which are implicated in sleep and arousal regulation (Szymusiak et al.,

2007; Hu et al., 2016). Our results, showing a large number of double-labeled neurons, which projects simultaneously to different cortical areas suggest that the B nucleus is in the best nodal point to control arousal level. Our results also show that SI had a similar connection pattern that of the B nucleus. Recently, it has been published that orexinergic neurons, which play an essential role in promoting arousal, have strong reciprocal connections with SI neurons (Agostinelli et al., 2017); thus, SI and orexin neurons probably work in concert to promote arousal.

So far, concerning our anatomical studies and results of the BF-cortical circuits and its characteristic features, we can propose that complex behaviors require the integration of different synaptic inputs in the brain. These functions cannot be performed using the traditional description of the FB cholinergic system as a diffusely organized neuromodulator system with widespread influence on information processing across large portions of the cortex. Recent evidence supports an alternative hypothesis that proposes that the cognitive functions of cholinergic projections are determined in part by BF-cortical circuitry controlling cholinergic synaptic neurotransmission release in a more specific manner than previously assumed (Hasselmo and Sarter, 2011; Zaborsky et al., 2015). Our results agree with this alternative hypothesis and further suggest that the cortex and BF are integrated in specific neuronal networks with different roles in sensory processing, motor planning or arousal control.

Taken together, previous and present results indicate that stimulus evoked responses HDB corticofugal neurons can contribute to sensory processing by selecting different cortices responses as preferred or non-preferred inputs, in a modality-specific manner, contributing to the perception of specifically sensory information. In a same manner, contralateral projections may play an important role in sensory inputs processing.

Once we concluded that BF-cortical circuitry may be implicated in the integration and processing of specific sensory input processing, we now focus on the results concerning the BF cholinergic neuronal implication in Alzheimer´s Disease model and the role of neuronal death and toxicity in its pathogenesis. Our

results showed a decrease in the number of cholinergic neurons in B nucleus (Cantero et al., 2016) but also in HDB. This neuronal lost is more acute in females than in males. IGF1 is demonstrated to be implicated in long term potentiation process, facilitates sensory processing in the cortex and enhances EEG activity (Trueba et al 2013; Nishijima et al 2010), and BF cholinergic neurons induce cortical activation and facilitates sensory processing (Oldford and Castro-Alamancos 2003; Sarter et al 2009). We observed an increased amount of IGF1 receptor in the HDB of APP/PS1 mice compared with control. That could explain the initial neuronal lost in B nucleus but not in HDB since IGF1 may be playing a protective role of these neurons which presents higher concentration of IGF1 receptor. In this way, in the first stages of AD, when there is neuronal lost in B nucleus, the HDB projecting circuits, which have more specific targets, may be overtaking the functional roles of these death neurons in B nucleus. Moreover, in our opinion, the neuronal death might be a consequence of the neuronal toxicity gain. We support this hypothesis by our in vitro results. We have studied, in microglia and BB2 cells, the role of TDP43 and its implication in the possible involvement in Alzheimer's disease. Two different experiments were performed with different approaches. First *in vitro* experiment studied the BV2 cells where the knockout was induced by siRNA transfection. The second experiment studied the role of TDP43 in primary microglia isolated from loxP/loxP knockout mice. The efficiency of the knockdown in BV2 cells was studied by WB and reveal the reduction of TDP43 in TDP pool, oligo1, oligo2, but not oligo3, oligo4. Hovewer, our preliminary results show the increased phagocytosis of Aβ and lysotracer in BV2 as well as TDP oligomers in PM in all cases. Lysotracer is acknowledged as an indicator of acidic structures in the cells. Specifically, the increased amount of lysotracer in the cells corresponds with increased activity of lysosomes and late endosomes. Additionally, the phagocytosis was attenuated with higher doses and/or with increased time in both experiments. The increased clearance of Aβ in all knockout samples also corresponded with our previous results and may reflect the increased removal of Aβ from the cells. Conclusively, establishing the direct link between TDP43 and AD has not been easy. The principal difficulty comes from the huge number of processes that can be aberrantly affected by TDP43 aggregations in neurons and microglia, and by the nuclear depletion of TDP43. The

basic characteristics of TDP43 should be considered because they may ultimately control the disease. The balance between such complicated processes should be the aim of further research (the effect of intracellular inclusions in the gain of toxicity or loss of function, phagocytosis resulting in increased removal of amyloid plaques or dendritic spines)

All the above mentioned could lead to a gain of neuronal toxicity which might leads to the death or loss of function of the neurons. HDB projecting neurons (both ipsi and contralateral) could be important in the AD during first stages of the disease due to their specific projection circuits patterns. In contrast, B nucleus, since it is not displaying specific circuits but spread-wide projecting pathways to all the modality cortices but the mPfC, might not be playing a decisive role in sensory input discrimination. Moreover, taking into account first, the specificity in projecting circuits in HDB but not in B nucleus, second, that we observed increased levels of IGF1 receptor in cholinergic neurons of HDB than in B nucleus, and third that the neuronal lost its observed in B nucleus in the first stages of AD when attention, learning and memory is not affected yet, those three facts leads us to think about the importance of HDB in the facilitation of a specific information processing. This could be implicated in dysfunctional sensory-motor integration and in AD pathological stages (Butcher and Woolf, 2004; Ballinger et al, 2016). Thereby, the neuronal circuits are not working as in physiological conditions. In the first stages of the disease that might be able to be compensated between neuronal circuits of B and HDB acquiring the functions of B nucleus ones. That could explain the progress of the AD symptoms, since in early stages of the disease, learning, attention and memory are not affected, corresponding that with the integrity of the mPfC-HDB-sensory cortices circuits we have described, but, leading in late stages of the disease when we observed also neuronal lost in HDB, with the characteristic features of AD symptoms.

Conclusions

6. CONCLUSIONS

1. **The Basal Forebrain in rodents is a heterogeneous area in which there are segregated neurons in different neuronal groups that project to different circuits.**

2. **Most HDB neurons project to the S1 cortex, indicating that this area must be specialized in the processing of the tactile stimuli, while the nucleus B shows a similar proportion of neurons projecting both S1 and A1.**

3. **The optogenetic stimulation of the cholinergic neurons of the different nuclei of the BF evokes different sensory responses in the different crusts.**

4. **Cholinergic projections to the cortex are organized into segregated groups of neurons that could modulate specific cortical areas.**

5. **The modulation carried out by the BF in the sensory cortex goes through separated channels from HDB, however the modulation carried out by the B neurons is by both separate and joint pathways.**

6. **The neurons of the prefrontal cortex maintain a preferential reciprocal circuit with HDB but not with B.**

7. **IGF1 levels are higher in HDB neurons in APP / PS1 than the AD model with respect to controls.**

8. **TDP-43 could play an important role in the development of AD pathogenesis.**

Conclusiones

7. CONCLUSIONES

1. **El BF en roedores es un área heterogénea en la cual existen neuronas segregadas en diferentes grupos neuronales que proyectan a distintas cortezas.**

2. **La mayoría de neuronas localizadas en HDB proyectan a la corteza S1, indicando que éste área debe estar especializada en el procesamiento de los estímulos táctiles, mientras que el núcleo B muestra una proporción similar de neuronas que proyectan tanto a S1 como a A1.**

3. **La estimulación optogenética de las neuronas colinérgicas de los distintos núcleos del BF evoca distintas respuestas sensoriales en las diferentes cortezas.**

4. **Las proyecciones colinérgicas a la corteza están organizadas en grupos segregados de neuronas que podrían modular áreas corticales específicas.**

5. **LA modulación llevada a cabo por el BF en las cortezas sensoriales va por vías separadas desde HDB, sin embargo la modulación llevada a cabo por las neuronas de B es mediante vías tanto separadas como conjuntas.**

6. **Las neuronas de la corteza prefrontal mantienen un circuito recíproco preferencial con HDB pero no con B.**

7. **Los niveles de IGF1 son más elevados en neuronas del HDB en el APP/PS1 del modelo de AD con respecto a los controles.**

8. **TDP-43 podría tener un papel importante en el desarrollo de la patogénesis de la AD.**

References

REFERENCES

Agostinelli LJ, Ferrari LL, Mahoney CE, Mochizuki T, Lowell BB, Arrigoni E, Scammell TE (2016). Descending projections from the basal forebrain to the orexin neurons in mice. J Comp Neurol. doi: 10.1002/cne.24158.

Aravanis AM, Wang LP, Zhang F, Meltzer LA, Mogri MZ, Schneider MB, Deisseroth K (2007). An optical neural interface: in vivo control of rodent motor cortex with integrated fiberoptic and optogenetic technology. J Neural Eng 4(3): S143-56. doi: 10.1088/1741-2560/ 4/3/s02.

Ayala YM (2011). TDP-43 regulates its mRNA levels through a negative feedback loop. EMBO J 30: 277-288.

Barros-Zulaica N, Castejón C, Núñez A (2014). Frequency specific response facilitation of supra and infragranular barrel cortical neurons depends on NMDA receptor activation in rats. Neuroscience 281: 178-194. doi: 10.1016/j.neuroscience.2014. 09.057.

Bedwell SA, Billet EE, Crofts JJ, Tinsley CJ (2014). The topography of connections between rat prefrontal, motor and sensory cortices. Front Syst Neurosci 8:177.

Bedwell SA, Billet EE, Crofts JJ, McDonald DM, Tinsley CJ (2015). The topography of connections between rat prefrontal and temporal cortices. Front Syst Neurosci 9:80.

Bigl V, Woolf NJ, Butcher LL (1982). Cholinergic projections from the basal forebrain to frontal, parietal, temporal, occipital, and cingulate cortices: a combined fluorescent tracer and acetylchilinestersse analysis. Brain Res Bull 8:727-749.

Bloem B, Schoppink L, Rotaru DC, Faiz A, Hendriks P, Mansvelder HD, van de Berg WDJ, Wouterlood FG (2014). Topographic mapping between basal forebrain cholinergic neurons and the medial prefrontal cortex in mice. J Neurosci 34:16234-16246.

Bondareff W, Mountjoy CQ, Roth, M (1982). Loss of neurons of origin of the adrenergic projection to cerebral cortex (nucleus locus ceruleus) in senile dementia. Neurology 32: 164-168 (1982).

Boyden ES, Zhang F, Bamberg E, Nagel G, Deisseroth K (2005). Millisecond-timescale, genetically targeted optical control of neural activity. Nat Neurosci 8: 1263-1268.

Broussard JI, Karelina K, Sarter M, Givens B (2009). Cholinergic optimization of cue-evoked parital activity during challenged attentional performance. Eur J Neurosci 29:1711-1722. Doi: 10.1111/j.1460-9568.2009.06713.x.

Bueno-Junior LS, Lopes-Aguilar C, Riggiero RN, Romcy-Periera RN, Leite JP (2012). Muscarinic and nicotinic modulation of thalamo-prefrontal cortex synaptic plasticity *in vivo.* PLoS One 7:e47484. doi: 10. 1371/journal.pone.0047484.

Buratti E (2010). Nuclear factor TDP-43 can affect selected microRNA levels. FEBS J 277: 2268-2281.

Buzsáki G, Bickford RG, Ponomareff G, Thal LJ, Mandel R, Gage FH (1998). Nucleus basalis and thalamic control of neocortical activity in the freely moving rat. Neuroscience 8: 4007-4026.

Cantero JL, Zaborszky L, Atienza M (2016). Volume loss of the nucleus basalis of Meynert is associated with atrophy of innervated regions in mild cognitive impairment. Cereb Cortex doi : 10.1093/cercor/bhw195.

Cardin J A, Carlén M, Meletis K, Knoblich U, Zhang F, Desselroth K, Tsai, L-H, Moore C I (2010). Targeted optogenetic stimulations and recording of neurons in vivo using cell-type-specific expression of Channelrhodopsin-2. Nat Protoc 5:247-254. doi: 10.1038/nprot.2009.228.

Carro E, Torres-Aleman I (2004). The role of insulin and insulin-like growth factor I in the molecular and cellular mechanisms underlying the pathology of Alzheimer's disease. Eur J Pharmacol 490: 127-133.

Chandler DJ, Lamperski CS, Waterhouse BD (2013). Identification and distribution of projections form monoaminergic and cholinergic nuclei to functionally differentiated subregions of prefrontal cortex. Brain Res 1522: 38-58.

Chaves-Coira I, Barros-Zulaica N, Rodrigo-Angulo ML, Núñez A (2016). Modulation of specific sensory cortical areas by segregated basal forebrain cholinergic neurons demonstrated by neuronal tracing and optogenetic stimulation in mice. Frontiers in Neural Circuits 10 (28):1-13.

Chiba AA, Bushnell PJ, Oshiro WM, Gallagher M (1999) Selective removal of cholinergic neurons in the basal forebrainalters cued target detection. Neuroreport 10: 3119-3123. doi: 10.1097/00001756-199909290- 00044.

Collier B, and Mitchell JF (1966). The central release of acetylcholine during stimulation of the visual pathways. J Physiol 184: 239-254. doi: 10. 1113/jphysiol.1966.sp007913

Dalley JW, Cardinal RN, Robbins TW (2004). Prefrontal executive and cognitive functions in rodents: neural and neurochemical sustrates. Neurosci Behav Rev 28:771-784.

Deisseroth K (2011). Optogenetics. Nat Methods 8: 26-29. doi: 10.1038/nmeth.f.324. Epub 2010 Dec 20.

Détari L (2000). Tonic and phasic influence of the basal forebrain unit activity on the cortical EEG. Behav Brain Res 115: 159-170. doi: 10.1016/s0166- 4328(00)00256-4.

De Strooper B (2010). Proteases and proteolysis in Alzheimer disease: A multifactorial view on the disease process. Physiol Rev 90: 465–494.

Dolrap S, Leung LS (2008). Cholinergic modulation of hippocampal CA1 basal-dendritic long-term potentiation. Neurobiol Learn Mem 90: 382-388. doi: 10.1016/j.nlm.2008.05.013.

Eckenstein FP, Baughman RW, Quinn J (1988). An anatomical study of cholinergic innervation in rat cerebral cortex. Neuroscience 25: 457-474. doi: 10.1016/0306-4522(88)90251-5.

Fernández A M, Torres-Aleman I. (2012). The many faces of insulin-like peptide signalling in the brain. Nat Rev Neurosci 13, 225-239

Fernández de Sevilla D, Núñez A, Borde M, Malinow R, Buño W (2008). Cholineric-mediated IP_3 receptor activation induces long-lasting synaptic enhancement in CA1 pyramidal neurons. J Neurosci 28: 1469-1478. doi: 10.1523/JNEUROSCI.2723-07.2008.

Fournier GN, Semba K, Rasmusson DD (2004). Modality and region-specific acetylcholine release in the rat neocortex. Neuroscience 126: 257-262. doi: 10.1016/j.neuroscience.2004.04.002.

Geula C, Mesulam MM (1989). Cortical cholinergic fibers in aging and Alzheimer's disease: a morphometric study. Neuroscience 33:469-481.

Goard M, Dan Y (2009). Basal forebrain activation enhances cortical coding of natural scenes. Nat Neurosci 12: 1444-1449. doi: 10.1038/ nn.2402.

Golmayo L, Núñez A, Zaborszky L (2003). Electrophysiological evidence for the existence of a posterior cortical-prefrontal-basal forebrain circuitry in modulating sensory responses in visual and somatosensory rat cortical areas. Neuroscience 119: 597-609. doi: 10.1016/s0306-4522(03) 00031-9.

Gradinaru V, Thompson KR, Zhang F, Mogri M, Kay K, Schneider MB, Deisseroth K (2007).

Targeting and readout strategies for fast optical neural control in vitro and in vivo. J Neurosci 27: 14231-14238.

Gregory CW, DeGeorges A, Sikes RA (2001). The IGF axis in the development and progression of prostate cancer. Recent Research Developments in Cancer: 437–462. ISBN 81-7895-002.

Gritti I, Mainville L, Mancia M, Jones BE (1997). GABAergic and other noncholinergic basal forebrain neurons, together with cholinergic neurons, project to the mesocortex and isocortex in the rat. J Comp Neurol 383:163-177.

Gritti I, Manns ID, Mainville L, Jones BE (2003). Parvalbumin, calbindin, or calretinin in cortically projecting and GABAergic, cholinergic, or glutamatergic basal forebrain neurons of the rat. J Comp Neurol 458:11-31.

Groenewegen HJ, Uylings HB (2000). The prefrontal cortex and the integration of sensory, limbic and autonomic information. Prog Brain Res 126:3-28.

Hasselmo ME, Sarter M (2011). Modes and models of forebrain cholinergic neuromodulation of cognition. Neuropsychopharmacology 36:52-73. doi: 10.1038/npp.00870.2011.

Hebert LE, Weuve J, Scherr PA, Evans DA (2013). Alzheimer disease in the United States (2010–2050) estimated using the 2010 Census. Neurology 80: 1778–83.

Henny P, Jones BE (2008). Projections form basal forebrain to prefrontal cortex comprise cholinergic, GABAergic and glutamatergic inputs to pyramidal cells or interneurons. Eur J Neurosci 27:654-670.

Hoover WB, Vertes RP (2007). Anatomical analysis of afferent projections to the medial prefrontal cortex in the rat. Brain Struct Func 212:149-179.

Houser CR, Crawford GD, Salvaterra PM, Vaughn JE (1985). Immunocytochemical location of choline acetyltransferase in rat cerebral cortex: a study of cholinergic neurons and synapses. J Comp Neurol 234:17-34.

Hu R, Jin S, He X, Xu F, Hu J (2016). Whole-brain monosynaptic afferent inputs to basal forebrain cholinergic system. Front Neuroanat 10:98. doi: 10.3389/fnana.2016.00098.

Jones JI, Clemmons DR (1995). Insulin-like growth factors and their binding proteins: biological actions. Endocr Rev 16: 3–34. PMID 7758431. doi:10.1210/edrv-16-1-3.

Kalinchuk AV, Porkka-Heiskanen T, McCarley RW, Basheer R (2015). Cholinergic neurons of the basal forebrain mediate biochemical and electrophysiological mechanisms underlying sleep homeostasis. Eur J Neurosci 41:182-195. doi: 10.1111/ejn.12766.

Kawahara Y, Mieda-Sato A (2012). TDP-43 promotes microRNA biogenesis as a component of the Drosha and Dicer complexes. Proc. Natl. Acad. Sci. U.S.A. 109: 3347-3352.

Kim HJ, Kim NC, Wang YD, Scarborough EA, Moore J, Diaz Z, MacLea KS, Freibaum B, Li S, Molliex A, Kanagaraj AP, Carter R, Boylan KB, Wojtas AM, Rademakers R, Pinkus JL, Greenberg SA, Trojanowski JQ, Traynor BJ, Smith BN, Topp S, Gkazi AS, Miller J, Shaw CE, Kottlors M, Kirschner J, Pestronk A, Li YR, Ford AF, Gitler AD, Benatar M, King OD, Kimonis VE, Ross ED, Weihl CC, Shorter J, Taylor JP (2013). Mutations in prion-like domains in hnRNPA2B1 and hnRNPA1 cause multisystem proteinipaphy and ALS. Nature. 495 (7442): 467–473. doi:10.1038/nature11922.

Kim J-H, Jung A-H, Jeong D, Choi I, Kim K, Shin S, Kim SJ, Lee S-H (2016). Selectivity of neuromodulatory projections from the basal forebrain and Locus Coeruleus to primary sensory cortices. J Neurosci 36:5314-5327.

Knusel B, Michel PP, Schwaber J S, Hefti F (1990). Selective and nonselective stimulation of central cholinergic and dopaminergic development in vitro by nerve growth factor, basic fibroblast growth factor, epidermal growth factor, insulin and the insulin-like growth factors I and II. J Neurosci 10: 558-570.

Koyama Y (2012). Regulation of sleep and wakefulness through the monoaminergic and cholinergic system. Brain Nerve 64: 601-610.

Kristt DA, McGowan Jr RA, Martin-MacKinnon N, Solomon J (1985). Basal forebrain innervation of rodent neocortex: studies using acetylcholinesterase histochemistry, Golgi and lesion strategies. Brain Res 337: 19-39.

Kuo MC, Rasmusson DD, Dringerberg HC (2009). Input-selective potentiation and rebalancing of primary sensory cortex afferents by endogenous acetylcholine. Neuroscience 163: 430-441.

Kuo PH, Doudeva LG, Wang YT, Shen CK, Yuan HS (2009). Structural insights into TDP-43 in nucleic-acid binding and domain interactions. Nucleic Acids Research. 37 (6): 1799–808. doi:10.1093/nar/gkp013.

Laplante F, Morin Y, Quirion R, Vaucher E (2005). Acetylcholine release is elicited in the visual cortex, but not in the prefrontal cortex, by patterned visual stimulation: a dual in vivo microdialysis study with functional correlates in the rat brain. Neuroscience 132: 501-510. doi: 10.1016/j.neuroscience.2004. 11.059.

Lee MG, Manns ID, Alonso A, Jones BE (2004). Sleep-wake related discharge properties of basal forebrain neurons recorded with micropipettes in head-fixed rats. J Neurophysiol 92: 1182-1198. doi: 10.1152/jn. 01003.2003.

LeRoith D, Werner H, Beitner-Johnson D, Roberts CT (1995). Molecular and cellular aspects of the insulin-like growth factor I receptor. Endocr Rev 16: 143–163. PMID 7540132. doi:10.1210/edrv-16-2-143.

Lin S C, Brown RE, Hussain Shuler MG, Petersen CCH, Kepecs A (2015). Optogenetic Dissection of the Basal Forebrain Neuromodulatory Control of Cortical Activation, Plasticity, and Cognition. J Neurosci 35: 13896-13903, doi:10.1523/JNEUROSCI.2590-15.2015 (2015).

Luchicchi A, Bloem B, Viaña JN, Mansvelder HD, Role LW (2014). Illuminating the role of cholinergic signaling in circuits of attention and emotionally salient behaviors. Front Synatic Neurosci 6: 24. doi: 10. 3389/fnsyn.2014.00024.

Lysakowski A, Wainer BH, Bruce G, Hersh LB (1989). An atlas of the regional and and laminar distribution of the choline acetyltransferae immunoreactivity in rat cerebral cortex. Neiroscience 28: 291-336. doi: 10. 1016/0306-4522(89)90180-2.

Mackenzie IR, Neumann M, Baborie A, Sampathu DM, Du Plessis D, Jaros E, Perry RH, Trojanowski JQ, Mann DM, Lee VM (2011). A harmonized classification system for FTLD-TDP pathology. Acta Neuropathol 122: 111–3. doi:10.1007/s00401-011-0845-8.

Manns ID, Mainville L, Jones BE (2001). Evidence for glutamate, in addition to acetylcholine and GABA, neurotransmitter synthesis in basal forebrain neurons projecting to the entorhinal cortex. Neuroscience 107:249-263.

Martinowich K, Cardinale KM, Schloesser RJ, Hsu M, Greig NH, Manji HK (2012). Acetylcholinesterase inhibition ameliorates deficits in motivation drive. Behav Brain Funct 8:15. doi: 10.1186/1744-9081-8-15.

Massimini M, Huber R, Ferrarelli F, Hill S, Tononi G (2004). The sleep slow oscillation as a traveling wave. J Neurosci 24:6862.6870.

Mattis VB, Tom Chang CW, Lorson CL (2012). Analysis of a read-through promoting compound in a severe mouse model of spinal muscular atrophy. Neurosci Lett525: 72-75. doi: 10.1016/j.neulet.2012.07.024.

Mendez MF (2012) Early-onset Alzheimer's disease: nonamnestic subtypes and type 2 AD. Archives of Medical Research 43:677–85.

Mesulam MM, Mufson EJ, Wainer BH, Levey AI (1983). Central cholinergic pathways in the rat: an overview based on an alternative nomenclature (Ch1-Ch6). Neurosci 10: 1185-1201y

Mesulam MM, Mash D, Hersh L, Bothwell M, Geula C (1992). Cholinergic innervation of the human striatum, globus pallidus, subthalamic nucleus, substantia nigra, and red nucleus. J Comp Neurol 323:252-268.

Metherate R, Ashe JH (1993). Nucleus basalis stimulation facilitates thalamocortical synaptic transmission in the rat auditory cortex. Synapse 14: 132-143. doi: 10.1002/syn.890140206.

Miller EK, Cohen JD (2001). An integrative theory of prefrontal cortex function. Ann Rev Neurosci 24:167-202.

Mompean M, Romano V, Pantoja-Uceda D, Stuani C, Baralle FE, Buratti E, Laurents DV (2016). The TDP-43 N-Terminal Domain Structure at High Resolution. FEBS Journal 283: 1242–1260. ISSN 1742-4658. doi:10.1111/febs.13651.

Nadasdy Z, Varsanyi P, Zaborszky L (2010). Clustering of large cell populations: method and application to the basal forebrain cholinergic system. J Neurosci Meth 194:46-55.

Navarrete M, Perea G, Fernández de Sevilla D, Gómez-Gonzalo M, Núñez A, Martín ED, Araque A, (2012). Astrocytes mediate *in vivo* cholinergic-induced synaptic plasticity-PLoS Biol 10:e10 01259. doi:10.1371/journal.pbio.1001259.

Neumann M, Sampathu DM, Kwong LK, Truax AC, Micsenyi MC, Chou TT, Bruce J, Schuck T, Grossman M, Clark CM, McCluskey LF, Miller BL, Masliah E, Mackenzie IR, Feldman H, Feiden W, Kretzschmar HA, Trojanowski JQ, Lee VM (2006). Ubiquitinated TDP-43 in Frontotemporal Lobar Degeneration and Amyotrophic Lateral Sclerosis. Science. 314 (5796): 130–133.

Nishijima T, Piriz J, Duflot S, Fernández AM, Gaitan G, Gómez-Pinedo U, Verdugo JM, Leroy F, Soya H, Núñez A, Torres-Alemán I (2010). Neuronal activity drives localized blood-brain-barrier transport of serum insulin-like growth factor-I into the CNS. Neuron 67: 834-846.

Núñez A, Domínguez S, Buño W, Fernández de Sevilla D (2012). Cholinergic-mediated response enhancement in barrel cortex layer V pyramidal neurons. J Neurophysiol 108: 1656-1668. doi: 10.1152/jn.00156. 2012.

Oldford E, Castro-Alamancos MA (2003). Input-specific effects of acetylcholine on sensory and intracortical evoked responses in the "barrel cortex" in vivo. Neuroscience 117: 769-778.

Paolone G, Lee TM, Sarter M (2012). Time to pay attention: attentional performance time-stamped prefrontal cholinergic activation, diurnality, and performance. J Neurosci 32:12115-12128. doi: 10.1523/JNEUROSCI.2271-12.2012.

Parikh V, Kozak R, Martínez V, Sarter M (2007). Prefrontal acetylcholine release controls cue detection on multiple timescales. Neuron 56:141-154. doi:10.1016/j.neuron.2007.08.025.

Pauli WM, O'Reilly RC (2008). Attentional control of associative learning- a possible role of the central cholinergic system. Brain Res 1202: 43-53. doi: 10.1016/j.brainres.2007.06.097.

Paxinos G, Watson C (2007). The rat brain in stereotaxic coordinates. 6th Ed. San Diego. Academic Press.

Price JL, Stern R (1983). Individual cells in the nucleus basalis-diagonal band complex have restricted axonal projections to the cerebral cortex in the rat. Brain Res 269:352-356.

Rajendran L, Annaert W (2012) Membrane trafficking pathways in Alzheimer's disease. Traffic 13:759–770.

Ramanathan D, Tuszynski MH, Conner JM (2009). The basal forebrain cholinergic system is required specifically for behaviorally mediated cortical map plasticity. J Neurosci 29: 5992-6000. Doi. 10.1523/JNEUROSCI.0230-09.2009.

Rassmuson DD (2000). The role of acetylcholine in cortical synaptic plasticity. Behav Brain Res 115: 2015-218.

Rasmusson DD, Smith SA, Semba K (2007). Inactivation of prefrontal cortex abolishes cortical acetylcholine release evoked by sensory or sensory pathways stimulation in the rat. Neuroscience 149: 232-241. doi: 10.1016/j. neuroscience.2007.06.057.

Riga D, Matos MR, Las A, Amit AB, Spijker S, Van den Oever MC (2014). Optogenetic dissection of medial prefrontal corte circuitry. Front Syst Neurosci 8:230. doi: 10.3389/fnsys.2014.00230. eCollection 2014.

Romberg C, Bussey TJ, Saksida LM (2013). Paying more attention to attention: towards more comprehensive cognitive translation using mouse models of Alzheimer's disease. Brain Res Bull 92: 49-55.

Saeed O, Yaghmaie F, Garan SA, Gouw AM, Voelker MA, Sternberg H, Timiras PS (2007). Insulin-like growth factor-1 receptor immunoreactive cells are selectively maintained in the paraventricular hypothalamus of calorically restricted mice. Int J Dev Neurosci 25: 23–28. doi:10.1016/j.ijdevneu.2006.11.004.

Sarter M, Bruno JP, Givens B (2003). Attentional functions of cortical cholinergic inputs what does it mean for learning and memory?. Neurobiol Learn Mem 80: 245-256. doi: 10.1016/s1074-7427(03)00070-4.

Sarter M, Parikh V, Howe W M (2009). Phasic acetylcholine release and the volume transmission hypothesis: time to move on. Nat Rev Neurosci 10: 383-390.

Sarter M, Lustig C, Howe WM, Gritton H, Berry SA (2014). Deterministic functions of cortical acetylcholine. Eu J Neurosci 39:1912-1920. doi: 10.1111/ejn.12515.

Schwierin B, Achermann P, Deboer T, Oleksenko A, Borbély AA, Tobler I (1999). Regional differences in the dynamics of the cortival EEG in the rat after sleep deprivation. Clin Neurophysiol 110:869-875.

Schwarz A (2010). Study Says Brain Trauma Can Mimic A.L.S. The New York Times, Accessed August 18.

Semba K (2000) Multiple output pathways of the basal forebrain: organization, Chemical heterogeneity, and roles in vigilance. Behav Brain Res 115:117-141. doi: 10.1016/s0166-4328(00)00245-0.

Semba K, Reiner PB, McGeer EG, Fibiger HC (1988). Brainstem afferents to magnocellular basal forebrain studied by axonal transport immunohistochemistry and electrophysiology in the rat. J Comp Neurol 267: 433-453. doi: 10.1002/cne.902670311.

Semba K, Fibiger HC (1989). Organization of the central cholinergic system. Prog Brain Res 79:37-63. doi: 10.1002/cne.902670311.

Sephton CF, Cenik C, Kucukural A, Dammer EB, Cenik B, Han Y, Dewey CM, Roth FP, Herz J, Peng J, Moore MJ, Yu G (2011). Identification of neuronal RNA targets of TDP-43-containing ribonucleoprotein complexes. J Biol Chem 286 (2): 1204–15. doi:10.1074/jbc.M110.190884.

Szymusiak R, Alam N, McGinty D (2000). Discharge patterns of neuron in cholinergic regions of the basal forebrain during waking and sleep. Beahv Brain Res 115: 171-182. doi: 10.1016/s0166-4328(00)00257-6.

Szymusiak R, Gvilla I, McGinty D (2007). Hypothalamic control of sleep. Sleep Med 8: 291-301. doi: 10.1016/j.sleep.2007.03.013.

Talbot K, Wang HY, Kazi H, Han LY, Bakshi KP, Stucky A, Fuino RL, Kawaguchi RK, Samoyedny AJ, Wilson RS, Arvanitakis Z, Schneider JA, Wolf BA, Bennett DA, Trojanowski JQ, Arnold SE (2012). Demonstrated brain insulin resistance in Alzheimer's disease patients is associated with IGF-1 resistance, IRS-1 dysregulation, and cognitive decline. J Clin Invest 122: 1316-1338.

Tremblay C, St-Amour I, Schneider J, Bennett DA, Calon F (2011). Accumulation of transactive response DNA binding protein 43 in mild cognitive impairment and Alzheimer disease. J Neuropathol Exp Neurol 70: 788–98. doi:10.1097/nen.0b013e31822c62cf.

Trueba-Saiz A, Cavada C, Fernández AM, León T, González DA, Fortea Ormaechea (J, Lleó A, Del Ser T, Núñez A, Torres-Aleman I 2013). Loss of serum IGF-I input to the brain as an early biomarker of disease onset in Alzheimer mice. Transl Psychiatry 3, e330.

Tye KM, Prakash R, Kim SY, Fenno LE, Grosenick L, Zarabi H, Thompson Kr, Gradinaru V, Ramakrishnan C, Deisseroth K (2011). Amygdala circuitry mediating reversible and bidirectional control of anxiety. Nature 471:358-362. doi: 10.1038/nature09820.

Unal CT, Golowasch JP, Zaborszky L (2012). Adult Mouse basal forebrain harbors two distinct cholinergic populations defined by their electrophysiology. Front Behav Neurosci 6: 21. doi: 10.3389/fnbeh. 2012.00021.

Uryu K, Nakashima-Yasuda H, Forman MS, Kwong LK, Clark CM, Grossman M, Miller BL, Kretzschmar HA, Lee VM, Trojanowski JQ, Neumann M (2008). Concomitant TAR-DNA-binding protein 43 pathology is present in Alzheimer disease and corticobasal degeneration but not in other tauopathies. J Neuropathol Exp Neurol 67: 555–564.

Whitehouse PJ, Struble RG, Clark AW, Price DL. 1982. Alzheimer disease: plaques, tangles, and the basal forebrain. Ann Neurol 12:494.

Whitehouse PJ, Price DL, Struble RG, Clark AW, Coyle JT, Delon MR (1982). Alzheimer's disease and senile dementia: loss of neurons in the basal forebrain. Science 215: 1237-1239.

Wilson FA, Rolls ET (1990a). Learning and memory is reflected in the responses of reinforcement-related neurons in the primate basal forebrain. J Neurosci 10: 1254-1267.

Wilson FA, Rolls ET (1999b). Neuronal responses related to reinforcement in the primate basal forebrain. Barin Res 509; 213-231. doi: 10. 1016/0006-8993(90)90546-n.

Wise SP (2008). Forward frontal fields: phylogeny and fundamental function. Trends Neurosci 31:599-608.

Xu Q, Malecka K L, Fink L, Jordan, EJ, Duffy E, Kolander S, Peterson JR, Dunbrack RL (2015). Identifying three-dimensional structures of autophosphorylation complexes in crystals of protein kinases. Science Signaling. 8 (405): rs13. doi:10.1126/scisignal.aaa6711.

Yaghmaie F, Saeed O, Garan SA, Voelker MA, Gouw AM, Freitag W, Sternberg H, Timiras PS (2006). Age-dependent loss of insulin-like growth factor-1 receptor immunoreactive cells in the supraoptic hypothalamus is reduced in calorically restricted mice. Int J Dev Neurosci 24: 431–436. doi:10.1016/j.ijdevneu.2006.08.008.

Zaborszky L (2002). The modular organization of brain systems. Basal forebrain: the last frontier. Prog. Brain Res 136:359-372. doi: 10.1016/s0079-6123(02)36030-8.

Zaborszky L, Carlsen J, Brashear HR, Heimer L (1986). Cholinergic and GABAergic afferents to the olfactory bulb in the rat with special emphasis on the projection

neurons in the nucleus in the nucleus of the horizontal limb of the diagonal band. J Comp Neurol 243:488-509.

Zaborszky L, Gaykema RP, Swanson DJ, Cullinan WE (1997). Cortical input to the basal forebrain. Neuroscience 79:1051-1078. doi: 10.1016/s0306-4522(97)00049-3.

Zaborszky L, Buhlm DL, Pobalashinghamm S, Bjaaliem JG, Nadasym Z (2005). Three-dimensional chemoarchitecture of the basalforebrain: spatially specific association of cholinergic and calcium binding-protein-containing neurons. Neuroscience 136:697713. doi: 10.1016/j.neuroscience.2005.05.019.

Zaborszky L, Van Den Pol A, Gyengensi E (2012). The basal forebrain cholinergic projection system in mice. In *The Mouse nervous System*, eds C Watson, GM Paxinos, and L Puelles (Amsterdam: Elsevier): 684-718.

Zaborszky L, Csordas A, Mosca K, Kim J, Gielow MR, Vadasz C, Nadasdy Z (2015). Neurons in the basal forebrain project to the cortex in a complex topographic organization that reflects corticocortical connectivity patterns: an experimental study based on retrograde tracing and 3D reconstruction. Cereb Cortex 25:118-137. doi: 10.1093/cercor/bht210.

Zant JC, Kim T, Prokai L, Szarka S, McNally J, McKenna JT, Shukla C, Yang C, Kalinchuk AV, McCarley RW, Brown RE, Basheer R (2016). Cholinergic neurons in the basal forebrain promote wakefulness by actions on neighboring non-cholinergic neurons: an opto-dialysis study. J Neurosci 36:2057-2067.